SUPERCONDUCTING DC-SPUTTERED Nb_3Ge FILMS:

FABRICATION, STRUCTURE, AND PROPERTIES

by

JAMES ALLEN GREGORY

S. B., Massachusetts Institute of Technology
1973

Submitted in partial fulfillment of the requirements
for the degree of

DOCTOR OF SCIENCE

at the

Massachusetts Institute of Technology
February, 1979

Signature of Author ....
Signature redacted
Department of Materials Science
and Engineering, January 12, 1979

Certified by ....
Signature redacted
Thesis Supervisor

Certified by ....
Signature redacted
Thesis Supervisor

Accepted by ....
Signature redacted
Chairman, Departmental
Committee on Graduate Students

ABSTRACT

SUPERCONDUCTING DC-SPUTTERED Nb$_3$Ge FILMS:

FABRICATION, STRUCTURE, AND PROPERTIES

by

JAMES ALLEN GREGORY

Submitted to the Department of Materials Science and
Engineering on January 12, 1979 in partial fulfillment
of the requirements for the degree of Doctor of Science.

    Thin films of essentially single phase A15 Nb-Ge have
been fabricated by dc getter-sputtering with an argon atmos-
phere in a system with an oxygen background partial pressure
of approximately 4×10^{-5} Pa. A maximum of 23-24% Ge could be
incorporated in the A15 phase corresponding to a lattice para-
meter of .5142 nm and a superconducting transition temperature
onset of 22.4 K. The germanium and niobium concentrations of
the films depend almost solely on the composition of the sput-
tering targets in the deposition temperature range which pro-
duces A15 phase films. The A15 lattice parameter depends pri-
marily on the Ge content of the A15 phase, decreasing as Ge
content increases, and, perhaps, decreasing as the order of the
films improves and as the film thickens. The film thickness
limits grain size for very thin films ($\approx$ 100 nm) while for
thicker films the grain size increases with deposition temper-
ature until a saturated grain size is achieved ($\approx$ 400 nm) at
a deposition temperature which increases with Ge content of
the target.
    The second phases present in the films have a strong de-
pendence on the sputtering target composition as well as on
the annealing and deposition temperatures. There is a marked
increase in the amount of additional phases present for films
deposited from a 28 atomic percent Ge target as opposed to 21%
and 23% Ge targets. There is also an increase of second phase
material for samples deposited at temperatures above or below
a deposition temperature corresponding to a saturated grain
size as well as for films that were annealed for long periods
of time (7200 seconds). The elemental impurity concentrations
of carbon and oxygen, on the other hand, appear to be sub-
strate dependent, exhibiting different depth profiles with
substrate type.
    Consistent with these structural aspects of the films, re-
sistivity and residual resistance ratio appear to depend on
target composition, deposition temperature, film thickness, and
annealing temperature and duration. The film resistivity at
25 K decreases for multiphase films, for films deposited at a

high temperature, for films thicker than $\approx$ 100 nm, and for films that had been deposited at low temperature and then annealed. The residual resistance ratio increases with Ge content of the target, with deposition temperature, with film thickness, and with annealing of multiphase films deposited at high temperatures.

Substrate morphology is the primary determinant of breaking strain; maximum values for ceramic substrates were obtained for sapphire but underlayer and overlayer films of gold and epoxy raised the breaking strain of sintered alumina and Superstrate substrates to that of the sapphire. Metallic substrates bonded to the A15 films so that irreversible superconducting transition temperature degradation was observed before fracture strains could be reached.

The superconducting transition temperature increases as the stoichiometric composition is approached from the Nb rich side, as the grain size increases to saturation, and as the crystalline order of the film is increased. These parameters are in turn determined by target composition, deposition temperature, thickness, and annealing conditions. Moderate additions of oxygen to the sputtering atmosphere during deposition ($\approx 10^{-3}$ Pa) also increase T_c, while straining the films in tension or compression after deposition decreases T_c ($\approx$ .1 K).

To produce Nb_3Ge films with T_c values above $22^{\circ}K$, the film must have a composition near 25% Ge, be nearly single phase, possess high long-range order, have grain sizes near .4 μm, and be deposited on a material such as sapphire so there is little strain caused by thermal contraction mismatch.

A model for the mechanism for film growth and for the changes effected by annealing the films is presented which, contrary to the current literature, does not invoke the existence of a defect of unknown character to explain the dependence of T_c on film structure in Nb_3Ge.

Thesis Supervisors: J. Bostock
    Assistant Professor of Physics

    M. L. A. MacVicar
    Associate Professor of Physics

Table of Contents

List of Figures

target and deposition temperature: (a) 21%
Ge, 710 C (b) 21% Ge, 770 C (c) 23% Ge,
710 C (d) 23% Ge, 780 C (e) 28% Ge, 725 C
(f) 28% Ge, 770 C. The magnification is
20,000 x.

small numerals denote the heights of the

atoms in fractions of the vertical cell edge.

The respective unit cells are shown by the

solid lines, and the broken lines show the

A15 unit cell "block" surrounding the Nb(1)

atoms in Nb_5Ge_3. Used with permission of

D.E.Cox (ref. 49).

List of Tables

Acknowledgements

First, I should like to thank my advisors, Margaret MacVicar and Judy Bostock, for the training, guidance, and support they have given me during the long course of my graduate work. Their continual optimism was always encouraging.

I should also like to thank Bob Rose and Irvin Puffer for all they have taught me and for their encouragement during this work.

Thanks are due to Alex Braginski of Westinghouse and Don Rogowski of Pennsylvania State University for providing samples and for useful discussions. I am also grateful to the members of the Center for Materials Science and Engineering at M. I. T. for the aid they have given me during the course of this work.

I should also like to acknowledge the financial support of the Department of Energy, the Advanced Research Projects Agency, the National Science Foundation, and the Edwin Austin Fund at M. I. T.

I am also obliged to my many friends for their help, encouragement, and friendship which have made my years at M. I. T. much more enjoyable. In addition, I'd particularly like to thank (in chronological order) Myron Frommer, Tom Eagar, Vicky Diadiuk, and Keith Milkove. I'd also like to thank Walter Zwirble and Jim DeBroux for their excellent help in collecting data.

Finally, I'd like to thank my wife Nancy and our families; her understanding and support were essential to the successful completion of this thesis, as was the encouragement and support of both our parents.

I. Introduction

A. Opening Remarks

The utilization of superconductivity in everyday life
is still in the future. However, applications of wide impact
are approaching the preliminary stages of commercial develop-
ment. Large scale uses are dependent either on the perfect
diamagnetism or the concomitant perfect conductivity of the
superconductor: e.g., ac transmission lines, levitated trains,
and magnetic field coils for containing fusion plasmas or
for storing plasma-generated energy are of current
active interest.[1] Smaller devices such as Josephson junction
detectors and switches are being developed too, and in the
case of switches, are approaching semiconductor devices in
packing density and speed.[2]

Further developments for actual field tests require
higher upper bounds on the superconducting parameters of
state, that is, critical magnetic field, critical current
density, and critical temperature. At this time, we are
still learning how to attain these critical property maxima.
We cannot predict whether these values are absolute maxima
for a specific material or whether they are relative maxima
for classes of materials at hand. To increase the limits
of these critical parameters, we must learn more about super-
conductors already available: how properties depend on the

structure of the material and how we can influence the struc-
ture during processing. Only then can we hope to balance
advantageously the inevitable tradeoffs that accompany materials
processing.

The empirical trends discovered so far are those that
depend on the characteristics of free atoms or elemental
solids. Although generally reliable, these trends do not
form a sufficient set of requirements to accurately predict
the transition temperature, T_c, of an alloy, nor do they
resolve which of several mechanisms are responsible for en-
hanced superconductivity.[3] For instance, the e/a scheme
of Matthias[4] wherein one calculates the average number of
valence electrons for each atom in the alloy or compound,
has been quite useful in finding crystal structures with
a high T_c. This approach predicts a maximum in T_c at 4.7
and 7 electrons per atom; and, these are the e/a ratios where
the superconductors with the highest T_c's are actually found.
Matthias presents only a qualitative explanation based on
bonding concepts for this behavior;[4] the scheme does not
explain how to achieve or to predict the absolute maximum
in T_c for a given e/a. Another avenue which has been ex-
ploited in the search for high temperature superconductors
is the use of high Debye temperature, θ_D, constituents. The

Debye temperature is a measure of the strength of phonons
in the material; a larger θ_D implies a greater phonon strength
and a greater coupling of electrons and phonons. This last
interaction is believed to be responsible for the occurence
of superconductivity,[5] so, a larger θ_D and electron phonon
coupling leads to a higher T_c. This approach, however, is
of more questionable utility because there are no strict
rules for predicting the Debye temperature of an alloy or
if such an alloy or compound will be stable. A third empiri-
cal approach is the search for superconductors among materials
that have high electrical resistivity but still remain metals,[5]
e.g., Ag and Cu are not normally superconductors but are the
best elemental conductors. Aluminum is a good conductor
but only has a T_c of 1.2 K and Nb is a poor conductor but
has a T_c of 9.2 K. This behavior is again related to the
interaction of phonons and electrons in the material.

The high θ_D, e/a, and high resistivity trends that have
been exploited in the search for high T_c superconductors
can be related to the Bardeen, Cooper, and Schrieffer (BCS)
theory of superconductivity which predicts $T_c = 1.14\theta_D\exp(-1/N(0)V)$
where N(0) is the electron density of states at the Fermi
level, and V is the strength of the interaction of electrons
and phonons in the material. An increase in θ_D or N(0) will
increase T_c. Attempts to correlate e/a with N(0) have indeed

been successful,[6] giving qualitative justification to the
dependence of T_c on e/a based on electron bonding, a mechanism
that tells us very little, however, about V. A larger V
would, in itself, of course imply a higher T_c in the BCS
theory, which perhaps explains the dependence of T_c on θ_D
and the electrical resistivity in the normal state: the
stronger the interaction potential V, the higher θ_D or the
resistivity of the normal state electrons.

Since the BCS theory neglects the specifics of crystal
structure, it is very difficult to obtain a handle on V.
Indeed, neglecting the crystal structure of the superconductor
under consideration leaves us with very little information
about θ_D and N(0) which must certainly depend on interatomic
distances and force constants, bond angles, and point symmetry
of the ion cores as well as e/a. Therefore, if progress
is to be made towards finding superconductors with more de-
sirable properties, the structure of the material and how
it influences various properties must be considered. Here
structure as a generalized term is used to denote the arrange-
ment of parts of the whole; i.e., it includes composition,
lattice symmetry, grain size, second phase distribution,
long-range order, and crystalline defects. Since we have
such a poor view of how properties are quantitatively

affected by structure or partial elements of structure such
as e/a, samples must be examined for differences in properties
and these differences related to changes in the structure
on scales ranging from the atomic to the macroscopic.[7] Using
this approach, it might then be possible to predict desired
properties of a structure not yet fabricated or tested and then
to fabricate this structure and, indeed, measure those properties.
If this attempt is unsuccessful in obtaining the desired
properties, the now enlarged data base might be helpful in
examining other aspects of the structure to see if they are
the controlling parameters of the property in question.

In considering the elements of structure, it is important
to realize that the same basic units under consideration,
such as grain shape and size, may be either a structure or
a property depending on the aspects of the problem immediately
at hand. For example, if the critical current density is
considered to depend on a structural element such as grain
size, one must also consider whether elements which influence
the grain size, such as composition and processing temperatures,
also contribute directly to the critical current density of
the material. If the answer is affirmative, then one must
go to a finer gradation of structure than grain size and
examine its influence on the critical current density. This
process may continue indefinitely to finer and finer levels

in an effort to identify the controlling parameter, and still
not yield a quantitative relationship between the elements of
structure and property in question. Even in this eventuality,
however, one obtains an understanding of how the property de-
pends empirically on the intermediate levels of structure and
of how one can control the property through the structure by
appropriate processing techniques.

The approach outlined above defines the underlaying plan
of materials science experiments: to define and understand the
elements of structure that control the properties of a material
and to understand how processing of the material yields a
given structure. The aim of this thesis was to investigate the
intermetallic compound Nb_3Ge (which has at present the highest
observed T_c and extremely high J_c and H_{c2} values[8]) in order to
determine what controls the superconducting properties of this
material when produced by a dc sputtering technique and to
determine in what ways the properties can be varied within
this fabrication technique. The dependence of superconducting,
electrical, and mechanical properties of thin films on struc-
tural elements were examined and the influence of substrate,
deposition temperature, thickness, sputtering gas composition,
applied strain, and annealing on film structure were investi-
gated. Proceeding in this way one hopes to gain insight as
to why Nb_3Ge has the superconducting properties it does
and how one might improve these properties in Nb_3Ge or any

other material which is best fabricated by dc sputtering.

B. Superconductivity and the Nature of A15 Compounds

The material of interest, Nb_3Ge, possesses the A15 cry-
stal structure. The A15 compounds, which include many of
the other superconducting materials of current technological
interest, have the stoichiometric formula A_3B where A is
an early transition metal or combination of these elements
and B is a late transition metal, metalloid, or a combination
of transition metals or metalloids. The A15 phase, which
is formed peritectically in many cases, usually lies entirely
on the A-rich side of stoichiometry.[9] Further, there is
often substantial disorder of atoms from their preferred
sites in the Pm3n space group.[10,11] In those cases where the
stoichiometric composition can be made to include the single
phase region by alloying with a third element so that the
e/a ratio would predict an increased T_c, the actual T_c for
this pseudo-binary is always less than that of the higher
T_c of the two stoichiometric binary components.[8]

To understand the consequences of these conditions on
superconducting properties we consider the ionic and elec-
tronic structure of the A15 phase. A unit cell is shown in
Fig. 1. The B atoms are located on the body-centered cubic
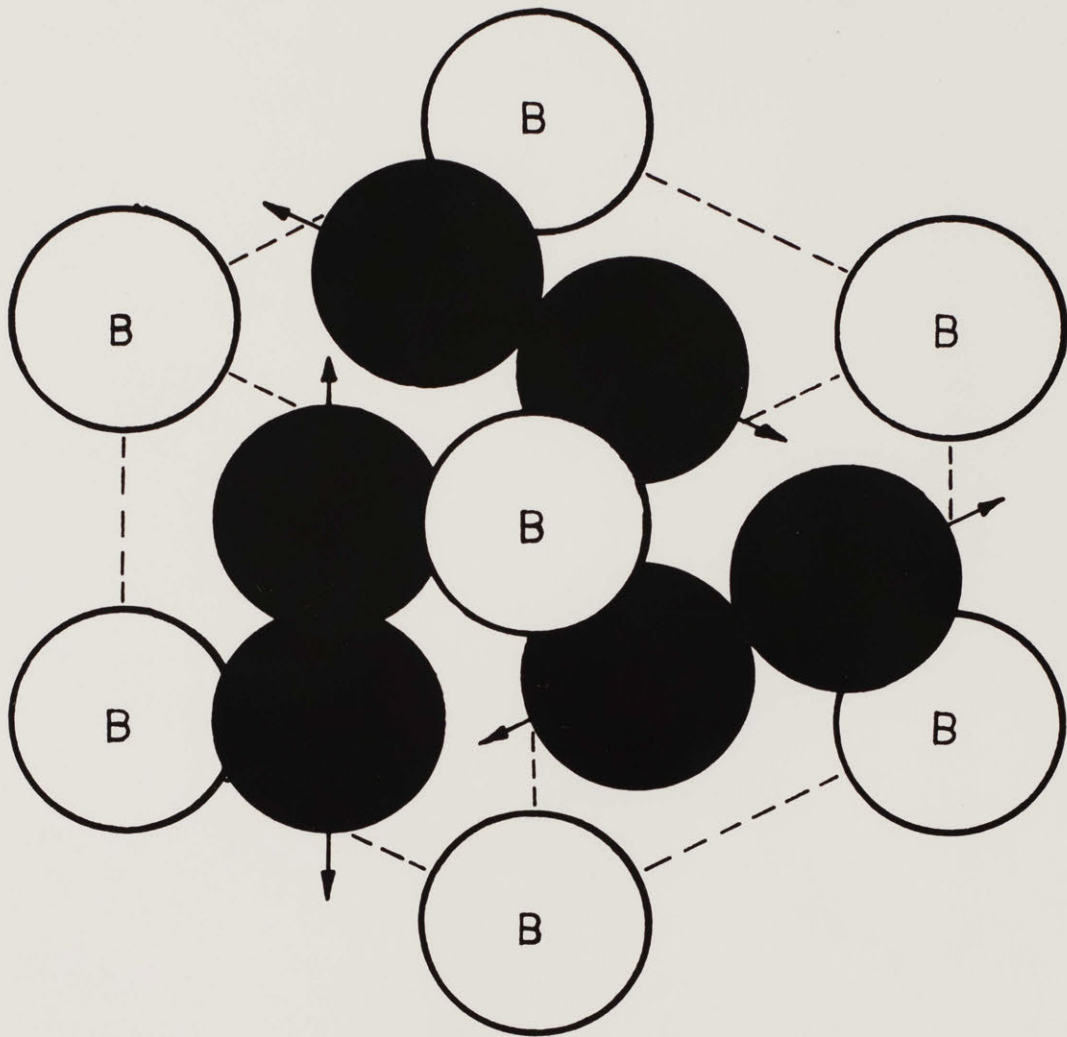
Fig. 1. A15 unit cell. The A atoms form three mutually orthogonal chains on the cell faces. The B atoms are on the body centered cubic cell positions.

sites and the A atoms are on the faces of the cube forming
three mutually orthogonal chains. The d electrons localized
at these sites are believed to interact only weakly with
electrons on the bcc sites and to have mutually cancelling
interactions with electrons on other chains; this A-atom
d-electron isolation along a cube face is believed to lead
to a high density of states that falls near the Fermi level
in these materials.[12] The results of computer calculations
of band structure of A15 materials are divided on the degree
of proximity of these peaks to the Fermi level.[13,14]

In an A15 compound with more than 75 atomic percent A,
the excess A atoms must go on the bcc sites;[8] the electrons
associated with these transition metal atoms then interfere
with those electrons localized on cube face A atoms. That
is, the wave functions of electrons on the chains of face
atoms are disturbed and the density of states at the Fermi
level decreases. According to the BCS theory this would
then lead to a decrease in T_c. The s-p elements disturb the
density of states of d-electrons at the Fermi level less
than other atoms with partially filled d-shells do, leading
to a higher T_c for compounds where the B element is a non-
transition element.[8] B atoms placed on the A sites also de-
grade T_c in those cases where the A15 phase extends to the
B rich side of stoichiometry[15] again because the density
of states at the Fermi level decreases due to the interruption

of the d-electron chains along the faces.

By the same line of reasoning simply interchanging A
and B atoms in a stoichiometric sample (anti-site defects)
could be expected to lower the density of states and T_c be-
cause the chain electron wave functions are disrupted when
A and B atoms are exchanged.[16] Similarly, T_c is lowered when
disorder is caused by thermal agitation[17,18] or neutron
bombardment.[19] In the case of disorder, however, if another
phase is not precipitated during an ordering anneal ($\approx$1000K),
the T_c of the ordered phase can always be recovered.[19] For
almost all A15 systems studied the maximum T_c for given A
and B elements is found in the ordered phase closest in atomic
ratio to exact A_3B stoichiometry.[8]

Another aspect of A15 materials that has attracted
attention is the decrease of elastic stiffness with lower
temperature, and in some cases, a low temperature structural
transformation from a cubic to a tetragonal system,[20] most
notable in V_3Si[21] and Nb_3Sn.[22] The precise relation between
the alterations of the phonon spectrum causing these struc-
tural changes and the superconducting properties is unclear
although it has been shown that after the onset of supercon-
ductivity further reduction of the elastic constants does
not occur.[23] It is also possible for the structural trans-
formation to be suppressed if the transformation temperature

is below T_c.[24] Theory cannot explain why a sample of a given material does or does not transform, or why the transformation can be suppressed by electroplating the sample with Cu,[25] or why samples with and without the the transformation have approximately the same T_c.

Determining the phonon dispersion curves as a function of temperature either by neutron scattering or by measuring the electron-coupled phonon density of states by electron tunneling might aid in establishing a connection between the softening of the elastic constants and T_c. Unfortunately, neutron scattering experiments require single crystals of a size and perfection rarely available,[26] and, tunnel junctions of sufficient quality are very difficult to fabricate.[27-29]

C. Superconductivity of Nb_3Ge

Interest in the Nb_3Ge system lies in the dependence of T_c on composition,[30,31] atomic order,[19,32] and strain, in the apparent ability of impurity atoms to extend the phase boundary,[33,34] and in the effect of a defect state on stability and on superconducting and mechanical properties.[19,35,36]

In accordance with general practice, in this thesis "Nb_3Ge" will be used to refer to a compound of variable composition that possesses the A15 structure. A sample of specific composition will be referred to in atomic percent.

The history of the compound Nb_3Ge is interesting because it illustrates what influence structure may have on the properties of a particular material. The compound Nb_3Ge was first synthesized in the A15 structure in 1954.[37] Work done in 1955 indicated the range of solid solubility at 1600 C was between 13 and 18% Ge.[38,39] It was pointed out that the lattice parameter of this compound suggested the samples were off stoichiometry;[40] subsequently, the T_c of the sample was raised from the vicinity of 5 to 7 K for bulk samples[41,42] to a transition onset as high as 17 K in samples formed by splat-cooling.[32] The lattice parameter of the splat-cooled material indicated the sample was closer to stoichiometry than were previous types of samples and its wide superconducting transition was attributed to low long-range order as determined by x-ray measurements.[32] Subsequent investigations of $Nb_3(Al, Ge)$ psuedo-binaries showed the T_c of some of these alloys to be over 21 K.[43,44] These high T_c values were believed due to the fact that the combination of the Al and Ge leads to a composition closer to a 3 to 1 ratio of A and B atoms than does Ge alone.

It was nearly ten years before Gavaler was successful in producing Nb_3Ge samples with T_c's above 22 K by dc-sputtering onto heated substrates.[45,46] This improvement was attributed to a closer approach to stoichiometry and greater long-range order in the Nb_3Ge films than can be

obtained from bulk equilibrium processing. The maximum T_c was later raised[30] to above 23 K; T_c's in this same range have also been produced by rf-sputtering,[31,47] chemical vapor deposition,[48-50] and codeposition.[34,51]   The J_c of such samples[52] at 4.2 K can be higher than 10^{10} A/m^2 at 20 T and the value[53] of H_{c2} at 0 K is believed to be close to 40 T.

The properties of the samples are not, however, always reproducible; this may be due to fluctuations in the composition or deposition temperature,[46] absence of an unspecified defect in the A15 phase,[30] or the partial pressure of an impurity gas necessary to stabilize the elements to near stoichiometric values.[33,51]   The need for the presence of low partial pressures of background gases may account for part of the variation of properties in films fabricated in systems where background gas levels are uncontrolled; however, there is still some scatter in data obtained from samples produced under ostensibly identical conditions.

This thesis describes a full characterization of Nb_3Ge samples produced by dc-sputtering in our laboratory, in part to determine the controlling variables which allow fabrication reproducibility of the highest T_c samples. Besides this determination, lattice parameter, grain size, film composition, failure strain, and T_c vs. uniaxial strain have been measured for films deposited on both ceramic and metallic

substrates. The effects on film properties of "in situ"
annealing both during and after deposition were also deter-
mined. An attempt to correlate these observed properties
with the structure of the material to determine how the
structure might be influenced by processing conditions has
been made and a model consistent with these correlations
is presented.

II. Previous Work on the Superconductivity of Nb_3Ge

There has been a great deal of research on the fabrication of high T_c Nb_3Ge. This chapter reviews the literature and compares the findings of different groups using various fabrication procedures. Since few of these studies are complete with respect to examination of materials properties and to the influence of several different processing parameters on the film structure and properties, the prime motivation in the author's work is a systematic characterization of Nb_3Ge as a function of fabrication. This approach should result in a data base of far higher consistency than one constructed from comparing the results of samples prepared by different means in different systems by different authors.

A. Fabrication of High T_c Films

As previously mentioned, there are three means of vapor deposition that have been successful in producing high T_c Nb_3Ge: sputtering, both dc[30,46] and rf,[31,47] chemical vapor deposition,[48,50] and codeposition.[34,51] Sputtering, the procedure used in this work, depends on the transfer of momentum from positive ions to a cathodic target, allowing the target material to gain enough energy to be ejected into the gas phase. The sputtering gas is usually argon although krypton[47] and argon-germane mixtures[54] have been used. Deposition rates in sputtering systems are usually on the order

of .2 nm/s. Sputtering has been used by the majority of
researchers because compared to the two alternatives, it
is inexpensive, can be brought on-line rapidly, and control
of film composition is easily realized. Furthermore, sputter-
ing can yield T_c's above 23 K while the other two methods
have not yet done so for reasons not yet clear.[55] The low
deposition rate limitations on the sputtering process, how-
ever, require relatively clean vacuum systems (10^{-4} Pa =
7.5×10^{-7} Torr) to avoid contamination of the samples.

Chemical vapor deposition, or CVD, relies on the changes
of chemical equilibrium constants with temperature to achieve
mass transport. Chlorine gas is passed over Nb and Ge form-
ing gaseous chlorides. These chlorides are mixed and then
H_2 and a He carrier gas are added.[48,50] The temperature
of the deposition chamber is higher than that of the mixing
chamber so in the former equilibrium favors the formation
of HCl and precipitation of Nb and Ge. Care must be taken
to ensure the precipitation of Nb_3Ge near stoichiometry and
the homogeneity of the deposit because, as the film is deposited,
the partial pressures of the $NbCl_4$ and $GeCl_2$ change which
alters the equilibrium gas mixture and leads to variations
in thickness and composition in the deposition zone.[48]
Consequently, CVD systems require greater expense and care
during set-up than sputtering systems. CVD systems are also
inherently dirtier due to impurities in the carrier and

reactive gases and the greater outgassing and leak rates of
the systems, which are larger and more complicated than sputter-
ing systems. Deposition rates for CVD are on the order of
10 nm/s, however, and are more amenable to commercial pro-
duction of material.

Codeposition of the constituent elements to produce a
film requires electron beam evaporation of the Nb and a good
vacuum ($\approx 10^{-4}$ Pa or less) in contrast to the sputtering gas or
CVD methods where a higher gas pressure is required during sam-
ple fabrication to volatize the Nb and Ge chlorides. Fur-
ther, the vapor in codeposition is not in thermal equilibrium
with the substrates, which may lead to energetic Nb and Ge
atoms damaging the film as they impinge on it from the gas
phase.[30] Automatic feedback control of the evaporation rate
of the constituents is required to achieve a homogeneous film
composition.[34] The typical deposition rate is similar to
that of CVD, about 10 nm/s.

All three of these methods of fabrication produce deposited
Nb-Ge films with a composition between 22% to 27% in the
A15 phase. This is the range of composition which is believed
to be necessary for high T_c films, since it allows most of
the Nb and Ge atoms to be on the A and B sites, respectively.[46,56]
Common to all three methods of fabrication is the fact that
the substrate must be heated to obtain high T_c samples,[46]
although the estimates of appropriate deposition temperatures

(T_d) vary by as much as 400 C.[51,57] It is a difficult matter
to measure the temperature of a thin film accurately and
most reported deposition temperatures are estimates based
on optical pyrometry and fine thermocouples in contact with
the film; these estimates have a precision of about $\pm$ 50 C.[30]
Despite this imprecision in measuring the deposition temper-
ature, it appears that the optimum substrate temperature
for codeposition[34,51,58] and CVD[48,50] is 50 - 150 C higher
than for sputtering.[30,46,47] This difference may depend
on the lower rate of sputtering deposition since it has been
noted in codeposition studies[58] that to maintain a given
value of T_c for decreasing values of T_d, the deposition rate
had to be reduced. At temperatures below the optimum, an
amorphous or very fine-grained deposit is obtained and at
high T_d the film properties, including T_c, tend towards those
encountered on the equilibrium phase diagram.[30,47]

The effect of total gas pressure during deposition on
the properties of sputtered, evaporated, or CVD films has
not come under close scrutiny; however, it is known an im-
purity partial pressure on the order of 10^{-5} Pa has a marked
effect on T_c of the films.[33,34,51,54] Among other gases,
O_2[33] and N_2[51] have had a beneficial effect. The role of these
impurities is not well established, but they are believed
to be responsible for extending the solubility of Ge in the
A15 phase of the thin films.[34]

Perfection of the deposited material also has an effect on T_c. Irradiation of Nb_3Ge films with neutrons[19] and α-particles[35] has, at high fluences, decreased the T_c of the sample to 3 K and increased the lattice parameter from .514 nm to .519 nm, as well as decreased the degree of long-range order. Subsequent annealing of the irradiated films for short periods of time has restored the high T_c and long-range order of the material and lowered a_o to its original value.[19] (In unirradiated films the lattice parameter increases from about .514 nm for 24% Ge to .517 nm for 18% Ge in the A15 phase.[34]) Short term anneals of undamaged films have led to increases in T_c, presumably due to increasing long-range order and grain growth.[59] On the other hand, annealing un-damaged films for long periods of time has either left T_c unchanged or else degraded T_c and increased the amount of second phase present.[46]

The T_c's of thin films have been lower than those of thick films prepared under the same conditions.[33,58] The reason for this behavior is uncertain, although it may be related to the smaller grain size of thin films[53,60] since films deposited at low temperatures have smaller grains and a low T_c.[47]

High T_c's have been observed in samples deposited on A15 Nb_3Ir and Nb_3Rh film substrates that have lattice parameters

close to those of Nb_3Ge.[56,61] The high T_c's are presumably
due to constraining the Nb_3Ge to form with a lattice para-
meter close to that of $Nb_{75}Ge_{25}$, inhibiting the formation
of the equilibrium phase. Therefore, using an A15 substrate
may eliminate the need for an impurity background pressure
to obtain high T_c's.[61] Other materials have also been success-
fully used for high T_c films, presumably due to a small thermal
contraction mismatch of these materials and Nb_3Ge.[30] These
materials include sapphire,[34,46] beryllia,[30] Hastelloy B,[48]
and copper.[50] This mismatch, in the case of Hastelloy sub-
strates, also appears to degrade the superconducting current
density due, perhaps, to the residual strain.[62] Indeed, the
J_c of such films on Hastelloy has been increased slightly
by straining the film to counter the strain applied by the
difference in thermal contraction between the deposition
temperature and 4.2 K.[62]

In summary, to obtain a film with a high T_c the composi-
tion should be near stoichiometry,[46,48] T_d should be in the
vicinity of 700 - 800 C.[46] Partial pressures of impurities
such as O_2 or N_2 should be present at least at levels around
10^{-4} Pa.[33,54] A substrate for the films should be chosen
so as to minimize strain due to thermal contraction mismatch.[30,62]
The film should not be too thin or the grain size too small,[33,58]
nor should it be subjected to a long term anneal,[46] although

short term anneals may increase T_c.[59]

B. Structure and Property Relations

One of the strongest influences on the T_c of Nb_3Ge is
the composition of the film.[34] As related in Chapter I, T_c
is seen to increase from 6 to 23 K as the A15 composition
of the film approaches 25% Ge. That this increase in T_c is
due to approaching stoichiometry, however, has not always
been accepted.[30] Part of the controversy over the impor-
tance of composition in determining T_c may stem from an error
in arithmetic. An early source stated the maximum Ge com-
position of A15 Nb-Ge[39] was $NbGe_{.22}$ and had a T_c[32] around
7 K. However, a later study seems to have misinterpreted
this composition as $Nb_{78}Ge_{22}$[32] (vs. 18% in $NbGe_{.22}$) causing
a serious disagreement between the T_c of sputtered films
containing 22% Ge and the bulk material of supposedly the
same composition.[30] This possible misunderstanding was
then compounded by an error in converting the Ge concentra-
tions expressed in atomic percent to the form Nb_xGe.[30]

The lattice parameter of the A15 phase follows a nearly
linear relation with composition and then remains constant
above a certain Ge composition.[31,34,61,63] This behavior
is typical of a change from a single phase to a two phase
region: when the lattice parameter ceases to change further
the composition is that which occurs at the single phase

field boundary.[64] This data implies that T_c's over 21 K
occur for samples with Ge concentrations between 23 and 26%
in the A15 lattice.[31,61]

One means of incorporating more than the equilibrium
amount of Ge in the A15 lattice (i. e., $\approx$ 18% near 800 C)
is to quench the sample from the liquid and obtain a meta-
stable Nb_3Ge that has passed through the temperature range
of significant diffusivity too rapidly to approach equili-
brium.[32,63] Indeed, it has been proposed that the equili-
brium Nb-Ge diagram can include A15 material that contains
22% Ge and has a T_c around 17 K; Flukiger and Jorda believe
that an insufficiently rapid quench is responsible for pre-
vious studies estimating the maximum solubility[63] of Ge in
Nb_3Ge at about 18%.

Although there have been unconfirmed reports of T_c's
near 22 K in bulk samples that were rapidly quenched,[65] im-
plying 23 - 24% Ge in the A15 phase,[56] in general, to ob-
tain the highest T_c material (greater than 17 K) methods
besides quenching must be used. In particular, the method
must be such that the mobility of the Nb and Ge atoms in a
metastable configuration corresponding to a high supersaturation
of Ge in the A15 Nb-Ge is reduced. Thus sputtering, codeposi-
tion, and CVD processes, in which the temperature of the
niobium and germanium is between 700 K and 1200 K,

allow the mobility to be sufficient to form supersaturated Nb_3Ge but do not allow fabrication of the low T_c equili-brium phase. In fact, atomic mobility <u>after</u> deposition appears to be the key factor in obtaining specified ratios of Nb to Ge atoms in an A15 phase.[46] Deposition temperatures that are above the optimum lead to degraded T_c's,[51] presumably due to the precipitation of Nb_5Ge_3 and the growth of equili-brium Nb_3Ge from the metastable material that is deposited. Deposition temperatures that are too low lead to the forma-tion of amorphous material or small grains[30,47,49] with re-duced T_c's. The smaller grain size agrees well with Thornton's model of film properties,[66] wherein a film deposited at a low temperature will have very fine grains and undergo a dramatic increase in grain size at T_d's near .5 T_m, where T_m is the melting point. Therefore, it appears that the maximum T_c is obtained when the deposition temperature is high enough so that the perfection of the material is not marred by a high incidence of grain boundaries or disorder as it would be for fine-grained or amorphous material, but, also, when the deposition temperature is not so high that the equili-brium Nb_3Ge phase grows. Even when the films are deposited at an optimum T_d (i. e., a T_d which results in very high T_c material) some very fine grained Nb-Ge may be present.[49]

The properties of the film also appear to depend on

vacuum system geometry and pressure. It has been determined
that convection currents are present in certain sputtering
systems, affecting film thickness, homogeneity, and T_c.[67]
The effect of convection on film homogeneity may be especially
pronounced in a sputtering system with an inhomogeneous tar-
get.[67] It also appears that in general, an impurity gas
in the system is required to obtain high T_c material,[33,34,51]
Most analytic work has been done on O_2 additions,[33,62] but
ambient air,[51] N_2,[51,54] SiH_4,[54] and Cl_2[68] have also been
used to make high-T_c Nb_3Ge. Oxygen must be admitted at
partial pressures between 10^{-5} to 10^{-2} Pa to obtain a bene-
ficial effect on T_c[33,51] and must be present in the bulk of
the film but only[33] at a level of .1% to 2%, although some
impurities, such as hydrogen,[69] are known to decrease and not
increase T_c. The role of the impurity in increasing T_c and in
increasing the extent of the solid solution region of Nb_3Ge
is still not clear. Oxygen, for example, is known to stabilize
other phases in A15 compounds[70,71,72] and appears to stabilize
the hexagonal Nb_3Ge_2 phase relative to tetragonal Nb_5Ge_3.[63]
The oxygen may raise the free energy of the tetragonal phase
relative to that of the A15 also, although attempts to ex-
tend the phase range of Nb_3Ge by addition of oxygen to the
bulk have been unsuccessful.[63]

Oxygen is clearly one of the most important impurities

that can be present in the Nb_3Ge film. Very thin films
have an oxygen content perhaps as high as 20% and an a_o at
least .004 nm larger than it should be for that Nb/Ge ratio.[33]
These films also have very fine grains, raising the possibility
of expansion of the lattice parameter by enhanced thermal
vibration in small grains. However, a_o for thinner films made
of material with a lower melting point increased by only
0.001 nm[73] suggesting enhanced thermal vibrations are not
adequate to account for the .004 nm increase in the Nb_3Ge
lattice parameter.

A layer of fine-grained material with a high O content
is also found if sputtering is interrupted and is resumed
several minutes later.[60] This result suggests the oxygen
adsorbed at the surface is responsible for the formation of
A15 grain nuclei.[33] As the films thicken, either from deposi-
tion on a clean substrate or on a previously sputtered Nb_3Ge
film, the oxygen content and a_o decrease while T_c and the
grain size increases.[33,60] It is believed that maintaining
coherency as the film grows stabilizes the A15 phase and
prevents precipitation of the tetragonal phase.[33]

The presence of oxygen can also determine the effective-
ness of a particular substrate. Films grown on clean metallic
substrates have lower T_c's than films grown on oxides of those
metals,[33] suggesting, along with the relationship of oxygen
concentration and grain size in thin films, that oxygen

promotes the nucleation of high T_c A15 grains. On the other hand, the choice of substrate can also apparently eliminate the need for O_2 or other impurity gases. It has been reported that the amount of Ge dissolved in the A15 lattice has reached 26% in the absence of O_2 when samples are deposited on Nb_3Ir and Nb_3Rh substrates.[61] In this case, Nb_3Ge is believed to grow epitaxially on A15 substrates, which stabilize it against precipitation of the tetragonal phase and depletion of Ge from the A15 grains.[61] The Nb_3Ge deposited on A15 films formed with an a_o close to that expected from the Ge composition when its lattice parameter was well matched to that of the substrate. In the case of a .5% mismatch to the substrate lattice, two sets of lattice parameters were observed for the Nb_3Ge, one set constant around .514 nm and the other set close to the a_o of the underlying Nb_3Ir of varying composition.[61] The low a_o A15 material has a high T_c, but the reason for its formation is unclear. Other observations of discrete multiple a_o's in individual samples have been made;[55,74] these discrete A15 phases are presumably due to inhomogeneities in deposition that lead to a high T_c metastable phase and a phase closer to equilibrium phase.[55]

It has been reported that, in addition to other requirements, the long-range order of the Nb_3Ge samples, as in other A15 materials, is important in obtaining a high T_c.[19] Neutron

and x-ray diffraction and ion channeling studies of irradiated V_3Si[75-77] and Nb_3Sn[78] indicate the atoms are randomly dis-placed from their equilibrium positions. For Nb_3Sn the mag-nitude of this displacement decreases as the order parameter rises,[78] implying the displacement might be due to changes in the valence or size of nearest neighbors, a phenomenon known as the Huang-Borie or size effect.[79]

Disordering the films also increases the resistivity[36,80] and the lattice parameter.[19,35] (Both of these effects are reversed when the samples are annealed.[19,80]) When the films are irradiated, the residual resistance ratio, $R_{300 K}/R_{25 K}$, or Γ, decreases.[36] This has been interpreted as an increase in defect population which reduces the T_c. The existence of this "defect" was introduced to explain what was perceived to be a large difference between the T_c of the film and bulk of ostensibly the same composition.[30] Models for this hypo-thetical defect have included the atomic displacements ob-served upon irradiation[77] or ordered arrays of point defect clusters.[81] However, aside from a peculiar transformation in the A15 lattice around 220 C, which might be explained by antisite defects or vacancies,[28] and striations in some grains of Nb_5Ge_3[82] no defect structure other than precipitates and stacking faults have been observed in TEM studies.[28,82-84]

In addition to T_c and resistivity being influenced by

the processing conditions, so are grain size and shape. As
the films thicken the grains increase in mean diameter and
become columnar,[60] although equiaxed grains have been reported.[34]
Strong preferred orientation of the A15 and tetragonal Nb_5Ge_3
phases has been observed[85] and in certain directions the
growth of nonsuperconducting hexagonal Nb_3Ge_2 seems to be
favored.[86] The low deposition temperature and compositional
fluctuations may favor the formation of both the hexagonal
and tetragonal phases. This may be due to the structural
resemblence of the A15 and second phase unit cells.[49,86]
In addition, it has been observed that high O_2 partial pressures
lead to an increase in the amount of hexagonal second phase
present in the films.[86]

In summary, Nb_3Ge films have exhibited high T_c's
when the composition of the film is near stoichiometry during
deposition; this is apparently made possible by the presence
of a background gas during deposition[33,51,54] or by using
an appropriate A15 substrate.[61] Long-range order is impor-
tant in obtaining high T_c films,[19] and there is an optimum
deposition temperature for maximizing T_c.[51] At low deposi-
tion temperature the grain size is small and other phases
may be present[74] which degrade T_c. At high deposition tem-
peratures the films tend toward their equilibrium properties.[47]
At intermediate deposition temperatures T_c is at a maximum

and preferred orientation of the phases is observed.[86]

There are still many unanswered questions about the A15 Nb_3Ge phase. The precise role of O_2 or other impurities in film fabrication is unknown: it is not certain if oxygen actually is present in the A15 phase and if so, where it is located in the unit cell; it is not certain if the impurity acts to increase the solubility of Ge in the A15 lattice or if it raises T_c in some other fashion; nor is it known if the impurity introduced during deposition is required once a high T_c film is initiated. In addition it is not even clear if impurities must be present given appropriate substrates. The situation is even more murky in the case of thin films where the influence of thickness, grain size, impurity concentration, and annealing time on T_c have not been separated.

The general influence of annealing on the structure and properties of the films is also not understood. It is not known how the elimination of defects in the film and growth of equilibrium tetragonal material are intertwined or what the effect of these competing processes are on T_c. Indeed, even the nature of defects in Nb_3Ge and other A15's is unknown.

III. Description of Apparatus and Materials

In the first section the apparatus built in the course of
this thesis project and used both to fabricate the Nb-Ge
films and to test their superconducting properties will be
described. These include the sputtering system, the resis-
tive T_c measuring device, and the four-point bending device.
The experimental procedures adopted for the use of these
instruments is also described. In a second section the
specifics of materials used as targets, substrates, and stan-
dards in the course of the research are discussed. The actual
procedures in film fabrication and characterization of other
film properties are then detailed in Chapter IV.

A. Apparatus

The sputtering system design is based on the getter-
sputterer of Theurer and Hauser;[87,88] similar systems have
been widely used to obtain superconducting films.[30,57,87-91]
The author's system consists of a liquid nitrogen cooled
stainless steel can which contains a high tension cathode
alloy target and a heated substrate table (see Fig. 2). The
assembled system is shown in Fig. 3; the target and dark
space shield are shown in Fig. 4. The can is approximately
100 mm high and 70 mm in diameter. A view of its inside
is shown in Fig. 5, with three deposited films in place on
the heater table. The power supply for the sputtering can
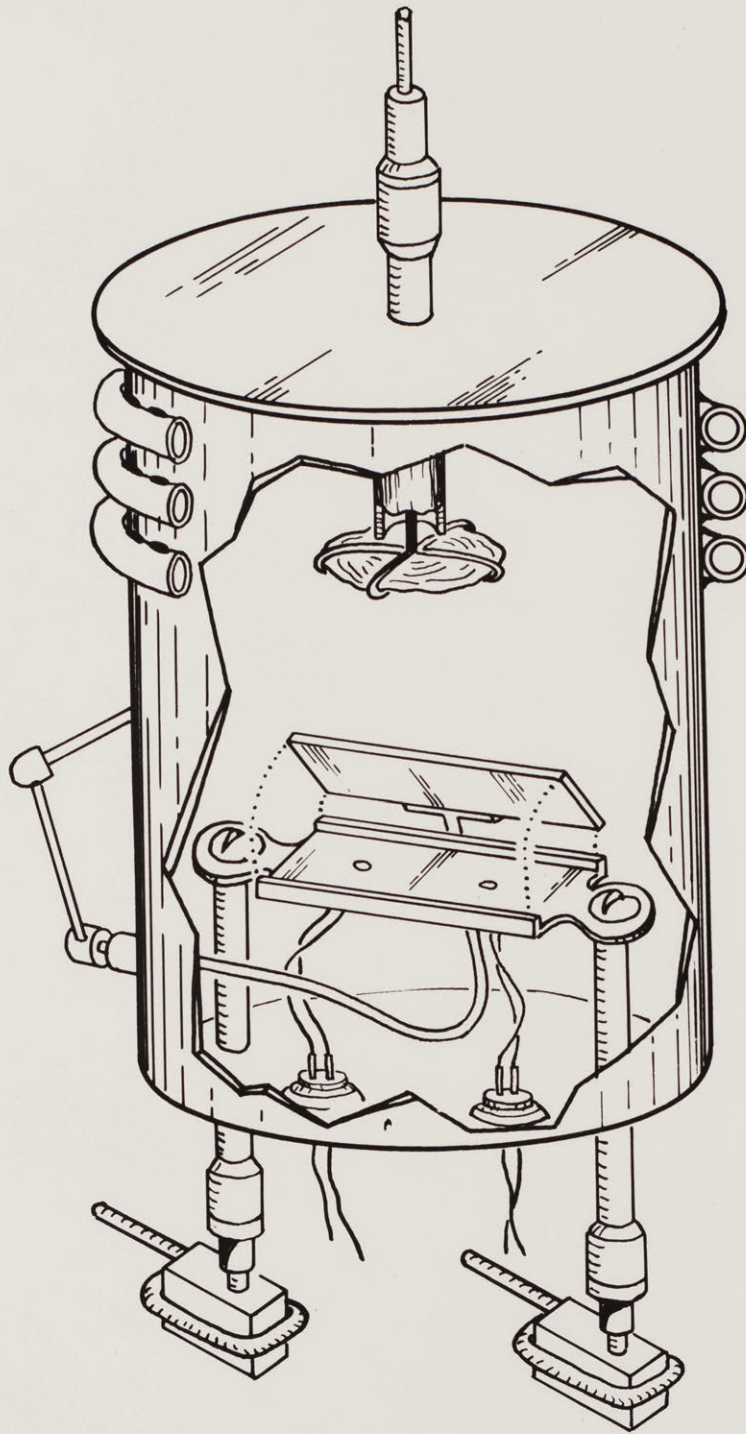
Fig. 2.   Cutaway Schematic of Sputtering System.
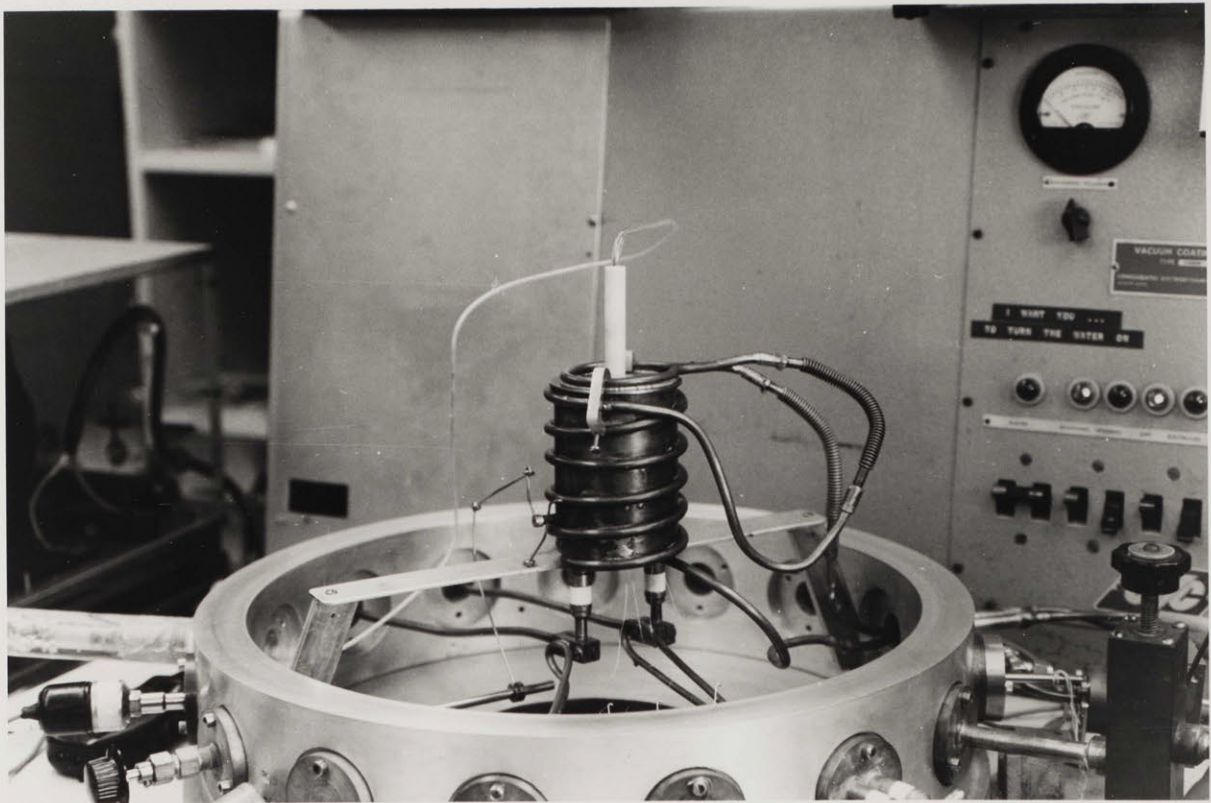
Fig. 3.   Assembled Sputtering System.
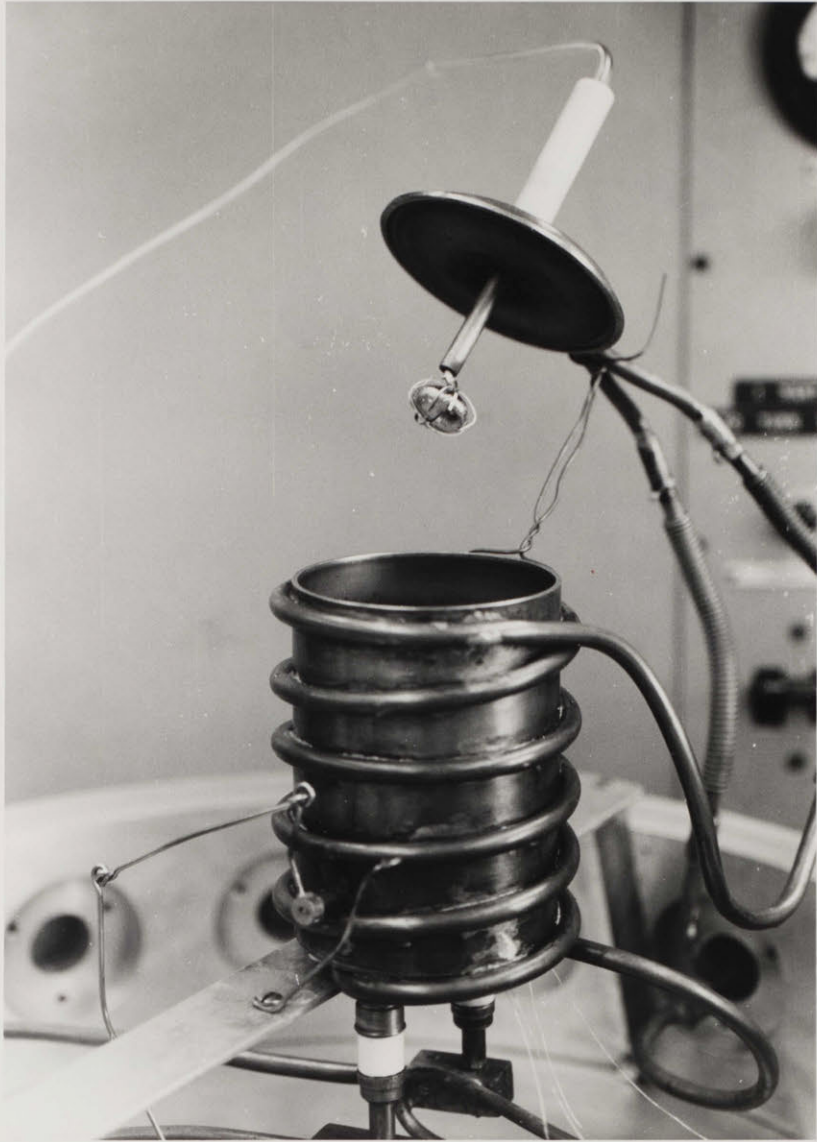
Fig. 4.   Open Sputtering System.   Note target
          and dark space shield.
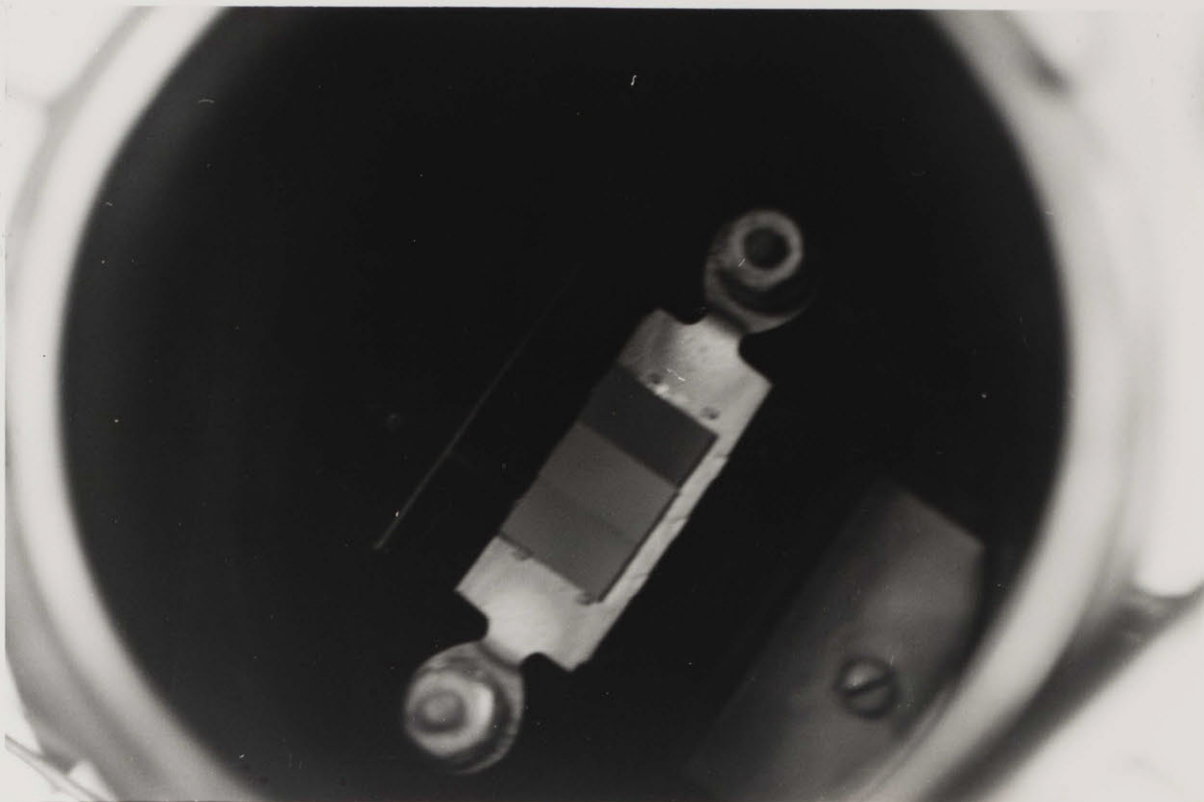
Fig. 5.   Inside of sputtering system with three
           films in place on heater table. Note
           edge of shutter to the left of the heat-
           er table.

(Fig. 6) is a full-wave-rectified power source from Alexander
Kusko, Inc. of Needham, MA. Filtering maintains the ripple
in the output voltage below approximately .2%.

The operating procedure for sputtering was as follows:
after 36 to 48 hours of pumping the VHS-6 diffusion pump
(supplied by NRC of Lexington, MA) reduced the system to
a pressure of 2 to $3x10^{-5}$ Pa (2 to $3x10^{-7}$ Torr). Water cool-
ing to the table feedthroughs was then turned on, as were
the heater table itself and the liquid nitrogen flow. After
30 minutes, with the pressure at $1x10^{-5}$ Pa, the high vacuum
valve was throttled down to 2/3 of a turn from fully closed to
yield a steady background pressure of 4 to $5x10^{-5}$Pa. This throt-
tling allowed a throughput of .3 to .4 Pa·m^3/s (2 to 3 Torr·l/s)
at 40 Pa of Ar, which is within the capacity of the diffusion
pump used. (RGA analyses of these vacuums and the lot analysis
of the ultra high purity Ar gas are given in Appendix A.)
Any desired impurity was added before the introduction of
the Ar gas through a needle valve regulating a storage tank
containing the impurity gas. To insure an even gas flow
during the entire sputtering process the impurity gas must
be held at a moderately high pressure ($\approx$ 3000 Pa in this study).
The partial pressure of the background gas is then determined
by dividing its volumetric flow rate by that of the Ar which
is introduced after the impurity gas. A ten minute equili-
bration period at the sputtering pressure (usually 40 Pa) was
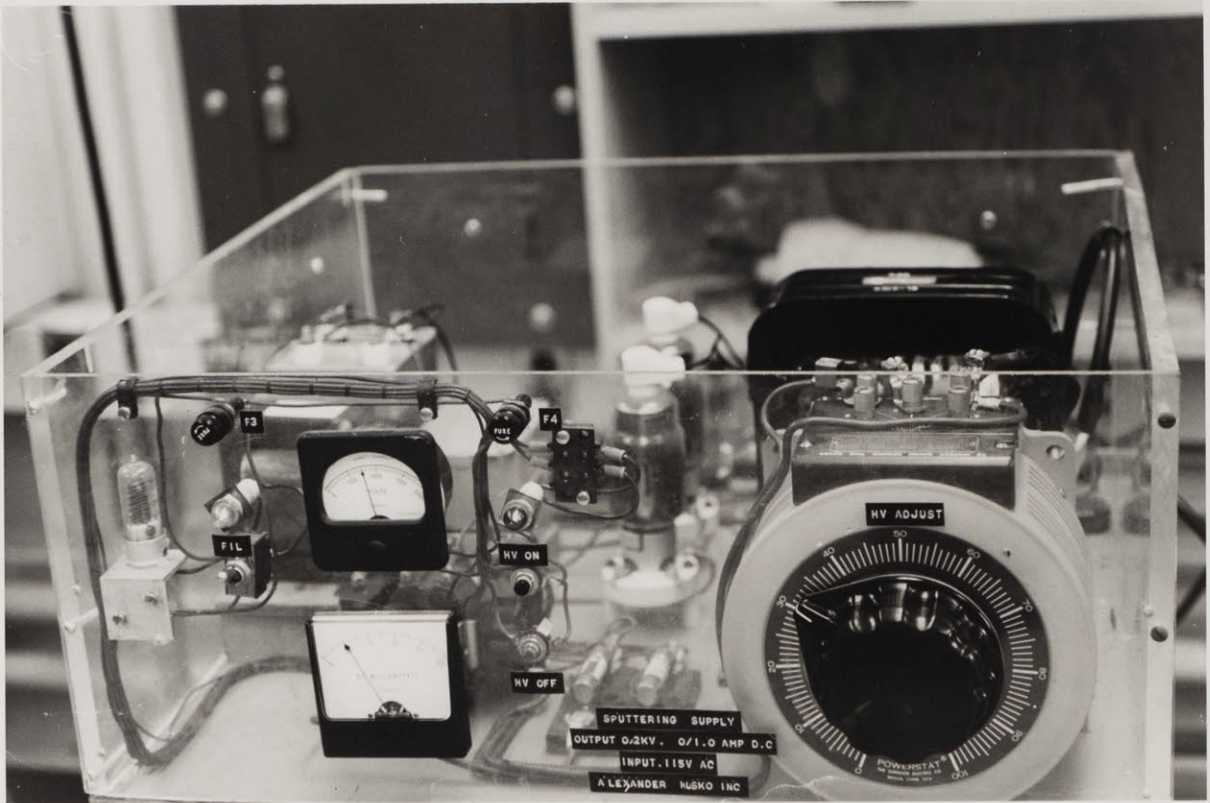
Fig. 6.   Sputtering power supply.

employed before sputtering was initiated.

The cathode voltage drop was increased slowly to 750 Vdc
to prevent arcing and shorting the cathode. Depending on the
sputtering pressure and target composition, this voltage cor-
responds to 15 to 30 mA current through the target. Sputter-
ing could be continued in this mode for an indefinite period
of time as long as adjustments to the system were made every
10 to 15 minutes to maintain a constant deposition temperature,
sputtering pressure, and liquid nitrogen flow.

Presputtering was not usually part of the fabrication
procedure because it made little observable difference in film
properties and because it was impossible to prevent at least
some Nb_3Ge from depositing on the substrate during presputter-
ing even though the shutter was closed during this period.
This was due to the fact that the substrate to shutter dis-
tance (1 to 3 mm) is much greater than the collision mean free
path (.25 mm) at these temperatures and pressures allowing some
material to diffuse between the shutter and substrate. This
material would then deposit around the edge of the substrate
causing the films made during presputtered runs to be thicker
at their edges.

To anneal the samples in situ after deposition the sputter-
ing voltage was turned down to zero, the Ar flow stopped and the
high vacuum valve fully opened. Liquid nitrogen and water
flows were maintained as long as power was supplied to the
heater table.

Once the power to the heater table was terminated the liq-uid nitrogen flow was stopped and the samples were then allowed to cool and the sputtering can to warm for 30 minutes. After this period, the system was backfilled to approximately ½ atm N_2. Following an additional 30 minutes waiting period the va-cuum could be broken without the condensation of water on the stainless steel can or liquid nitrogen lines.

The temperature of the films resting on the heater table was determined optically using a Leeds and Northrup 8622C op-tical pyrometer. The absolute readings of the optical pyro-meter, calibrated by observing samples placed in a resistive tube furnace in a flow of Ar gas, were observed to be 30 to 50 C higher than the temperature of the tube furnace and the sam-ples, as measured by the furnace thermocouple. Thus the tem-perature values of the substrates were recorded to be 40 C lower than the pyrometer reading. The two end films on the table were also observed to be at a somewhat lower temperature than the middle film ($\approx$ 10 C) by direct observation using the optical pyrometer. It was observed by monitoring temperatures of the substrates and the heater table for a given heater table current that the heater was about 180 C hotter than the sub-strates. This temperature differential is thought to be real.

Direct observation showed the heater table stopped radi-ating in the visible frequency range 15 seconds after power was cut off to the table of initial temperature of 1000 C.

The table reached 100 C in approximately 90 seconds, as determined by thermocouples spot-welded to the table. The samples resting on the table lost their glow in the visible frequency range approximately 40 seconds after power to the table was turned off suggesting the films remain hotter than the table temperature for a significant period of time, contrary to what was previously assumed.[91]

The resistive T_c device is shown in Fig. 7. The copper can on the left in the figure is heated by a non-inductively wound heater. The teflon holder is inserted in the copper can after four gold wires attached to the sample with silver paint are soldered to the binding posts with indium solder. The binding posts, in turn, are connected to twisted pairs of #36 copper wire leading to the top of the header. The sample holder also contains a Ge thermistor from Scientific Instruments, Inc. of Lake Worth, FL. which was calibrated against a precision calibrated thermistor (from Cryocal, Inc., Riviera Beach, FL) in the gaseous He environment in which all T_c's were determined. To check the calibration of the thermistor a sample had its T_c measured in pumped liquid hydrogen; the temperature at which the sample had 99%, 80%, 60%, 50%, 40%, 20%, and 1% of its normal state resistance were measured. The temperature of these points were redetermined for this sample in
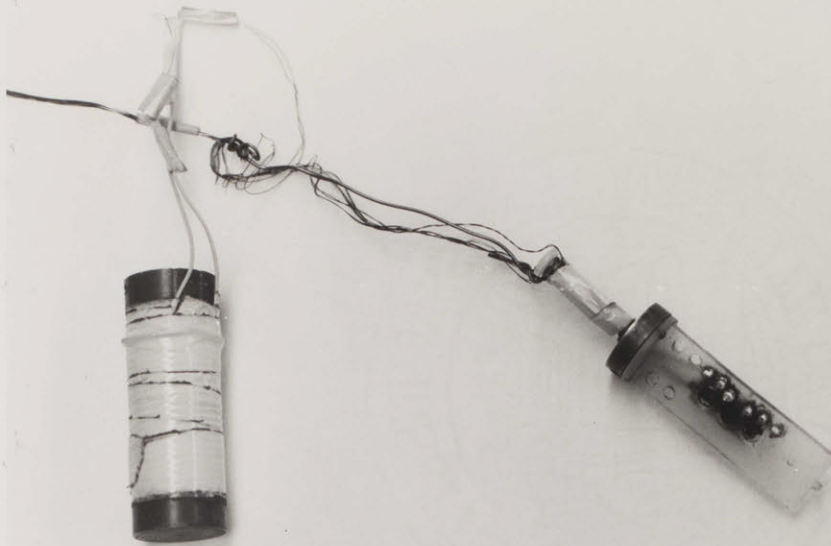
Fig. 7.   Resistive T_c apparatus. Note heater wound about copper can.

a liquid He dewar. At 15 K on the liquid H_2 vapor pressure
scale, the thermistor in the liquid He bath indicated a tem-
perature .2 K higher for the above set of resistive points.
At 20 K on the liquid H_2 vapor pressure scale, the thermistor
indicated a temperature .4 K higher. Correcting the Cryocal
thermistor derived temperatures to those obtained from the
liquid hydrogen bath results in a calibration accurate to ±.5 K
at temperatures up to 25 K for the thermistor-sample configura-
tion used in this work. Repeated measurement of samples cycled
between room temperature and 4.2 K indicated the precision of
the thermistor is within ±.2 K.

The effect of applied strain on the transition temperature
of the films was investigated using a four-point bending appa-
ratus in which the loading of the film samples was varied by
controls extended to the cryostat. The temperature correspond-
ing to 50% normal state resistance of the sample was monitored
as a function of the resistance of a thin film strain gauge
bonded to the sample substrate. The temperature was varied by
changing the current going to a non-inductively wound heater
sheath that slipped over the body of the bending device and
used He exchange gas to remain in thermal contact with the
sample.

The thermistor in the four-point bending device was
calibrated against a calibrated thermistor placed in the

sample position from 4.2 K up to the liquid hydrogen boiling point (20.6 K). The resistive T_c and the bending device thermistor agree to within .4 K for the same sample, which is within the accuracy of both thermistors. In the bending device, however, the important aspect of temperature determination was the precision of T_c of a sample during a single run. The precision of this measurement, determined by repeated measurement of T_c of a sample by cycling through its transition temperature, is believed to be the same as the thermistor resolution, .05 K.

One full clockwise turn of the wheel at the top of the four-point bending device header (shown in Fig. 8) advances the tip of the differential screw drive shown in Fig. 9a by 34 μm. This displacement is transferred to the teflon block containing the thermistor (shown as A in Fig. 9b) and advances two (points B) of the four knife edges down, into contact with the sample (C). The section between these two inner knife edges is 5 mm long and is the region over which the transverse strain is constant in a four-point bending device. A four-point voltage probe is attached to the sample in this region at points D and the strain gauge (E) is glued to the opposite side of the sample within this same section. The sample is supported by the other two knife edges (points F) of a teflon block that also holds the voltage probe binding
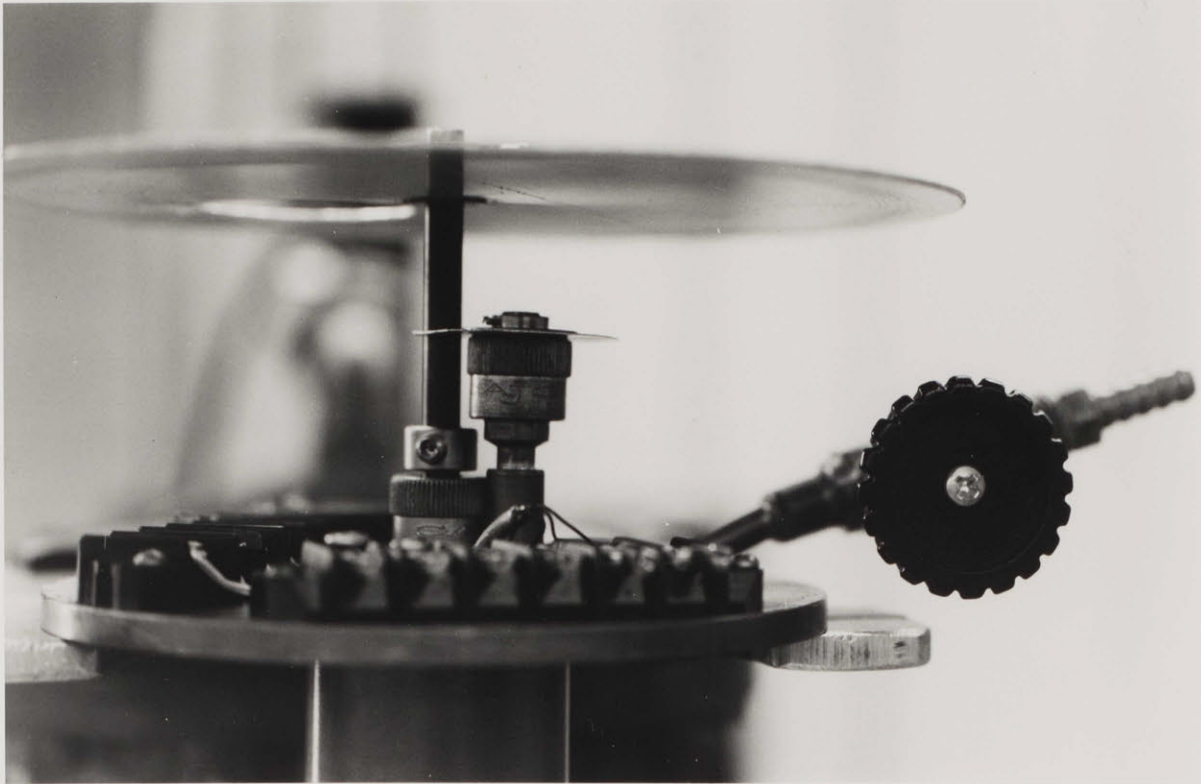
Fig. 8.   Top of four-point bending device header.
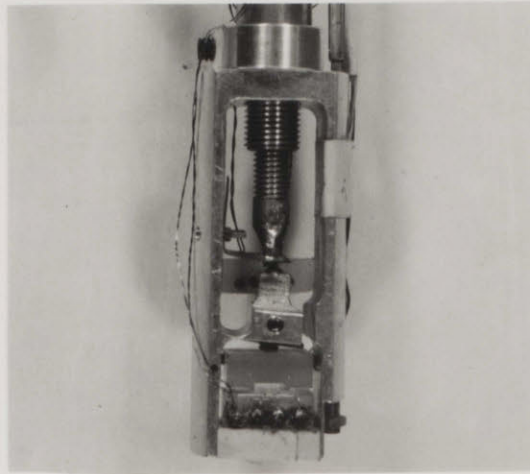
(a)
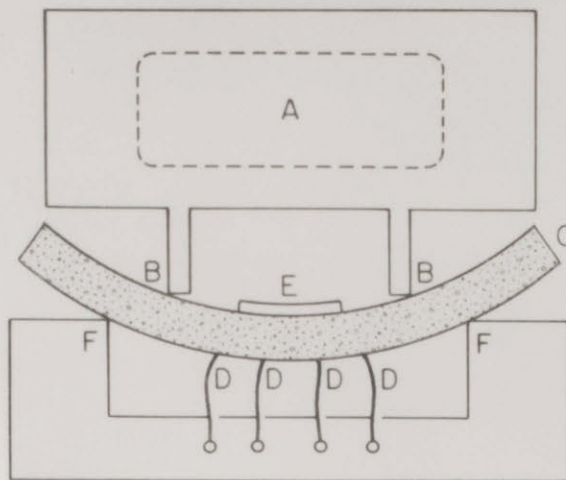
(b)

Fig. 9.   (a) Body of four-point bending device.
Note the differential screw mechanism
and the sample held between the two tef-
lon blocks. (b) Schematic of four-
point bending device. A. Teflon block
containing thermistor. B. Two of four
knife edge contact points. C. Sample.
D. Four-point resistance probe.
E. Strain gauge bonded to sample.
F. Two of four knife edge contact points.

posts. The drive mechanism is reversible so that the applied strain could be removed without changing the sample-device configuration. Thus, after testing the sample in tension or compression the device could be warmed to room temperature and the sample inverted so it could be strained in the opposite sense. Since the thickness of the substrates is about .6 mm, the A15 film about .001 mm, and that of the strain gauge and epoxy is about .05 mm, the film, gauge, and epoxy contribution to the moment of inertia of the samples was neglected; consequently the neutral axis in bending is assumed to be along the axis of symmetry of the substrate and the film and strain gauge are strained in opposite senses.

The gauge factor, a coefficient which relates the change in resistance to the change in length of the gauge was determined by plastically deforming a sample to .5% at room temperature and then measuring its apparent strain at cryogenic temperatures. After correcting this low temperature reading for the estimated difference in thermal contraction of the gauge and substrate, the resulting difference in the strain readings was attributed to the gauge factor having increased by about 10% between room temperature and 4.2 K.

B. Materials

The Nb powder used in the arc melted targets, in the

splat-cooled Nb-Ge flakes, and for the Nb-Ge calibration standard was obtained from Wah Chang, Inc., of Albany, Oregon; it is 325 mesh and 99.5% pure. The Ge and Si used for the targets were single crystals obtained from Professor A. Witt, MIT Materials Science and Engineering Department, and were at least 99.995% pure. These single crystals were ground to 325 mesh, mixed with the Nb powder, and compacted before being inserted into the arc melter. Arc melted samples were fabricated by melting several times and turning between each melt. The Nb_3Ge sample used as a standard for the microprobe was annealed at 1850 C in vacuum for ten hours. The Nb-Ge arc melted buttons were analyzed by W. W. Correia, MIT Center for Materials Science and Engineering, and found to contain $\leq$ 1 weight percent oxygen.

A variety of substrates were used in this study: sintered alumina, sapphire, Superstrate, Hastelloy B, pure Nb sheet, and splat-cooled Nb-Ge films. Sintered alumina and sapphire substrates were obtained from Adolf Meller, Inc. (Providence, RI) and were then cut to 12 mm x 6 mm size. They are of 99.99% purity and polished with diamond dust; under the microscope gouges in the surface of the alumina could be seen while the sapphire is without flaws to at least 400 x. The orientations of the sapphire substrates were close to $[10\bar{1}0]$, $[11\bar{2}0]$, or $[0001]$. The Superstrate (Lucalox) substrates were

obtained from Professor R. L. Coble, MIT Materials Science and Engineering Department, and consisted of sintered grains about 50 μm in size. These substrates were usually .6 mm thick, although three sapphire substrates were only .1 mm thick.

The Hastelloy B Sheet was obtained from the Stellite Division of the Cabot Corp. (Kokomo, Indiana). The composition of the Hastelloy was 66% Ni, 24% Mo, and 10% other metals, mainly Fe and Cr. The .5 mm thick sheet was cut to 12 mm x 6 mm size for use as substrates. They were then annealed for 16 hours at 900 C in vacuum to dissolve precipitates in the matrix. Scanning micrographs of these substrate surfaces showed large grains, precipitates at grain boundaries, and numerous twins. Niobium sheet .25 mm thick and 99.5% pure was obtained from Wah Chang, Inc., it also was cut to 12 mm x 6 mm size for use in this work.

Nb-Ge flake substrates were made by splat-cooling. The Nb-Ge is melted by rf induction coils; as the drop falls it trips an electric eye, releasing the massive spring-loaded copper plates that converge on and solidify the molten drop.[92] The resulting flake substrates were approximately .05 mm thick and 5 to 15 mm across. They contained approximately 24% Ge (microprobe analysis) and had superconducting onsets between 12 and 16 K; the superconducting transition, however, was not complete by 4.2 K.

All substrates were degreased in reagent acetone or

trichloroetheylene and dried in a freon gas stream before

being inserted into the sputtering can for Nb_3Ge deposition.

IV. Outline and Plan of Work

The objective of this research is to relate structure to
the observed physical properties of dc-sputtered Nb_3Ge films
and to determine the means of control of structure by fabrica-
tion parameters. In this chapter the overall plan of the re-
search and details of experimental procedures are given. The
initial step was the fabrication of Nb-Ge films under the vari-
ous sputtering conditions which produce essentially A15 struc-
ture films. These films were then characterized with respect
to structure, phase distribution, transition temperature (T_c),
resistivity (ρ), lattice parameter (a_o), breaking strain,
and T_c vs. applied strain. Comparative studies of the film
properties for films deposited either on ceramic or metallic
substrates were also undertaken. An important part of the re-
search concerns the changes in film properties which accompany
both annealing during deposition and post-deposition _in situ_
annealing.

A. Fabricating Nb_3Ge Films

The target composition, deposition time and temperature,
and sputtering gas composition, could all be varied over
relatively large ranges of values and still produce A15 struc-
ture films. Changing the composition of the sputtering tar-
get changes the composition of the resulting Nb_3Ge film.
Generally, target composition changes were accomplished by
adding or removing extra turns of Nb wire wrapped around an

arc-melted bare target. This target configuration was found
to be quite stable; in only one run did the Nb wire about
the target shift position during sputtering. (Consequently,
the data from this run was discarded.) The composition of
such composite targets was estimated to within one atomic
percent by observing the change in sputtering current of
the bare target (of known composition) before and after Nb
wire was added, and attributing this change in current to
the sputtering of pure Nb. This estimate of effective tar-
get composition agrees with the new estimated composition
calculated from the total target area and the change in Nb
fraction due to the addition of the Nb wire. The final tar-
get compositions used are estimated to have been 19, 21, 23,
and 28% Ge. Since the 28% Ge target composition produced
the films with the highest T_c's, a large majority of the films
made in this study were fabricated from this target composi-
tion.

Although the range of substrate temperatures resulting in
good, superconducting A15 films is from 700 to 920 C, most of
the films reported on in this work were fabricated between 750
and 850 C. Almost all of the films were annealed at the deposi-
tion temperature in the 10^{-5} Pa range following completion of
sputter deposition. A degree of annealing also occurred during
deposition, however, because variation of the duration of

sputtering time was used to effect variation in thickness
of the film without changing sputtering pressure or voltage.
Thicknesses from .1 μm to 6 μm were obtained for intervals
between several minutes and several hours, respectively.
Varying thickness in this manner automatically varies the
interval of time films are held at the fabrication temperature,
T_d. To examine the consequence of this, thinner films were
held at T_d for an amount of time comparable in duration to
that of the deposition interval for more common, thicker
films.

Most samples were sputtered at 40 Pa Argon pressure;
however, to see the effects of sputtering gas pressure on
film properties, a few films were made at various pressures
between 33 and 53 Pa (1 Pa=7.5 mTorr). Although it is difficult
to measure the outgassing rate of the system accurately, the
background pressure in the system while sputtering was es-
timated to be less than $3x10^{-4}$ Pa total pressure and less
than 10^{-4} Pa O_2 in the absence of a controlled leak. How-
ever, O_2 could be introduced during sputtering; the O_2 dynamic
partial pressures were introduced at two levels, $5x10^{-4}$ and
$2x10^{-3}$ Pa.

The type of the substrates was also varied. Sintered
alumina, Superstrate (Lucalox), sapphire, Hastelloy B, Nb,

and splat-cooled Nb_3Ge were used. The Al_2O_3 substrates were
placed directly on the heater table, while the metallic sub-
strates were placed on a ceramic holder resting on the heater
to prevent welding of the metallic substrates to the heater.
All substrates were generally between .5 mm and .6 mm thick,
although three films were prepared on sapphire substrates
.1 mm thick. In every run Nb_3Ge was deposited simultaneously
on three substrates, each 6 mm x 12 mm. Although effects
of substrate orientation were not detected in this work (nor
searched for on a microscopic level), it should be noted
that the sapphire substrate orientations were close to $[11\bar{2}0]$,
$[10\bar{1}0]$, and $[0001]$ and that the Hastelloy B substrates had
at least some degree of preferred orientation since a very
strong (111) Hastelloy diffraction peak was observed in the
final Nb_3Ge film x-rays.

The thickness of a given sample was determined in either
of two ways. One way was to weigh the substrates before and
after deposition; then using the bulk specific gravity[39] of
8.7 along with the area of the deposited film the thickness
of the film can be determined. The accuracy of this deter-
mination is the same as the experimental error in determining
the change in weight: 15 to 20%. The other method consists
of fracturing the samples in a three-point bending configura-
tion and observing the sample cross-section in a scanning

electron microscope (SEM). (To avoid charging of the Al_2O_3

substrate when viewing the cross-section of samples in the

SEM, a gold layer about 50 nm thick was sputtered onto the

fractured surface.) The thickness determinations for the

two methods agree to within the limits of error of each tech-

nique.

B. Characterization of Samples

Films produced under the various sputtering conditions

were characterized with respect to composition, a_o, phase

assembly, grain size, T_c, ρ, and breaking strain. An elec-

tron microprobe (model MAC-5, ETEC Corp., Hayward, CA) was

used to determine film composition. This instrument has a

nominal accuracy of two atomic percent using MAGIC IV correc-

tions and pure Nb and Ge standards, and a precision of one

atomic percent as determined from repeated analysis of one

film on different dates. An absolute calibration was per-

formed by using it to analyze a carefully prepared and homo-

genized Nb-Ge arc-melted sample. This Nb-Ge sample was pre-

pared by melting the constituent compacted powders and turn-

ing them several times between melts to insure homogeneity.

(The arc melter with a nonconsumable tungsten electrode was

manufactured by Materials Research Corp. of Orangeburg, NY.)

The weight loss indicated that $\approx$ .3% Ge had evaporated leaving

a final sample composition of 18.3% Ge. This sample was

annealed for ten hours at 1850 C, sectioned, and polished.

Analysis of the microprobe data indicated its Ge composition

was 17.4% averaged over several determinations. (The stan-

dard deviation of composition of this bulk sample is only

1%, compared to the 2% standard deviation of the films.)

Consequently, all Ge microprobe concentrations were increased

by one atomic percent to agree with the composition of the

arc melted standard. (Incidentally, this procedure brought

the data obtained in this work into closer agreement with

the compositions reported by other researchers.) Since the

microprobe was not able to detect oxygen, the Nb and Ge com-

positions (and Si if applicable) were normalized to sum to

100%, neglecting the O expected from the partial pressure

in the system and the impurities in the target. (An x-ray

dispersive analyzer attached to the SEM indicated the Nb and

Ge were the only elements clearly above the noise level.)

The chemical composition of the surface layers of various

samples were analyzed by Auger electron spectroscopy (on a

Varian Scanning Spectrometer: Varian Surface Analysis Labora-

tory, Palo Alto, CA and on a model 545 Physical Electronics

Industries scanning spectrometer: University of Pennsylvania,

Philadelphia, PA). In particular, the 261eV C peak, 500eV

O peak, 1118eV Ge peak, and the 1898eV Nb peak were monitored

during the Auger profiling. The Auger signal through the
thickness of the film to the substrate was monitored for
three films on two different substrates and five films were
monitored only through the first 50 nm of film material.
For the films monitored through to the substrate, the sub-
strate position was determined by observing the occurence
of a strong rise in the 1365eV Al peak for Al_2O_3 substrates
and the occurence of the 830eV Ni peak for the Hastelloy B
substrate. The absence of Nb-Ge standards of known surface
composition, and the inconsistency of derived composition
obtained from the same sample in different Auger systems
using standard sensitivities of the elements,[93] means that
the Auger data cannot be used to give absolute concentrations
of the elements in the samples. On the other hand, the Auger
data can give an accurate picture of both a change in elemental
bonding as a function of depth and of a change in composi-
tion as a function of sputtering depth.

The crystal structure of the films was determined by
analysis of x-ray diffraction patterns taken on a GE XRD-5
diffractometer using Cu K_α radiation (λ = .154 nm). The
phases present in the films were identified by the relative
intensities of peaks occuring at specified d-spacings in the
diffraction patterns corresponding to the individual phases
of interest.[49] Unambiguous identification of the phases

present could easily be made despite the existence of some
preferred orientation of the different phases in the films.
The amount of each phase present could, however, only be
estimated due to a large diffuse background present in the
x-ray patterns, the variable composition of the phases present,
the small volume of material available for the x-ray diffrac-
tion, and the considerable preferred orientation of the tetra-
gonal phase present in the films.

The observed x-ray peaks were characterized by determining
both their integrated intensities and the full-width-at-half-
maximum (FWHM) of each peak. So, for example, the integrated
intensities of the A15 (110), (210), (420), and (440) peaks
were obtained by scanning 2θ at a low speed (0.2 degrees
per minute) and taking the average value determined in two
separate scans. (These (110) and (440) peaks were selected
to measure changes in the long-range order parameter since
the use of parallel planes minimizes preferred orientation ef-
fects.) Similarly, the integrated intensity of the tetragonal
Nb_5Ge_3 (411) and (330) peaks and the hexagonal (112) peak
were determined in order to estimate the approximate amount
of these phases present in the film.

Since the hexagonal peaks in the diffraction patterns
did not exhibit any strong change in preferred orientation
as a function of film composition, the amount of this phase
present in any given film was estimated by determining the

ratio of the integrated intensity of the hexagonal (112)

peak to that of the A15 (210) peak. On the other hand,

the tetragonal phase did show variable amounts of preferred

orientation as a function of film composition which required

determining those tetragonal peaks that appear least sensi-

tive to the compositional variation of films made from a

given target. Analysis of films from targets of different

composition indicated that for all but the 28% Ge target,

the ratio of integrated intensity of the tetragonal (330)

to the A15 (210) peaks is a reproducible estimate of the

relative amount of these phases present in the film. How-

ever, for the 28% Ge target there is a considerable tetra-

gonal phase preferred orientation as indicated by the relative

size of the (330) peak to the (411) peak. For example, for films

deposited at T_d's of ≈ 840 C, the ratio of this tetragonal

(330) peak to the (411) peak was observed to be as much as

10:1 as compared to an ideal ratio of 1:9 expected from a

randomly oriented Nb-Ge sample; regrinding the powder samples

only lowered this ratio to 2-3:1 indicating a substantial

residue of preferred orientation in the tetragonal phase.

Thus, for the 28% Ge targets the amount of tetragonal A15

phase present as a function of film composition was estimated

by comparing the tetragonal (411) peak to the A15 (210) peak.

The FWHM of all of these peaks mentioned above were

measured to determine their variation with 2θ. In these

measurements care was taken to observe the recommended pro-
cedure for matching scanning speed, time constant, and re-
ceiving slit to optimize peak breadth and peak intensity.[94]

The lattice parameter of the A15 phase was determined
by measuring the d-spacing of several of the peaks in the
2θ range $80°$ to $145°$. The peaks of the sapphire substrates
acted as an internal standard in this analysis allowing an
accuracy of $\pm$ .0003 nm. Lattice parameters could not, however,
be obtained for very thin films, films deposited at very
low T_d, or for films deposited on metallic substrates, since
in the first two cases peak intensity was too low in the
high 2θ region, and in the latter case the existence of other
intermetallic peaks interfered with the d-spacing measure-
ments.

An SEM (a Cambridge Stereoscan Mark II with a resolution
of ≈ 50 nm) was used to determine grain size, second phase
distribution, and grain morphology. (To observe these proper-
ties, the samples were simply grounded and inserted in the
microscope.) An x-ray dispersive analyzer attached to the
SEM was used to determine qualitative elemental concentra-
tions of the films.

The resistivity and T_c of the samples were measured
sequentially in a standard liquid He dewar using a four point

probe technique. Four gold wires of .12 mm diameter were
attached to the film with conductive silver paint; the inner
pair of gold leads were voltage probes ($\approx$6 mm apart) and the
outer wires were used to provide current. The gold wires
were connected to binding posts with indium solder. (See
Fig. 7 in Chapter III.) The sample was then soldered in
place on its holder and assembled into a copper can equipped
with heater windings. This can was then placed into a pyrex
tube which was subsequently evacuated. Helium exchange gas
was introduced into the pyrex tube and the header precooled
to 4.2 K by placing it in a helium bath. The heater current
was then turned on and increased slowly until a temperature
of $\approx$25 K was reached. In raising the temperature to $\approx$ 25 K,
the transition from the superconducting state to the normal
metallic state of the sample was traced. The heater current
was then slowly decreased, retracing the original voltage
versus temperature plot to within the recorder pen width.
The current density through the sample was $\approx 10^6$A/m^2,
corresponding to 10mA for a 1 μm thick sample. Current den-
sities of $\approx 10^4$A/m^2 increased T_c by .1 to .3 K above the
values obtained at 10^6A/m^2 and decreased the transition in-
terval by $\approx$.1 to .4 K. For a given current density, the re-
sistivity of the film at 25 K was computed by determining
the resistance of the sample using the four point probe,
multiplying this by the cross-sectional area of the film,

and dividing by the voltage probe spacing. (Changing the voltage probe spacing from 2 mm to 9 mm had no effect on the value of the resistivity.) The T_c onset was taken to be that temperature at which the voltage drop across the sample was 99% of that in the normal state. The midpoint was taken to be at 50%, and the finish of the transition taken at 1%. (In this work "T_c" always refers to the superconducting on-set.)

The resistivity of the films at 300 K was determined by measuring the resistance of the sample in place in the resistive T_c rig immediately prior to cooling to 4.2 K. The resistance value was converted to resistivity by the same arithmetic operations for the resistance as at 25 K.

In addition to the T_c and ρ of the samples, the breaking strain and T_c vs. applied strain were measured at cryogenic temperatures. The mechanical properties of Nb_3Ge films were measured in a four-point bending device described in Chapter III. The T_c was determined in the manner first described except that the four gold wires were attached to the film within the section of the sample deformed to a constant radius of curvature. The strain (either tension or compression) was then changed and the effect on T_c observed. A thin film strain gauge (FSM series, BLH Electronics Inc., Waltham, MA) was attached with low temperature epoxy to the opposite side

of the substrate in the constant radius section to determine
the amount of strain applied to the substrate-film composite.
The change in gauge reading between the strained and un-
strained states of the composite is then normalized by the
gauge constant defined as $K = \frac{\Delta R/R}{\Delta L/L}$, where L and R are the
gauge length and resistance in the unstrained state, respec-
tively. The gauge constant increased by 10% upon cooling
to 4.2 K a sample that had been plastically deformed to a
0.5% strain at room temperature. This corrected gauge con-
stant must be taken into account in analyzing Nb_3Ge mechani-
cal behavior. The breaking strain of the samples was taken
to be the tensile or compressive strain at which the film
became electrically discontinuous.

The difference in thermal contraction of the film and
substrate between T_d and room temperature was determined
by measuring the bowing of a Nb-Ge film-sapphire substrate
composite at a magnification of 400 x in an optical micro-
scope. The details of the calculations relating the bowing to
differential thermal contraction are given in Appendix C.

C. Analysis of Experimental Data

Changes in T_c, resistivity, lattice parameter, and break-
ing strain were compared to changes of structure, i. e. com-
position, grain size, long-range order, substrate, and phase

volume fraction and distribution, to see if correlations exist-
ed. The influence of deposition parameters on the above ele-
ments of structure were also considered. Samples produced from
the 28% Ge target were the most intensively investigated because
these samples had the most interesting superconducting proper-
ties. Since many of the changes in properties of the films
were within the limits of error of the measurements, an attempt
was made to determine the trends in the data rather than to ana-
lyze individually the data points obtained under the various
experimental conditions. It should also be mentioned that al-
though $\approx$ 300 films were fabricated and tested for individual
properties, a characterization of all the above film proper-
ties was possible on only $\approx$ 35 films due to limitations on
the availibility of the analytical equipment (most particularly
the electron microprobe).

V. Results

The experimental characterization of the Nb_3Ge films
is reported in this chapter. In particular, the properties
measured were film composition, lattice parameter, phase
assemblage, grain size and film morphology, resistivity,
residual resistance ratio, breaking strain, and transition
temperature. The processing parameters which were varied
in investigating these film properties were target composi-
tion, substrate heater temperature, sputtering gas composi-
tion and pressure, heat treatment, film thickness, substrate
material, and applied strain.

In considering the data, the precision of the various
experimental methods (established in Chapters III and IV)
must be kept in mind. For example, the electron microprobe
is precise to only 1%, the deposition temperature only to
$\pm$ 20 C and onset T_c to $\pm$ .5 K. Thus, the discussion to follow
will rely heavily on observed changes in properties particular
to a given sample type. In addition, because most of the
samples investigated were made from a 28% Ge target, the
behavior of films made from other targets are compared to
that of films made from this target composition.

Unless otherwise specified, films were deposited on
sapphire substrates in 40 Pa argon with approximately 4×10^{-5}
Pa oxygen and 3×10^{-4} Pa other gases present. The sputter-
ing voltage was 750 Vdc. Films attained a thickness of

roughly 1 µm in a one hour deposition time.

A. Film Composition

Within the limits of error of the microprobe it appears
the overall film composition is the same as, or close to,
that of the target with the exception of that deposited
from the 19% target. (See Fig. 10.) Deposition temperature
also has an effect on the composition of the film and
other factors such as sputtering gas composition may influence
sample composition; such effects, however, were not observed
in this work.

In Figure 10, it appears that the films deposited from
the 28% Ge target increase in Ge content as the deposition
temperature, T_d, is increased. For the 21% and 23% targets,
however, there appears to be a peak in Ge concentration (c_{Ge})
as T_d is increased. As can also be seen in Fig. 10, the
effect of oxygen addition on the Ge composition of the film
is not that pronounced, but that may be due to the high level
of background oxygen in the system.

Auger analysis of the films indicate the thickness of
the films has little effect on the relative strength of the
Nb and Ge signals throughout the bulk of the film after a
transient layer about 10 to 20 nm thick is sputter etched
away. A typical Auger composition profile is shown in Fig. 11.
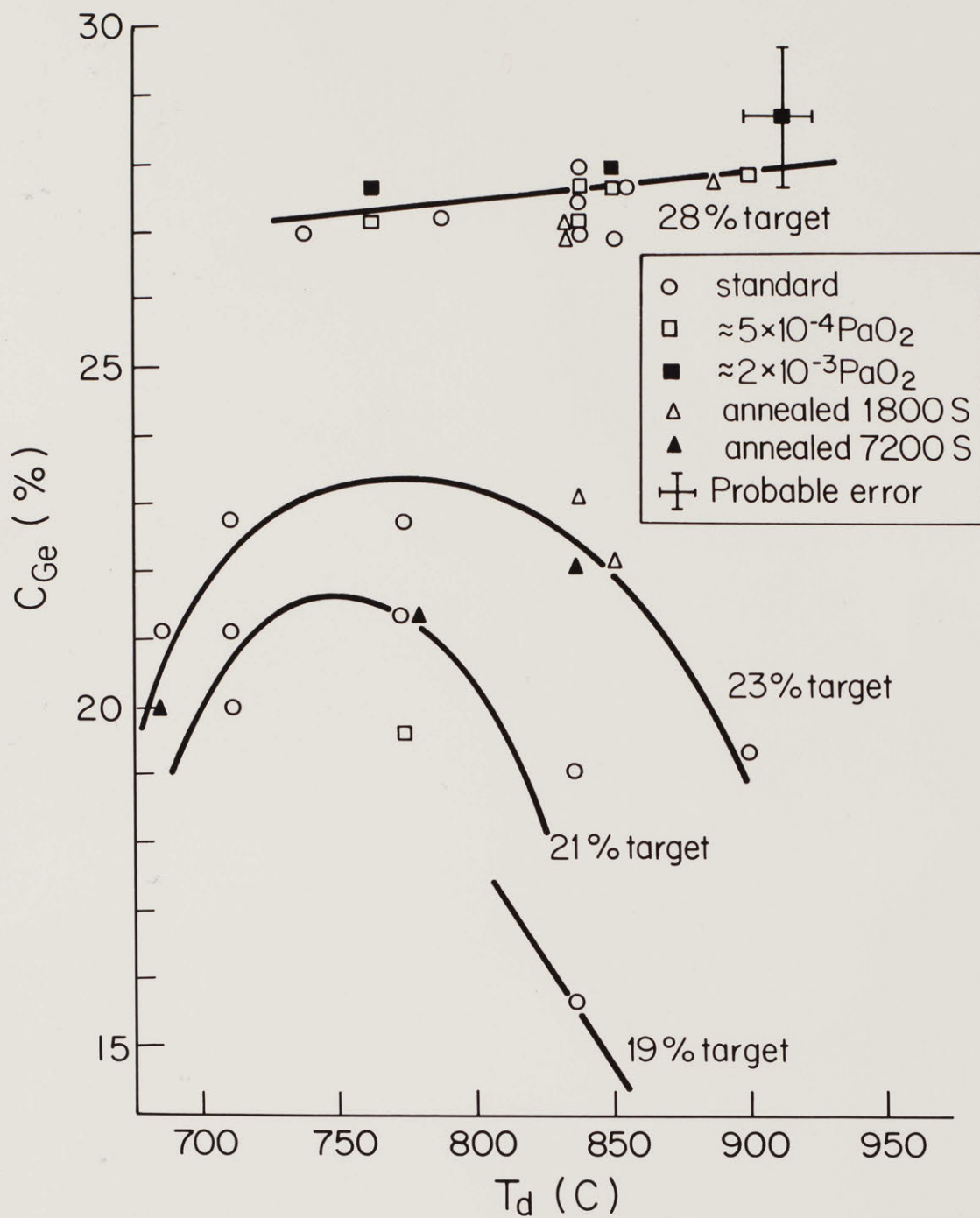
Fig. 10.   Ge composition of film vs. deposition
           temperature.
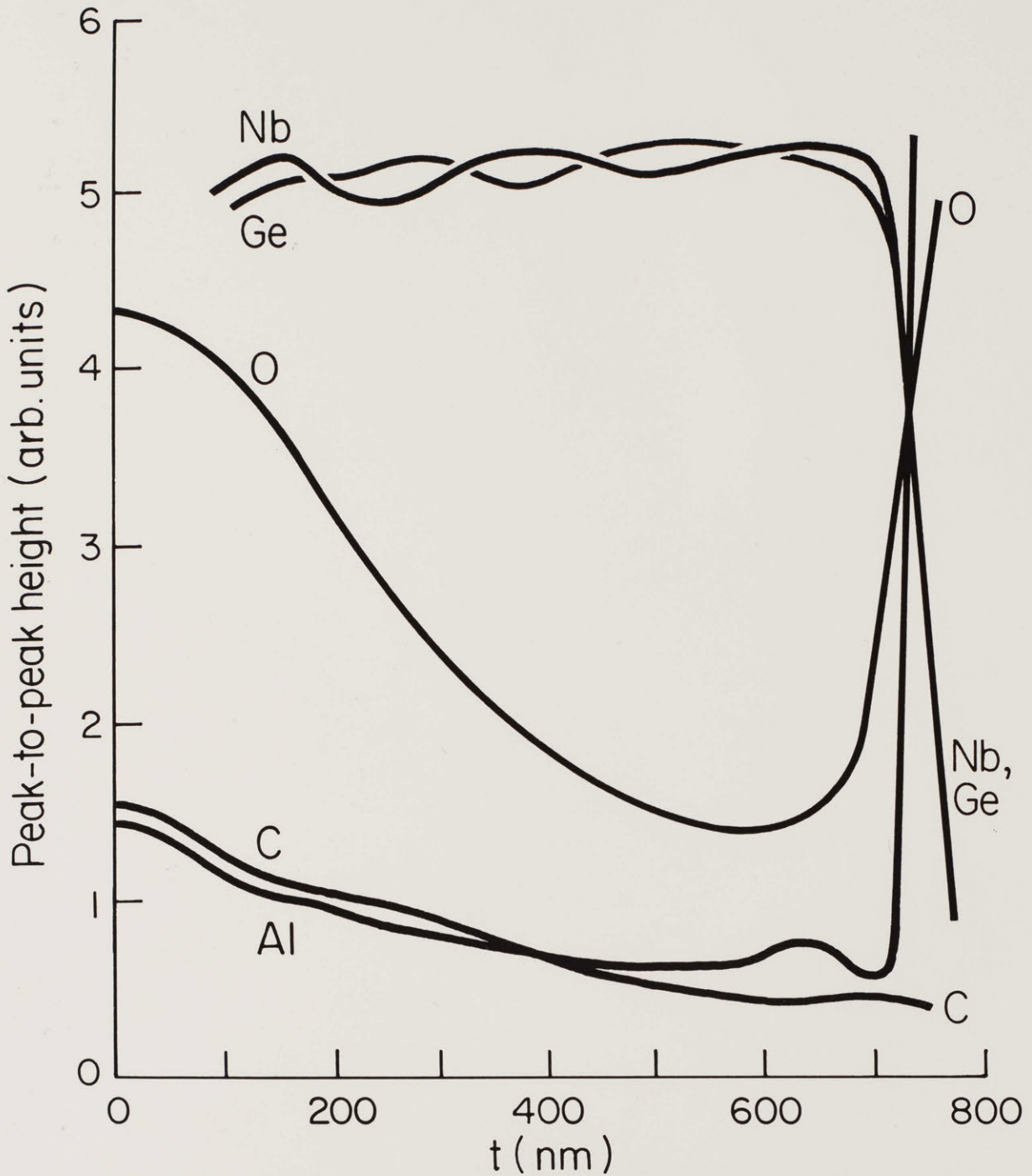
Fig. 11. Auger peak-to-peak height vs. distance from sample surface for sample deposited on sapphire at 840 C from the 28% Ge target and annealed for 1800 seconds.

The surface layers of the film have high O, C, and Al concentrations; undue weight should not be given to the strong Al peak as a large sampling window was employed for this element and stray signals may have originated from an Al sample holder. As the initial layers are sputtered away, the carbon lineshape, shown in Fig. 12, changes from an adsorbed to bonded type for all samples. This change in bonding is probably due to contamination of the sample surface between deposition and sputter-etching of the film in the Auger system.

Also apparent in Fig. 11 is a minimum in the O concentration as a function of distance into the film. The high O concentration near the surface of the sample is probably related to contamination of the sample after deposition is completed. The rise in O concentration near the film-substrate interface may be due to diffusion of O from the substrate into the film or peculiarities of film growth. It should be noted, however, that near the film-substrate interface the O concentration rises perceptibly over a distance somewhat greater than that of the rise of Al concentration and decreases in the Nb and Ge concentrations.

This minimum in oxygen concentration is not present in the depth profile of a sample deposited on a Hastelloy B substrate, as shown in Fig. 13. Here, the O concentration monotonically decreases, while the thickness of the layer where the Nb, Ge, and Ni are present in substantial amounts is approximately 500 nm, as opposed to the $\approx$ 60 nm layer over which the Al concentration

(a)   (b)

Fig. 12.   Auger carbon peak. (a) before sput-
ter etching (b) during sputter etch-
ing.
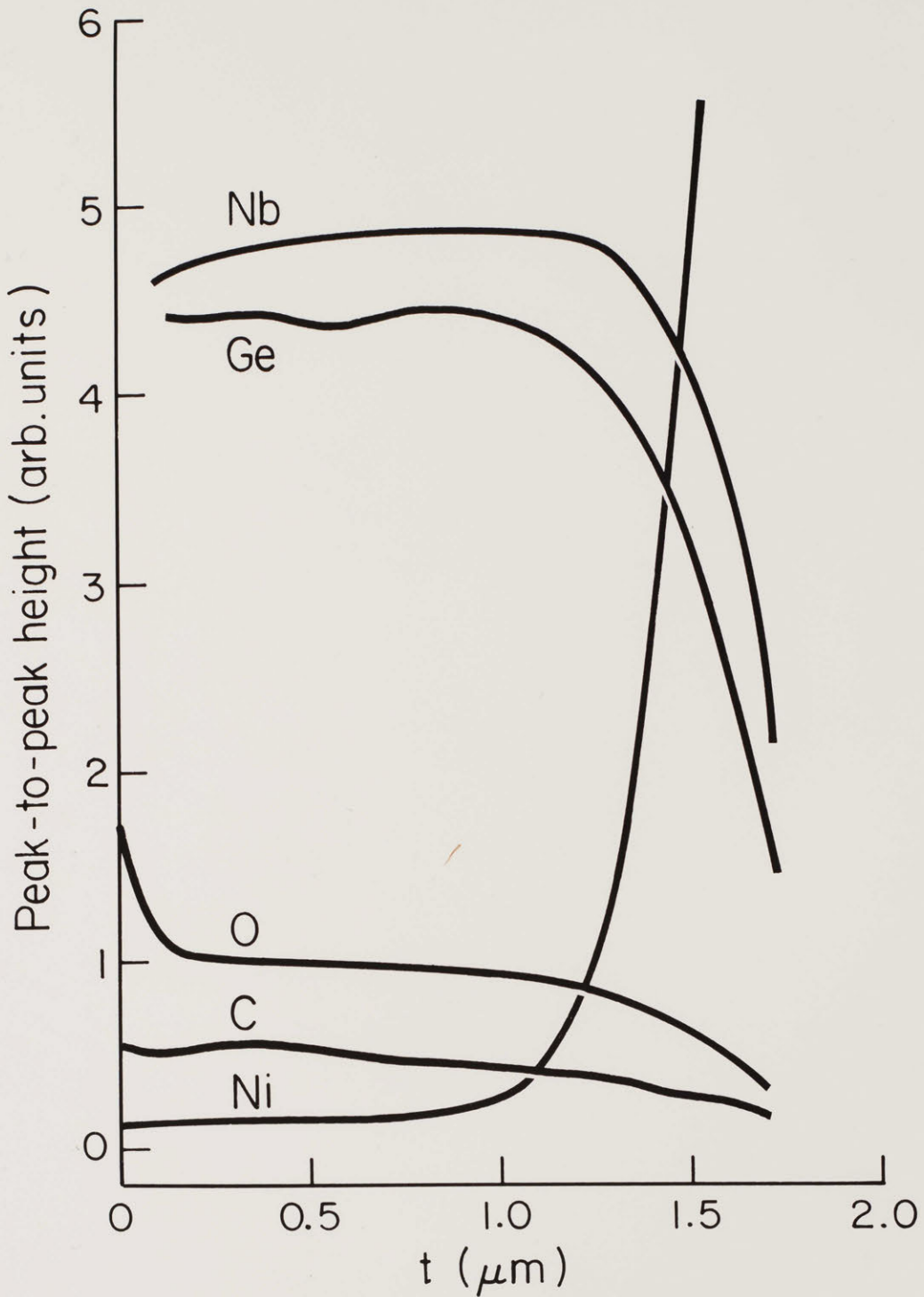
Fig. 13.   Auger peak-to-peak height vs. distance
            from sample surface for sample deposited
            on Hastelloy at 900 C from the 28% Ge
            target.

rises and the Nb and Ge concentrations fall for sapphire sub-
strates. On the other hand, the morphology and composition of
the substrate did not influence the bulk composition of the film
as determined by microprobe analysis, which samples on the or-
der of 500 nm.

Although the concentration of elements in the film cannot
be determined from the Auger results, the Nb peak-to-peak height
to Ge peak-to-peak height ratio qualitatively follows the change
in Ge target composition from sample to sample.

B. Lattice Parameter

The A15 lattice parameter, a_o, is a strong function of film
composition and decreases as the amount of Ge in the film in-
creases to $\approx$ 23% Ge, as shown in Fig. 14. At higher Ge concen-
trations a_o does not change substantially from the .5142 nm
value. The effect of annealing at T_d on the A15 lattice para-
meter is also shown in Fig. 14. The lattice parameter of Nb-
rich samples subjected to 7200 second anneals increases, al-
though the composition of the film as a whole does not change.

The thickness of very thin films was obtained by assuming
a constant rate of deposition, as determined by measurements
on films of 1 μm or greater thickness. Using these estimated
deposition rates it appears increasing film thickness from
$\approx$ 150 nm to 1 μm decreased a_o by .001 to .003 nm; this change,
however, may be due to determining a_o from low angle peaks
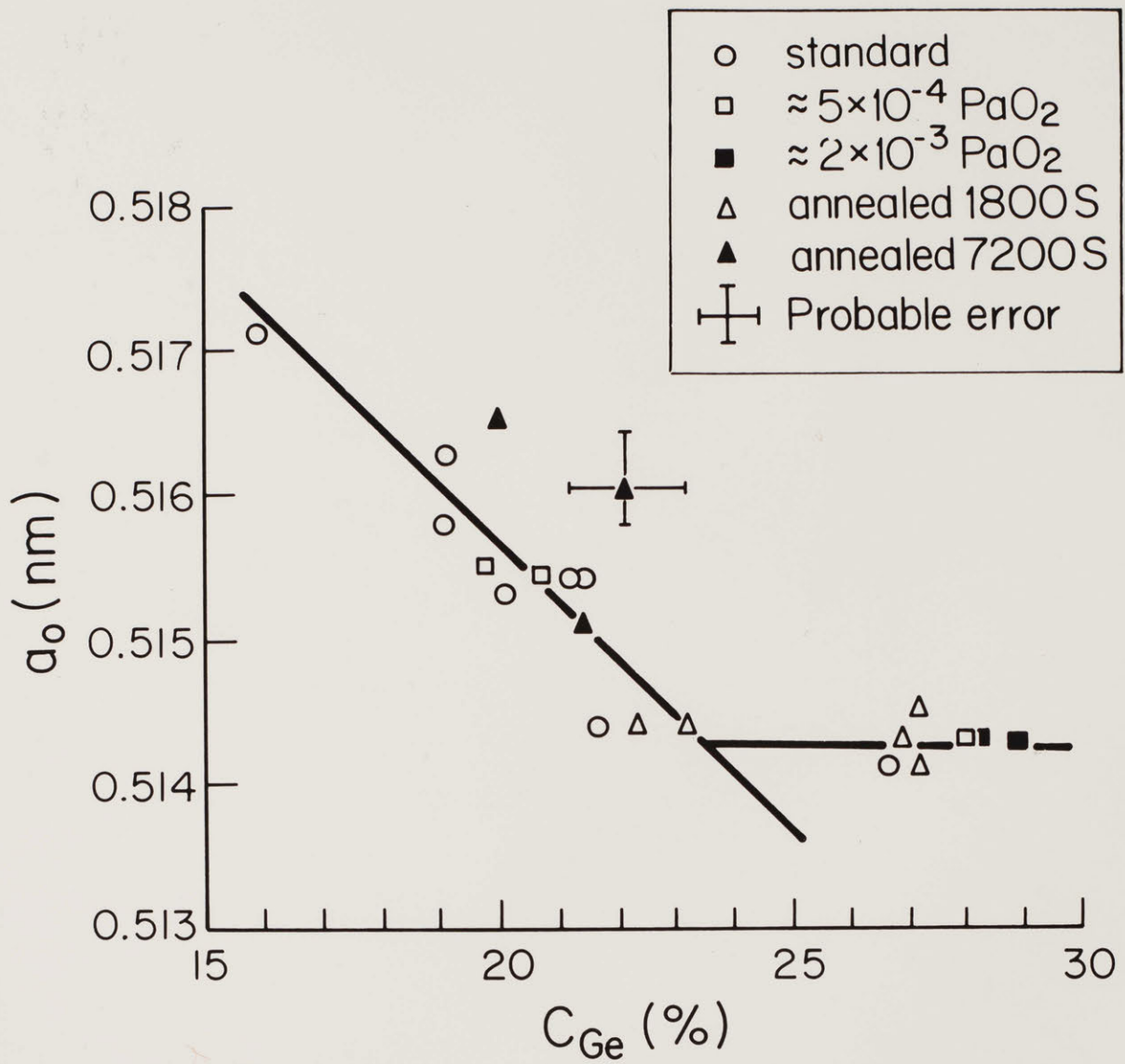
Fig. 14. Lattice parameter of A15 phase vs. Ge composition of the film.

for the thinnest films rather than to a change in film com-
position.

Along with composition, the lattice parameter for films
on the polycrystalline Al_2O_3 substrates did not differ from
those deposited on sapphire. Values of the lattice parameter
could not be obtained for films deposited on metallic sub-
strates because of interference of the substrate and inter-
metallic phase peaks with the weak A15 peaks.

C. Phase Assemblage

The phase distribution changes with target composition,
as seen in Fig. 15 and Table I. The amount of hexagonal
and tetragonal phase, as determined by the method indicated
in Chapter IV, appears to increase with Ge concentration,
especially between 23% and 28% targets. A comparison of
the sum of the integrated intensities of minor phases to
the sum of integrated intensities of A15 peaks of the diffracto-
meter traces in Fig. 15 indicates the films deposited from
the 28% Ge target have a higher proportion of second and
third phases present than do the other films. Indeed, con-
sideration of the peaks present in the 2θ range of $20°$ to
$150°$ suggests that the films deposited from the 19%, 21%,
and 23% targets are nearly single phase; i. e., they are
$\gtrsim 95\%$ A15 material.
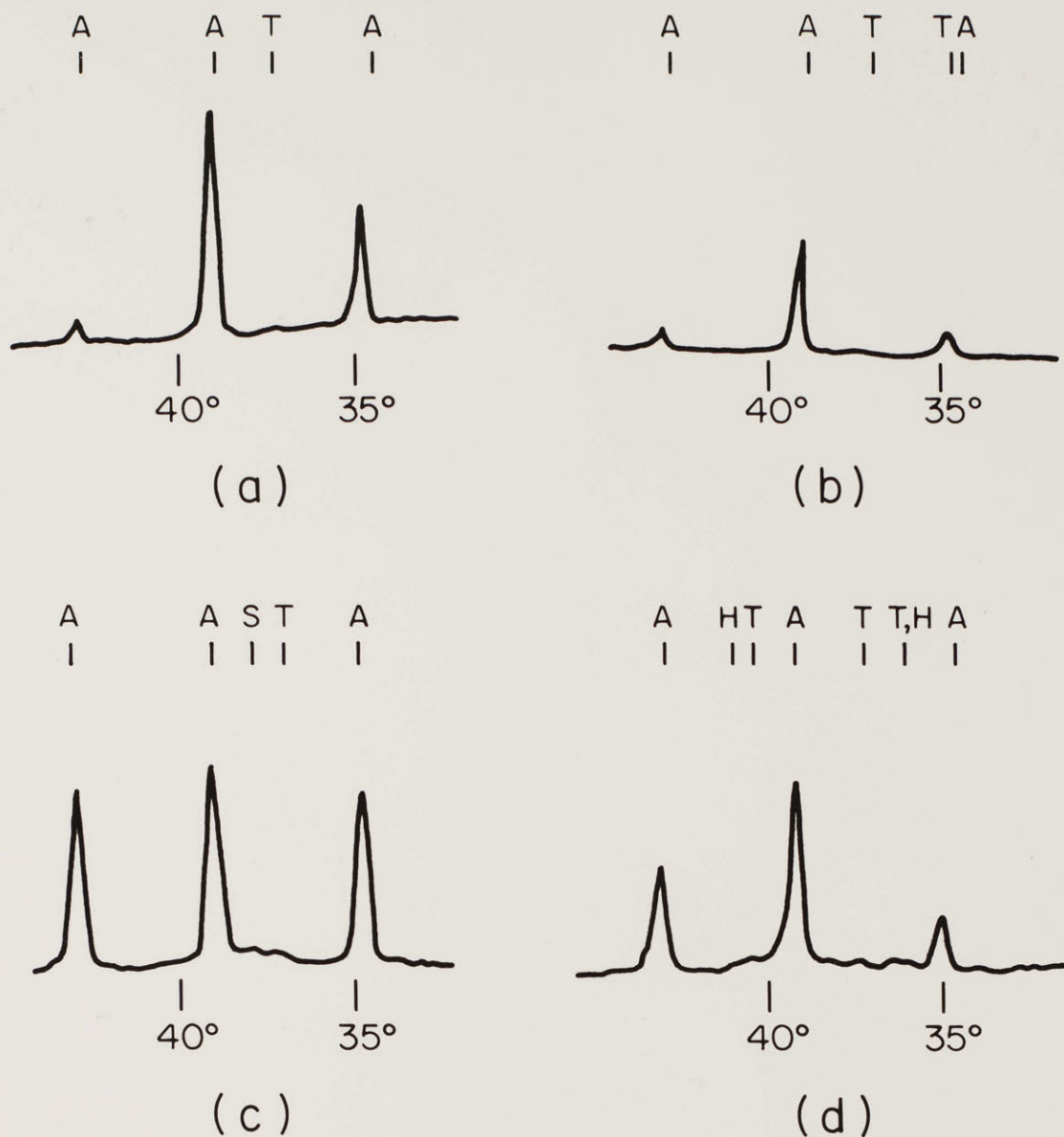
Fig. 15. Diffraction patterns for increasing Ge content target, T_d = 850 C: (a) 19% Ge (b) 21% Ge (c) 23% Ge (d) 28% Ge. Peaks present are identified.

Table I - Diffraction Peak Integrated Intensities and Peak Widths

Sample	T_d (C)	Tetragonal (%)	Hexagonal (%)	$\dfrac{I_{(110)}}{I_{(440)}}$ (%)	(110)	FWHM (°2θ) (210)	(420)	(440)	Comments
				19% Ge Target					
24162	850	3	2	78	.25	.25	.40	.70	
				21% Ge Target					
2591	710	3	3	—	—	,35	.70	—	
2592	720	1	2	—	—	.30	.60	—	
2542	780	7	—	54	.20	.28	—	.40	
25111	770	5	1	57	.25	.28	.38	.60	annealed 1800s
25112	780	4	0	72	.25	.23	.35	.50	"
25241	770	8	—	54	.22	.29	.47	.65	annealed 7200s
25242	780	10	1	60	.25	.25	.35	.55	"
25243	770	8	—	69	.27	.27	—	.50	"
25312	770	3	—	51	.28	.33	.62	.95	5 μm thick
24192	850	2	—	57	.25	.22	.40	.55	
				23% Ge Target					
2651	770	10	1	66	.35	.30	.45	.65	

Table I

Sample	T_d (C)	Tetragonal (%)	Hexagonal (%)	$\dfrac{I_{(110)}}{I_{(440)}}$ (%)	FWHM (°2θ) (110)	(210)	(420)	(440)	Comments
				23% Ge Target					
2652	780	15	1	57	.27	.29	.30	.70	
26221	840	4	—	54	.20	.30	.60	.85	
26222	850	4	—	51	.25	.27	.50	.70	
26241	840	10	—	63	.30	.28	.45	.60	annealed 1800s
26242	850	12	—	45	.23	.28	—	.55	"
2721	900	20	1	—	—	.30	.60	.75	
				28% Ge Target					
20262	760	36	6	—	.40	.75	—	—	annealed 1800s 5×10^{-4} Pa O_2
21122	760	45	—	—	.32	.55	.70	.65	5×10^{-4} Pa O_2
21123	750	45	—	—		.52	.70	.75	"
21162	760	35	4	108	.45	.57	.50	.75	annealed 7200s 5×10^{-4} Pa O_2
21232	750	33	2	—	.47	.57	.45	—	2×10^{-3} Pa O_2
19223	830	12	18	—	.22	.30	.60	.85	

Table I

Sample	T_d (C)	Tetragonal (%)	Hexagonal (%)	$\dfrac{I_{(110)}}{I_{(440)}}$ (%)	FWHM ($^\circ 2\theta$) (110)	(210)	(420)	(440)	Comments
				28% Ge Target					
19251	850	12	45	99	.28	.25	.50	.52	
19253	850	3	43	87	.30	.27	.70	.75	
20152	850	16	29	66	.28	.27	.45	.80	annealed 1800s 5×10^{-4} Pa O_2
20221	840	3	14	102	.27	.27	.40	.70	"
21143	840	35	8	90	.25	.40	.60	1.10	annealed 7200s 5×10^{-4} Pa O_2
21263	840	4	3	81	.32	.30	.60	.85	53 Pa Ar
21293	840	11	7	105	.32	.32	.65	.70	33 Pa Ar
19183	930	1	17	57	.28	.28	.35	.90	
19272	910	3	15	72	.22	.27	.45	.75	
19273	900	2	16	78	.22	.27	.45	.70	
20101	900	2	12	93	.27	.25	.32	.55	5×10^{-4} Pa O_2
20102	910	0	13	63	.22	.27	.30	.40	"
20103	900	0	13	75	.22	.25	.40	.50	"

Table I

Sample	T_d (C)	Tetragonal (%)	Hexagonal (%)	$\dfrac{I_{(110)}}{I_{(440)}}$ (%)	(110)	(210)	FWHM (°2θ) (420)	(440)	Comments
				28% Ge Target					
20121	900	6	17	39	.27	.25	.30	.30	annealed 1800s 5×10^{-4} Pa O_2
20122	910	1	10	66	.30	.30	.30	.35	"
21191	900	8	8	60	.25	.27	.35	.55	annealed 7200s 5×10^{-4} Pa O_2
21192	910	12	8	57	.25	.25	.32	.70	"
21212	910	33	2	59	.22	.27	.30	.60	2×10^{-3} Pa O_2

Deposition temperature also has an effect on phase distribution as can be seen in Table I and Fig. 16. The film deposited at very low T_d, shown in Fig. 16a is essentially amorphous, as indicated by the broad peak several degrees wide in 2θ centered about $39°$. As T_d increases this peak is observed to split and the diffuse background decreases as T_d is increased, indicating the formation of A15 and other crystalline phases. The precise change in phase distribution is uncertain as changes in preferred orientation may occur as T_d is varied. However, the data in Table I suggest that for a given annealing time the amount of tetragonal phase decreases as T_d is increased from 770 C to 840 C for both the 23% and 28% target samples. The change in amount of tetragonal phase present at higher T_d is uncertain. For the 28% target samples the amount of hexagonal phase increases with T_d up to 840 C for a given annealing treatment; for subsequent increases in T_d, the amount of hexagonal material remains about the same. An SEM of the hexagonal phase (light colored grains) corresponding to the diffraction pattern in Fig. 16d is shown in Fig. 17d.

Increasing oxygen partial pressure during deposition of the film appears to have little systematic effect on the intensity of the tetragonal and hexagonal peaks tabulated in Table I, with the possible exception of the 28% target samples where the amount of tetragonal phase increases and
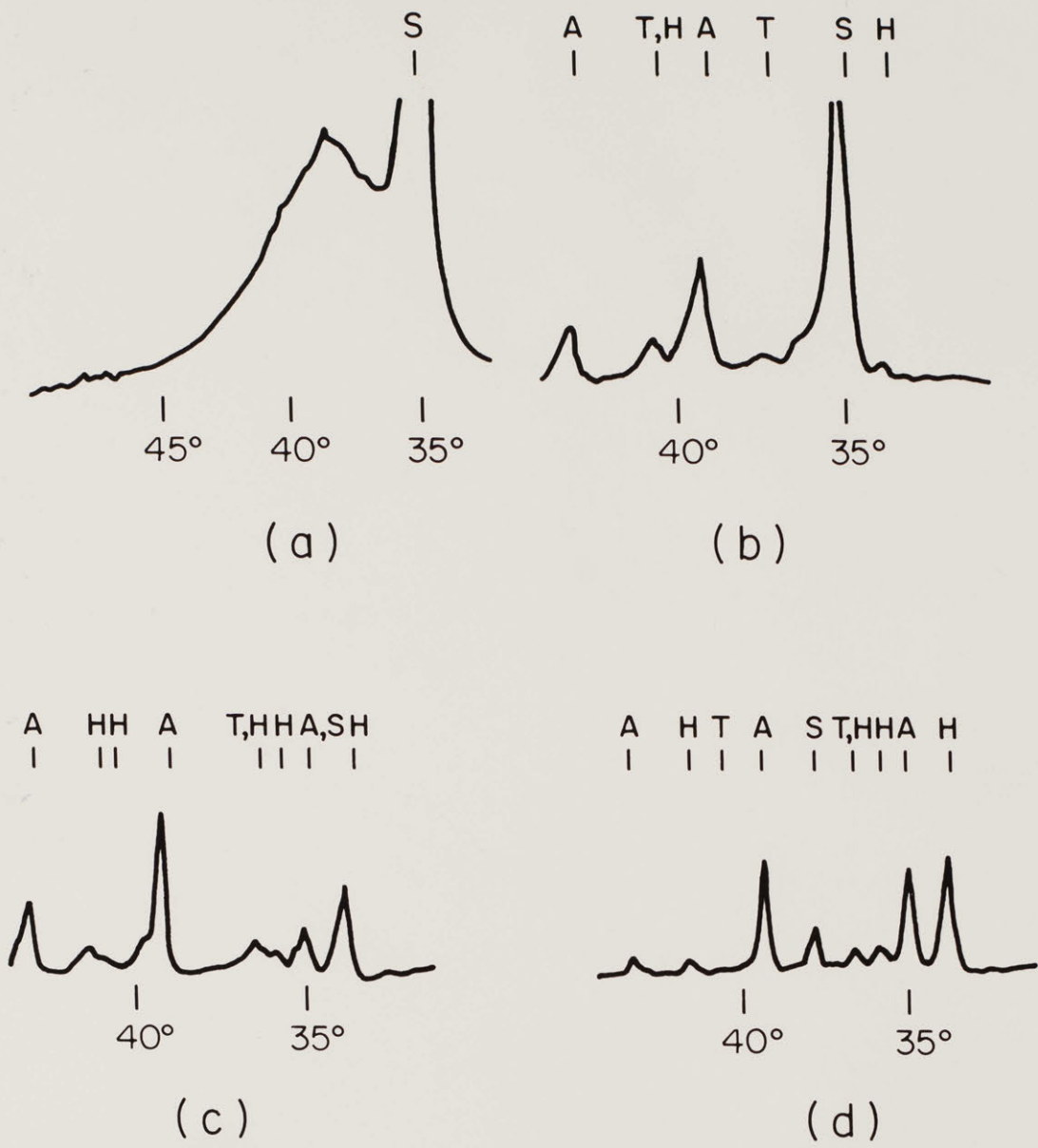
A   A15 Nb$_3$Ge
T   Tetragonal Nb$_5$Ge$_3$
H   Hexagonal Nb$_3$Ge$_2$
S   Sapphire

Fig. 16.   Diffraction patterns for increasing deposi-
tion temperature, 28% Ge target: (a) 710 C
(b) 790 C (c) 840 C (d) 910 C. Peaks present
are identified.
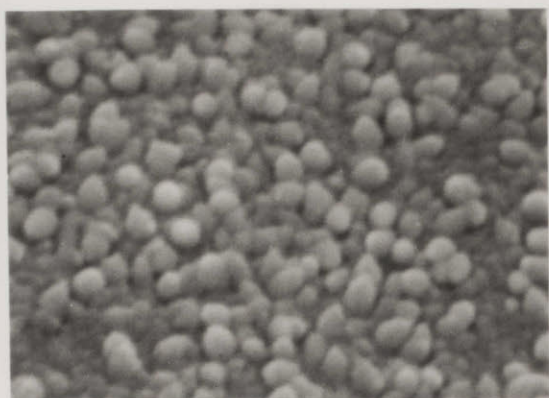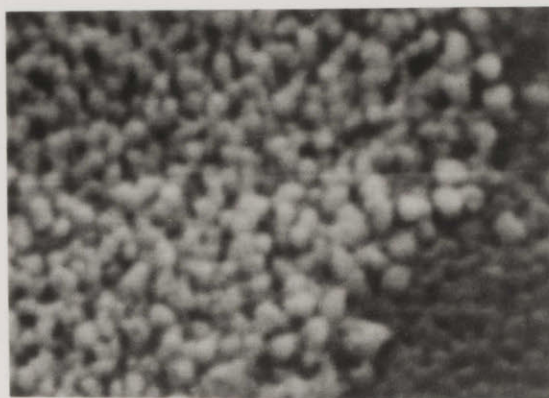
Fig. 17. Films deposited with increasing deposition
          temperature, 28% Ge target: (a) 720 C
          (b) 770 C (c) 850 C (d) 900 C. The magni-
          fication is 10,000 x.

hexagonal decreases for the highest O_2 level at 910 C. Table I
also shows the increase of tetragonal phase and associated
decrease of hexagonal phase present with long anneals for
a given composition, T_d, and O_2 partial pressure. There
is no clear systematic change in the amount of A15 phase
present in the samples. With annealing the FWHM of the high
angle peaks in Table I may increase slightly. If so, this
may be evidence for phase segregation and growth of the tetra-
gonal phase.

The type of substrate did not appear to influence the
phase distribution in the bulk of the films; for the metallic
substrates there is, however, an interface region between
the substrate and film which contains the various possible
intermetallic compounds of the two materials.

A typical diffraction pattern for a film deposited on
a Hastelloy substrate is shown in Fig. 18; note the presence
of additional structure, which is believed to be due to Nb-Ni
and Nb-Ni-Ge compounds, and also the strong Ni-Mo peak. The
presence of these peaks is consistent with the approximately
500 nm Nb-Ge-Ni layer detected during Auger profiling. Films
deposited on other metallic substrates, Nb foils and Nb-Ge
splat-cooled flakes, yielded diffraction patterns similar
to those shown in Fig. 18; intermetallic second phases, such
as tetragonal and hexagonal Nb-Ge were present in these samples.

BNN₃t NNTA NGT   T H t t

A HTA TT,HAH

A   N,At   AT H   t
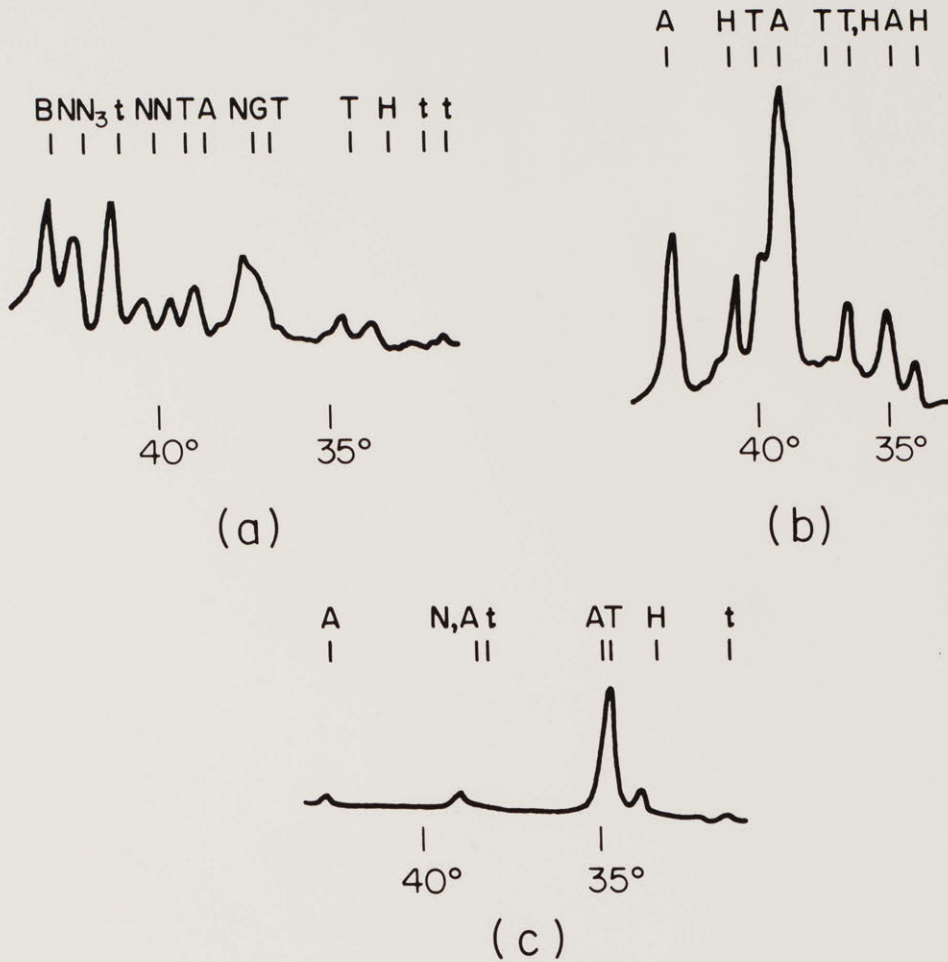
A   A15 Nb₃Ge
T   Tetragonal Nb₅Ge₃
t   Tetragonal Nb₅Ge₃
H   Hexagonal Nb₃Ge₂
N   Nb
B   Hastelloy B
NN   Nb-Ni
NN₃ Nb Ni₃
NG   Nb-Ni-Ge

Fig. 18. Diffraction patterns of films on varying
substrates: (a) Hastelloy B, 28% Ge target,
970 C (b) Splat-cooled Nb-Ge, 28% Ge target,
910 C (c) Nb, 28% Ge target, 850 C. Peaks
present are identified.

D. Grain Size

As the deposition temperature is raised, there is an
increase in grain size as shown in Fig. 17 for films deposited
from the 28% Ge target. The grain size increases from below
the resolution limit of the SEM (about 50 nm) at a $T_d \approx 710$ C
to the vicinity of 400 nm at a T_d near 850 C and remains
near that size for higher T_d. Films deposited from 21% and
23% Ge targets appear to reach the 400 nm grain size at a
lower T_d than those deposited from the 28% Ge target, as
shown in Fig. 19 for films deposited near 710 C and 770 C.
The 21% target sample has already reached the limiting grain
size at 770 C while the Ge rich films have progressively
smaller grains at that T_d.

This limiting grain size behavior is further substantiated
in Fig. 20, where the diffraction patterns suggest that the
temperature at which the single broad peak splits into in-
dividual peaks increases with Ge content of the film. Along
with changes in phase distribution and the decrease in diffuse
background, there appears to be a general trend in the data in
Table I for all targets towards a narrower FWHM for low-angle
peaks at higher T_d. This also implies the grain size grows
with increasing T_d.

The average grain size appears to increase slightly with
the Ar pressure, as shown in Fig. 21, although this change
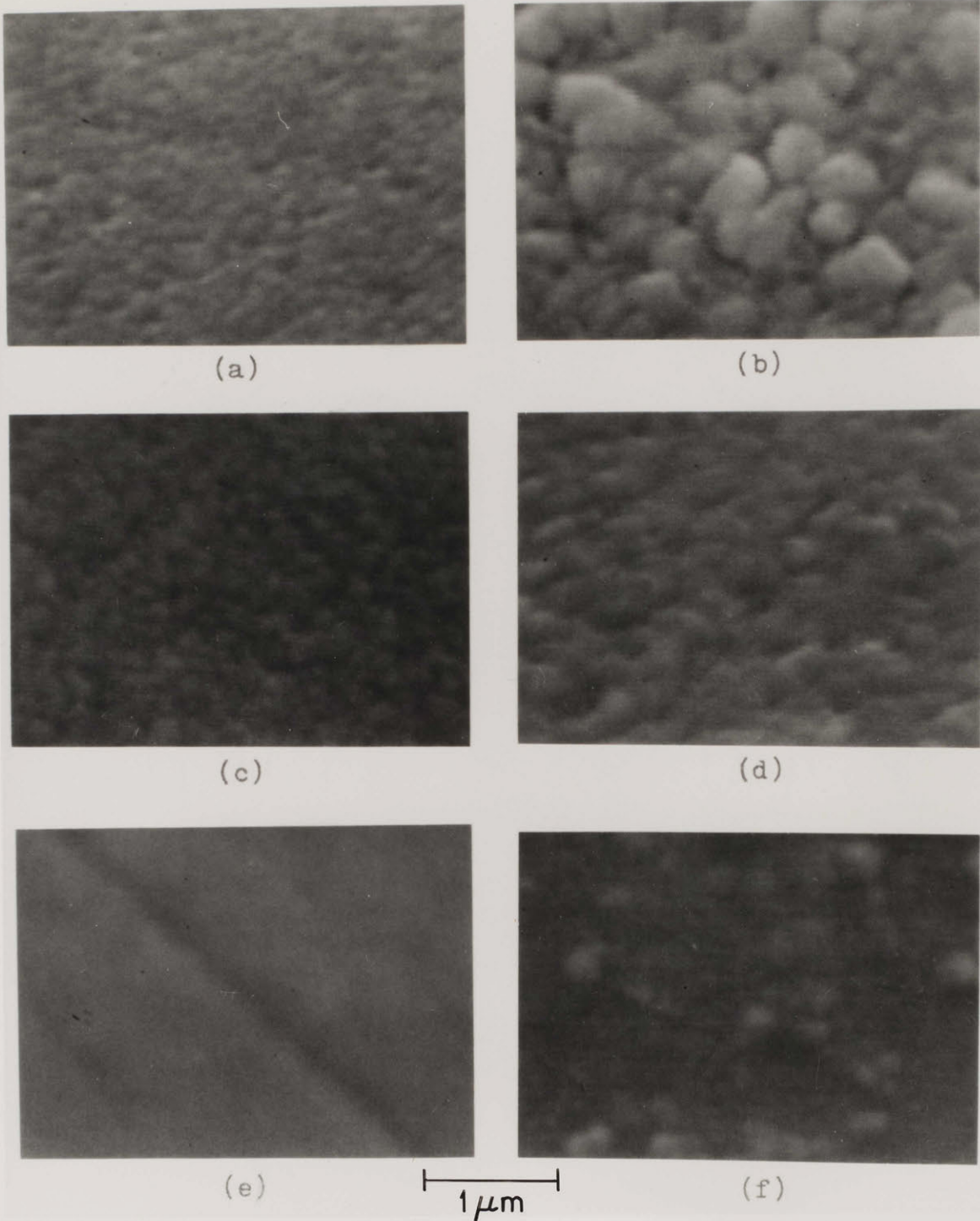
Fig. 19. Films deposited with increasing Ge content
target and deposition temperature:
(a) 21% Ge, 710 C (b) 21% Ge, 770 C
(c) 23% Ge, 710 C (d) 23% Ge, 780 C
(e) 28% Ge, 725 C (f) 28% Ge, 770 C.
The magnification is 20,000 x.
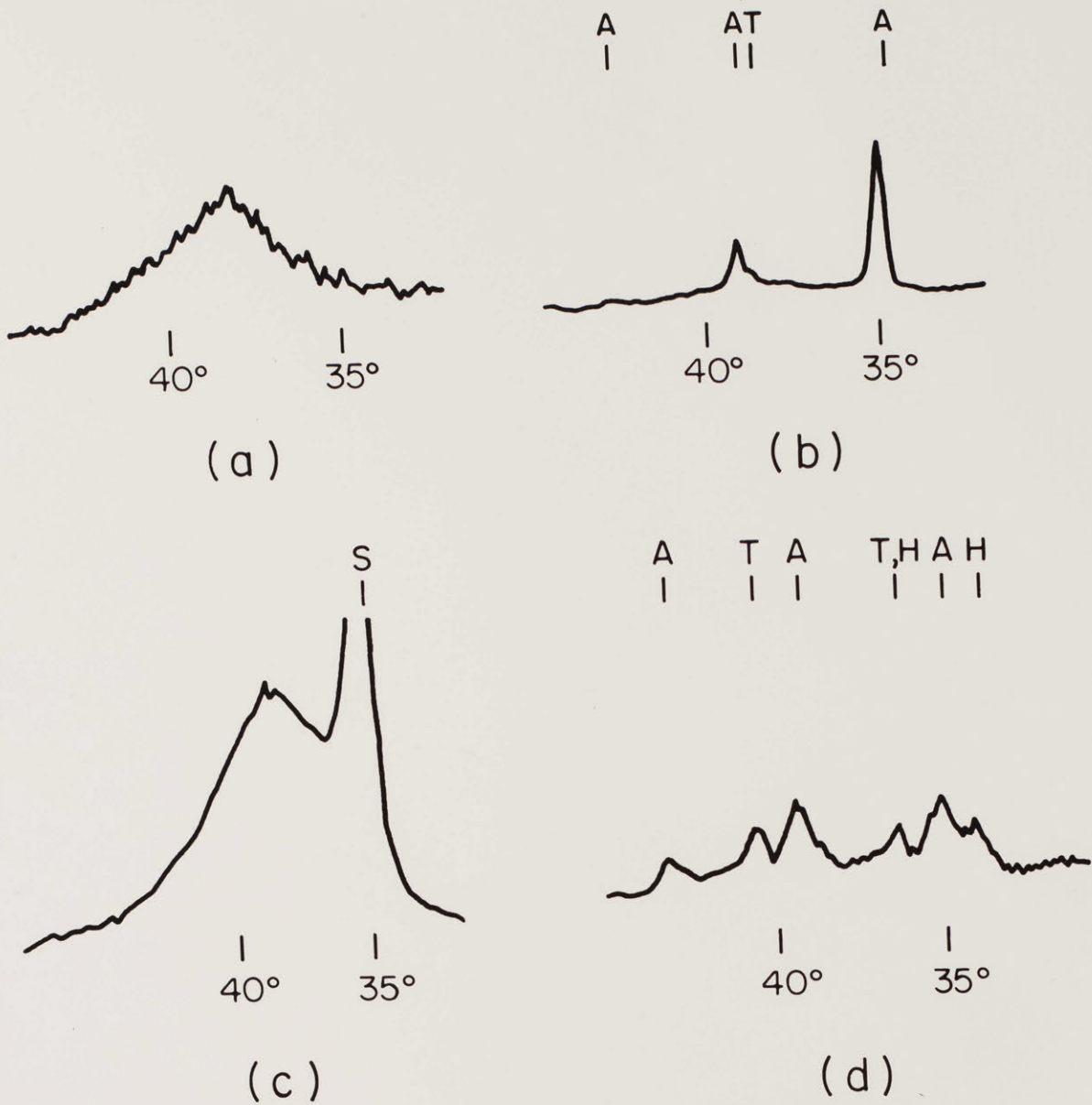
Fig. 20. Diffraction patterns for increasing Ge content target and deposition temperature: (a) 21% Ge, 660 C (b) 21% Ge, 690 C (c) 28% Ge, 710 C (d) 28% Ge, 760 C. Peaks present are identified.

(a)

(b)

(c)

├─────┤
1 μm

Fig. 21. Films deposited with increasing argon pressure.
28% Ge target, T_d = 840 C: (a) 33 Pa (b) 40 Pa
(c) 53 Pa. The magnification is 20,000 x.

might well be due to a change in thickness of the film result-
ing from the higher sputtering rate at higher Ar pressure.
Reinforcing this idea, it was found that changing the O_2 partial
pressure did not appear to change the average grain size.

Annealing does not change the grain size and shape sig-
nificantly either. Further, for very thin films (between 100
and 200 nm) whose grain size remains below the resolution of
the SEM, the FWHM do not change significantly on annealing which
implies that the grain size of these films does not increase.
For thicker films the SEM reveals the change in structure im-
plied by the decrease in FWHM for low angles of thicker films:
grain size increases as the films become thicker, as shown in
Fig. 22. The film cross section displayed in Fig. 23 shows the
grains become more columnar as their average size increases and
the film thickens.

Although the A15 grain size does not vary substantially
with substrate, as shown in Fig. 24, the nature of the sub-
strate affects the morphology of the films. For example, the
occurence of cracks and fissures is more widespread for the
polycrystalline alumina substrates than the sapphire substrates.
In the case of the Hastelloy substrates, the Hastelloy topology
is mirrored by the topology of the A15 films, as shown in Fig.
25. The grains of Hastelloy can clearly be seen, as can twins
and precipitates at the grain boundaries of the substrate.

A micrograph of a typical film deposited from a Si doped

(a)

(b)

(c)
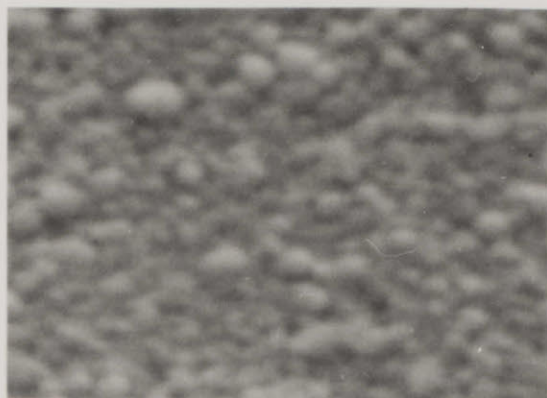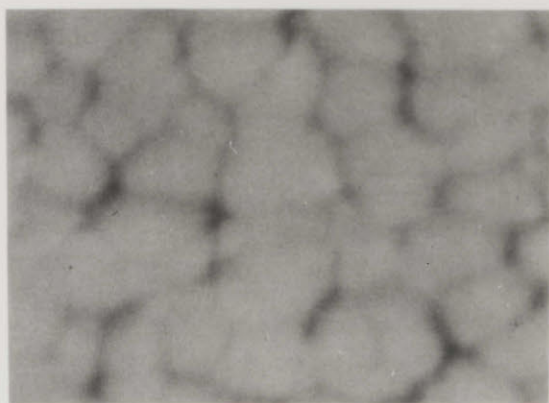
├─────┤
1 μm

Fig. 22. Films of varying thickness, 28% Ge target,
          T_d = 840 C: (a) .12 μm (b) .8 μm (c) 2.6 μm.
          The magnification is 20,000 x.

(a)

(b)

1μm

Fig. 23. Cross section of films of varying thickness, 28% Ge target, T_d = 840 C: (a) .7 μm (b) 2.6 μm. The magnification is 12,000 x.

(a)

⊢ ⊣
10μm

(b)

(c)

⊢———⊣
1μm

(d)
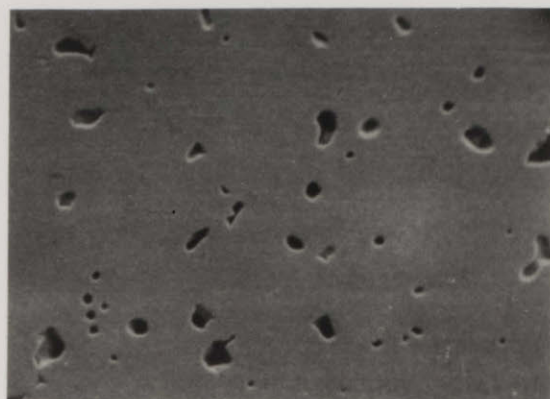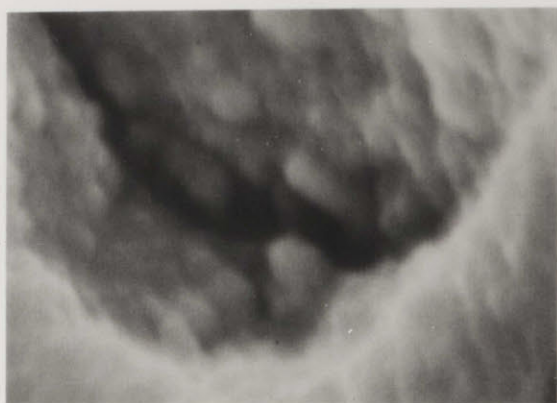
Fig. 24. Films deposited on different substrates,
23% Ge target, T_d = 770 C: (a) Sapphire
substrate, 500 x (b) Sintered alumina substrate,
500 x (c) Sintered alumina substrate, 20,000 x
(d) Superstrate substrate, 20,000 x.

(a)

├─┤
10μm

(b)

├────────┤
1μm

(c)

├────────┤
1μm

Fig. 25.   Films deposited on different substrates:
(a) 28% Ge target, T_d = 840 C, Hastelloy B
substrate, 500 x (b) 28% Ge target, T_d = 850 C,
Hastelloy B substrate, 20,000 x (c) 28% Ge
target, T_d = 850 C, splat-cooled Nb-Ge
substrate, 20,000 x.

target is shown in Fig. 26; the grain size is somewhat smaller than for a comparable Nb-Ge film deposited at the same temperature. The light colored grains may be the Nb_5Ge_3 phase present in the diffraction pattern of this sample (not shown).

E. Resistivity and Residual Resistance Ratio

Comparing the data in Figs. 27-29 it is apparent that for a given T_d, there is little difference in the resistivity, ρ, of the 21% and 23% Ge target samples; indeed the film deposited from the 19% Ge target has a resistivity of 1.5 $\mu\Omega m$ at 840 C, very close to that expected for 21% and 23% films (Figs. 27 and 28, respectively). There is, however, a large change in the resistivity between the nearly single phase films and the 28% Ge target films: the resistivity of the Ge rich films is substantially lower at a given T_d. There is a tendency towards a lower ρ at higher T_d, although the slope appears to decrease at higher T_d and the knee in the ρ vs. T_d curve appears to move to a higher T_d as c_{Ge} is increased. Indeed, for the highest c_{Ge} films the decrease in slope at high T_d, if present, is not fully developed at the highest T_d's tested. While the addition of oxygen has very little effect on the resistivity of the samples, the data in Figs. 27-29 suggest that for low T_d the resistivity of the films at 25 K is lowered by annealing.

1 μm

Fig. 26. Film deposited from Si-alloyed target:
          20% Ge, 2% Si target, T_d = 910 C. The
          magnification is 20,000 x.
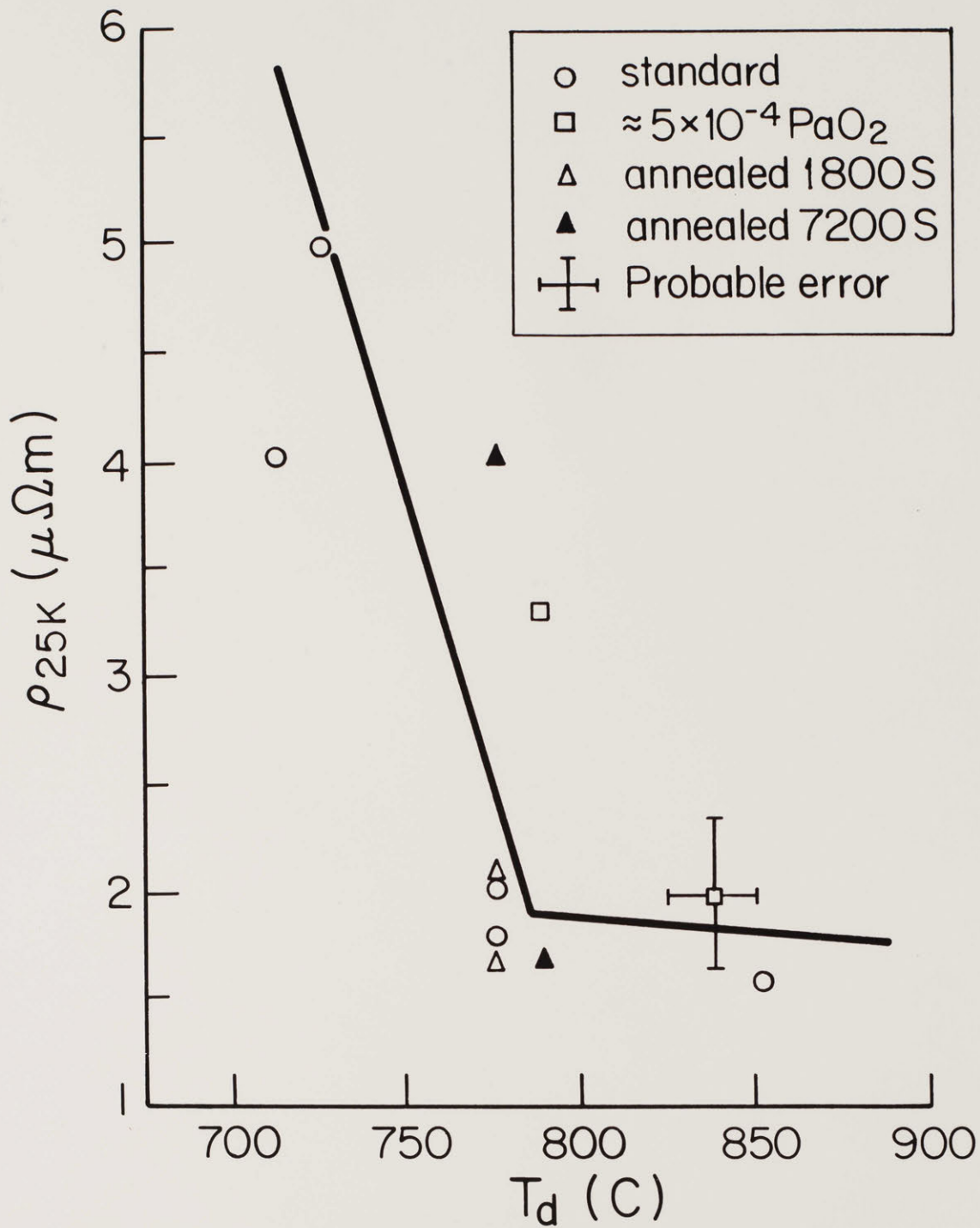
Fig. 27.   Resistivity vs. deposition temperature:
           21% Ge target.
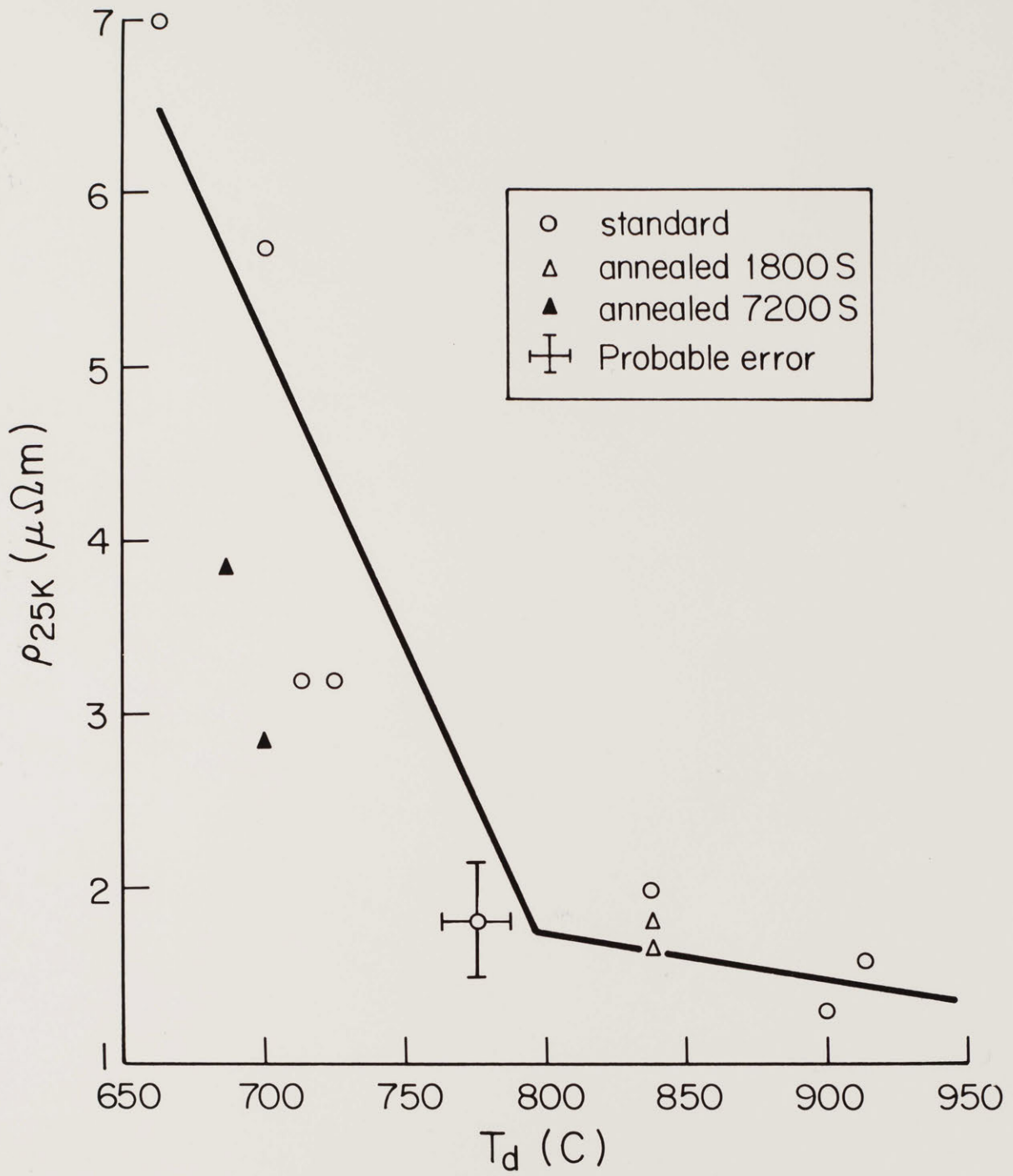
Fig. 28. Resistivity vs. deposition temperature:
23% Ge target.
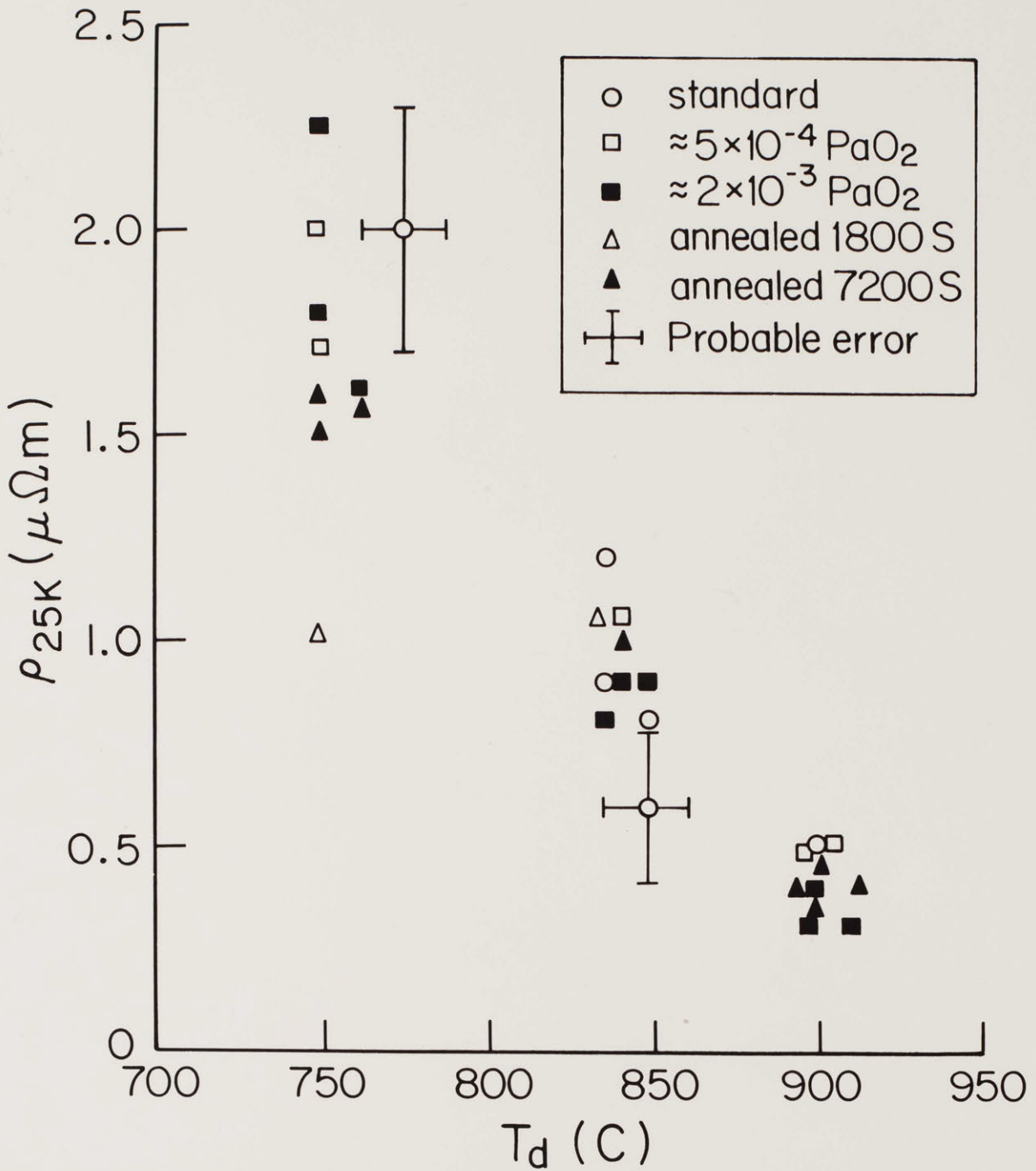
Fig. 29. Resistivty vs. deposition temperature:
28% Ge target.

The behavior of the residual resistance ratio (Γ) versus composition follows similar trends in Figs. 30-32: for a given T_d, heat treatment, and oxygen level the single phase films show little dependence of Γ on c_{Ge}. The multiphase films, however, have a much higher Γ . There also appears to be a trend towards a plateau in Γ with T_d except for high T_d - 28% Ge target films fabricated with high O_2 partial pressures or subjected to high T_d post deposition annealing. For films deposited at lower T_d or for the 21% or 23% Ge targets the influence of annealing on Γ is not clear.

The effect of thickness on resistivity is shown in Table II. The resistivity decreases between the .15 μm and 1 μm thickness for a given annealing interval and then remains relatively constant for greater thicknesses. There appears to be little dependence of Γ on film thickness. Finally, both the resistivities and the residual resistance ratios appear to be independent of ceramic substrate morphology. (See Table III and Figs. 27-32.)

F. Breaking Strain

The mechanical properties of the films are governed in large measure by the morphology of the underlying substrate. The data in Table IV suggest that the breaking strain of the films subjected to four-point bending seems to increase as
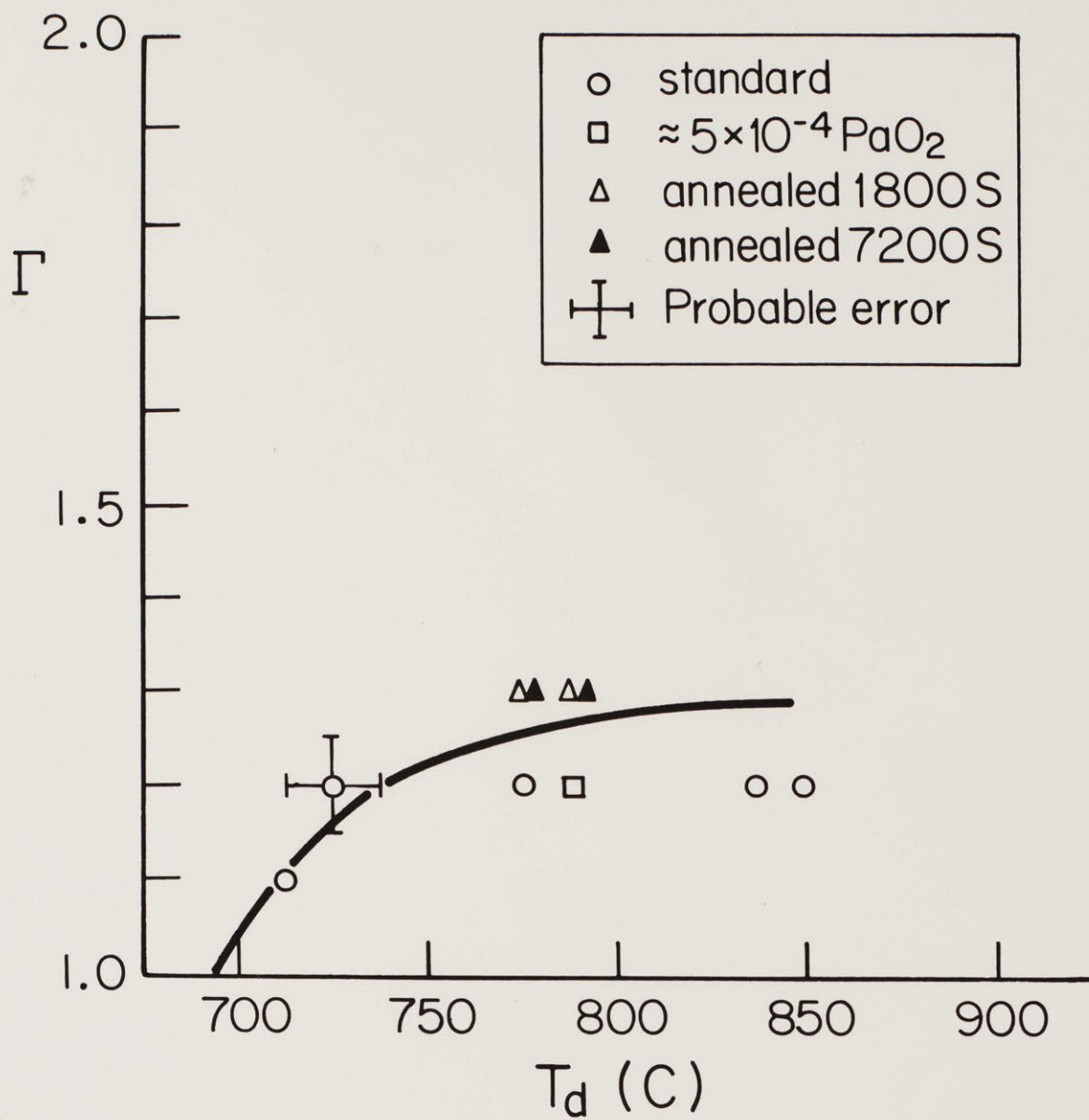
Fig. 30.   Residual resistance ratio vs. deposition
temperature: 21% Ge target.

Fig. 31. Residual resistance ratio vs. deposition
temperature: 23% Ge target.
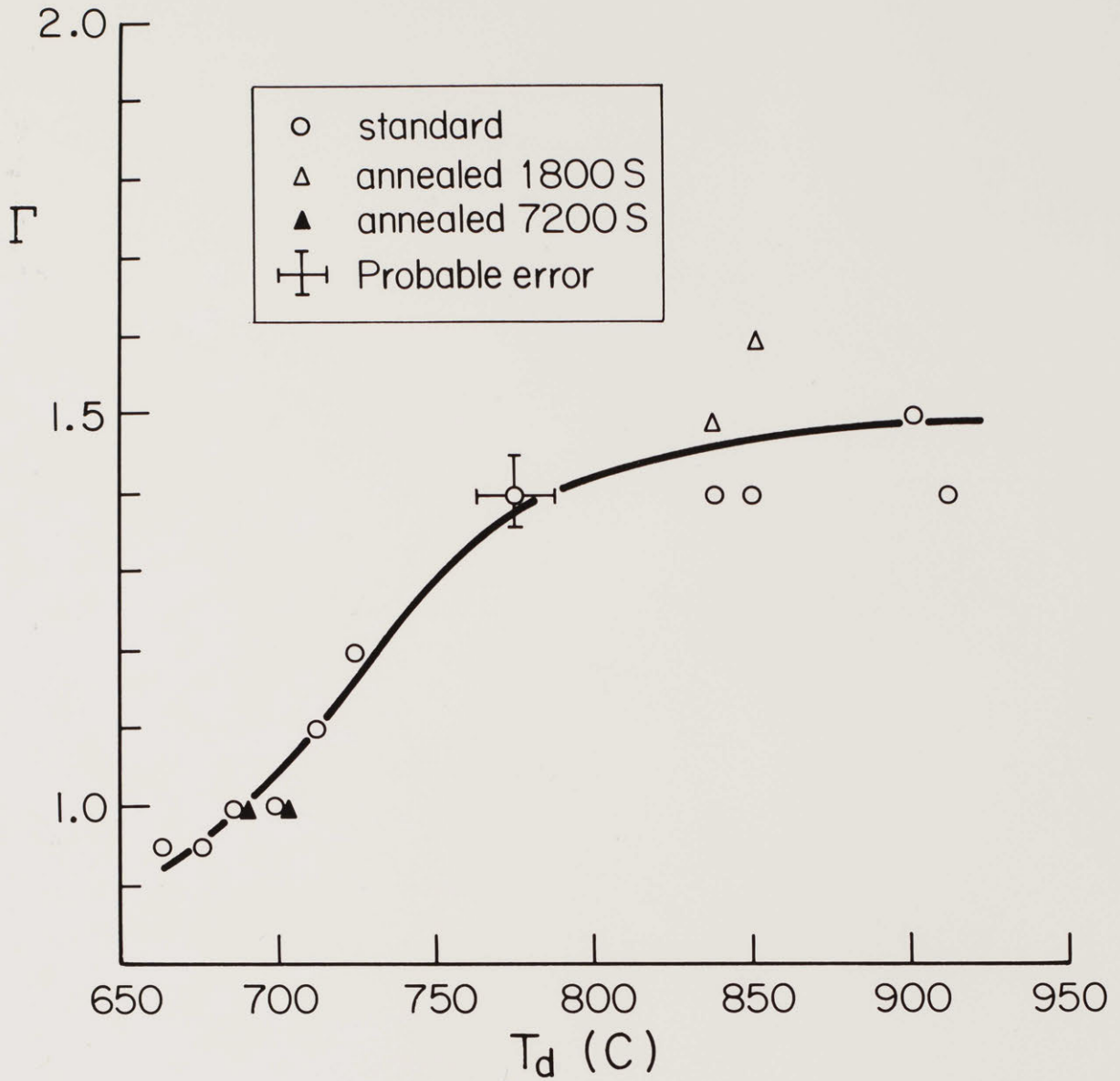
Fig. 32. Residual resistance ratio vs. deposition
temperature: 28% Ge target.

Table II - Sample Transition Temperature, Thickness, and Annealing Time.

Sample	Target (%Ge)	T_d (C)	Thickness (μm)	T_c onset (K)	T_c width (K)	ρ (μΩm)	Total Time at T_d (seconds)	Annealing Time (seconds)
2542	21	780	1.2	14.3	2.8	2.0	3,600	
25311		770	4.7	18.6	2.9	.9	14,400	
29222	23	850	.2	12.6	1.5	1.0	900	
29292		850	.2	14.5	1.7	1.0	3,600	2,700
3091		850	.2	16.8	2.0	.8	10,800	9,900
29242		840	1.2	14.8	2.3	1.1	3,600	
29312		850	3.6	18.1	2.5	.6	10,800	
21111	28	840	.12	18.7	4.7	1.2	600	
2161		840	.12	19.9	1.9	.7	3,600	3,000
30192		850	.12	19.7	3.9	.6	10,800	10,200
2011		840	.9	21.6	1.6	1.1	3,600	
21141		840	.8	21.8	1.6	.5	10,800	7,200
1762		810	2.6	21.3	1.5	.8	10,800	

Table III – Transition Temperature, Resistivity, Residual Resistance Ratio,
and Processing Parameters for Samples Deposited on Sintered
Alumina Substrates.

Sample	X-Ray Patterns	T_c (K)	Γ	ρ ($\mu\Omega$m)	Comments *
2341	Al_2O_3, A15, tetragonal, hexagonal	22.3	2.0	.7	
2342	"	21.8	2.0	.65	
2343	"	22.0	1.9	.6	
23101	"	22.3	2.1	.7	4×10^{-4} Pa O_2
23102	"	21.8	2.0	.75	"
23103	"	21.7	1.8	.8	"
23141	"	22.3	2.2	.8	annealed 1800 s
23142	"	21.8	2.2	.8	"
23143	"	22.1	2.2	.75	"
23161	Al_2O_3, A15, more tetragonal than 2314-, hexagonal	22.2	2.4	.7	annealed 7200 s
23162	"	21.8	2.4	.7	"
23163	"	21.9	2.2	.75	"
24163	Al_2O_3, A15, little tetragonal, little hexagonal	7.9			19% Ge target

Table III

Sample	X-Ray Patterns	T_c (K)	Comments *
24193	Al_2O_3, A15, little tetragonal, little hexagonal	13.0	21% Ge target
25313	"	17.9	deposition temperature 770 C, 21% Ge target, 4.8 um thick
26243	Al_2O_3, A15, intermediate tetragonal, little hexagonal	20.5	23% Ge target annealed 1800 s

*unless otherwise specified, the deposition temperature was 840 C, thickness .8 μm, at a sputtering pressure of 40 Pa Ar.

Table IV - Breaking Strain, Degradation of T_c with
Applied Strain, and Processing Parameters of Samples
Deposited on Ceramic Substrates.

Sample	Target (%Ge)	T_d (C)	Comments	Breaking Strain*	Strain (%)	$T_c^{\#}$ (K) Midpoint 10% resistance
			Alumina Substrate			
23143	28	840	annealed 1800s 5 x 10^{-4} Pa O_2	+.05	±.045	NC
23163	"	"	annealed 7200s 5 x 10^{-4} Pa O_2		+.04	NC
					−.05	NC
24163	19	"			±.05	NC
24193	21	"		−.05	−.05	NC
23163	28	"	annealed 7200s 5 x 10^{-4} Pa O_2 1 μm Au coat	+.14		
33202	"	"	1 μm Au underlayer	+.12	+.05	NC
					+.09	NC
			plain substrate	+.09		
			Superstrate Substrates			
29193	23	770	5 x 10^{-4} Pa O_2	−.14	0.0	13.10
					+.11	NC
					−.075	NC
					−.09	13.05
					−.10	13.00

Table IV

Sample	Target (%Ge)	T_d (C)	Comments	Breaking Strain*	Strain (%)	T_c# (K) Midpoint	10% resistance

Superstrate Substrates

Sample	Target (%Ge)	T_d (C)	Comments	Breaking Strain*	Strain (%)	T_c# (K) Midpoint	10% resistance
29223	23	840	.2 µm thick	−.11	0.0	12.30	
					+.08	NC	
					+.10	12.18	
					+.12	12.18	
					−.05	12.30	
					−.08	12.22	
29263	"	"	annealed 1800s		0.0	15.67	14.93
					−.05	NC	NC
					−.10	15.60	14.85
					+.12	NC	NC
29243	"	"		−.095	0.0	16.95	16.00
					−.08	16.77	15.80
29263	"	"	annealed 1800s	+.11	0.0	15.87	15.33
					+.05	NC	NC
					+.11	15.84	15.30
29313	"	"	3.5 µm thick, epoxy overlayer	−.16			
3023	"	"	5×10^{-4} Pa O_2, 1 µm Au overlayer	+.17			
			plain substrate	+.15			

Table IV

Sample	Target (%Ge)	T_d (C)	Comments	Breaking Strain*	Strain (%)	T_c[#] (K) Midpoint 10% resistance
			Sapphire Substrates			
26241	23	840		+.15	0.0	19.40
					−.05	NC
					+.11	19.32
			substrate with 1 μm Au overlayer	+.14		
33201	28	"	1 μm Au underlayer	+.18	0.0	20.40
					+.12	20.30

*These values have been corrected for differential contraction of the substrate and samples.

#Note T_c does not refer to onset in this table.

NC - No change

See Fig. 38 for graphical presentation of T_c vs. strain data.

the substrate changes from sintered alumina to Superstrate
to sapphire: ± .05%, ± .12%, and ±.15%, respectively. When
the films deposited on the ceramics were covered with a layer
of epoxy or 1 μm of Au, or when a 1 μm layer of Au was de-
posited on the substrate before deposition of the A15, the
breaking strain was increased to ± .15%, approximately the
same as the breaking strain of sapphire, regardless of the
particular morphology of the Al_2O_3 substrate. This included
ceramic substrates with intrinsic breaking strains of $\approx$ .09%.

Although the adhesion of the Au overlayer film on the
A15 was poor (e. g., the two films separated under thermal
cyling or light abrasion), the mechanical performance of
the overall Au-Nb_3Ge-substrate composite was equal to that
of the Nb_3Ge-Au substrate composite where a good mechanical
bond exists between the Au and both the A15 and substrate.

G. Transition Temperature

The overall composition of the film is the main deter-
mining factor of the transition temperature of the Nb_3Ge sample.
A plot of T_c vs Ge composition of the film, c_{Ge}, is given in
Fig. 33 and a least squares linear fit to the higher T_c data
is drawn in to indicate the best T_c obtained for a given
film composition. (The lower T_c points were not used in the
fit since the properties of these samples are likely to be
degraded by grain size, disorder, and/or defects.)
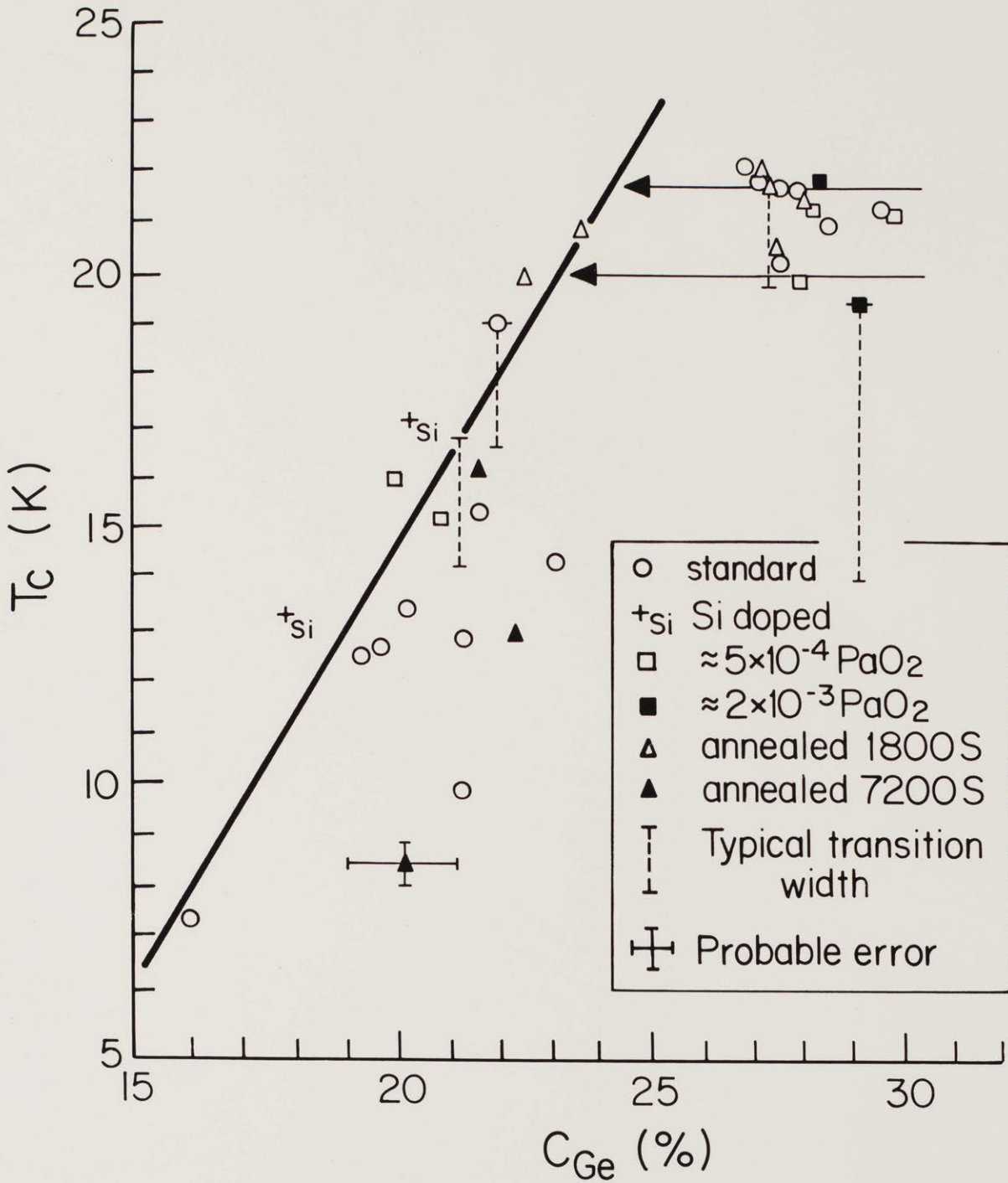
Fig. 33. Transition temperature vs. Ge composition of film.

Between approximately 16% and 23% Ge in the film the T_c increases, while for compositions above 25% there are two general clusterings of T_c, one between 21 and 22 K and the other near 20 K. The higher T_c group was observed to have narrower transitions.

Data from Nb-Ge-Si films deposited from a target where 10% of the Ge atoms had been replaced by Si are also given in Fig. 33. These samples have T_c's very close to those pre-dicted for binary Nb-Ge films in which only the Nb content of the film is considered; that is, the $1\frac{1}{2}$ to 2 percent Si in the film affects T_c in the same way as the Ge it replaces.

The effect of deposition temperature on T_c onset is shown in Figs. 34-36 for Nb-Ge samples produced from different compo-sition targets; typical transition widths are also given in the figures. It is seen that there is a deposition temperature at which T_c reaches a maximum, independent of oxygen pressure in the system or heat treatment, and this optimum T_d increases with c_{Ge}. Further, the width of the transition tends to in-crease as T_c decreases both above and below the optimum T_d with the exception of the samples deposited from the 23% target at 690 C (Fig. 35). At T_d's lower than the optimum there is a tendency for two transitions to appear in the samples deposi-ted from the 28% target.

The effect on T_c of increasing O_2 partial pressure in the sputtering system can also be seen in Figs. 34-36; T_c rises
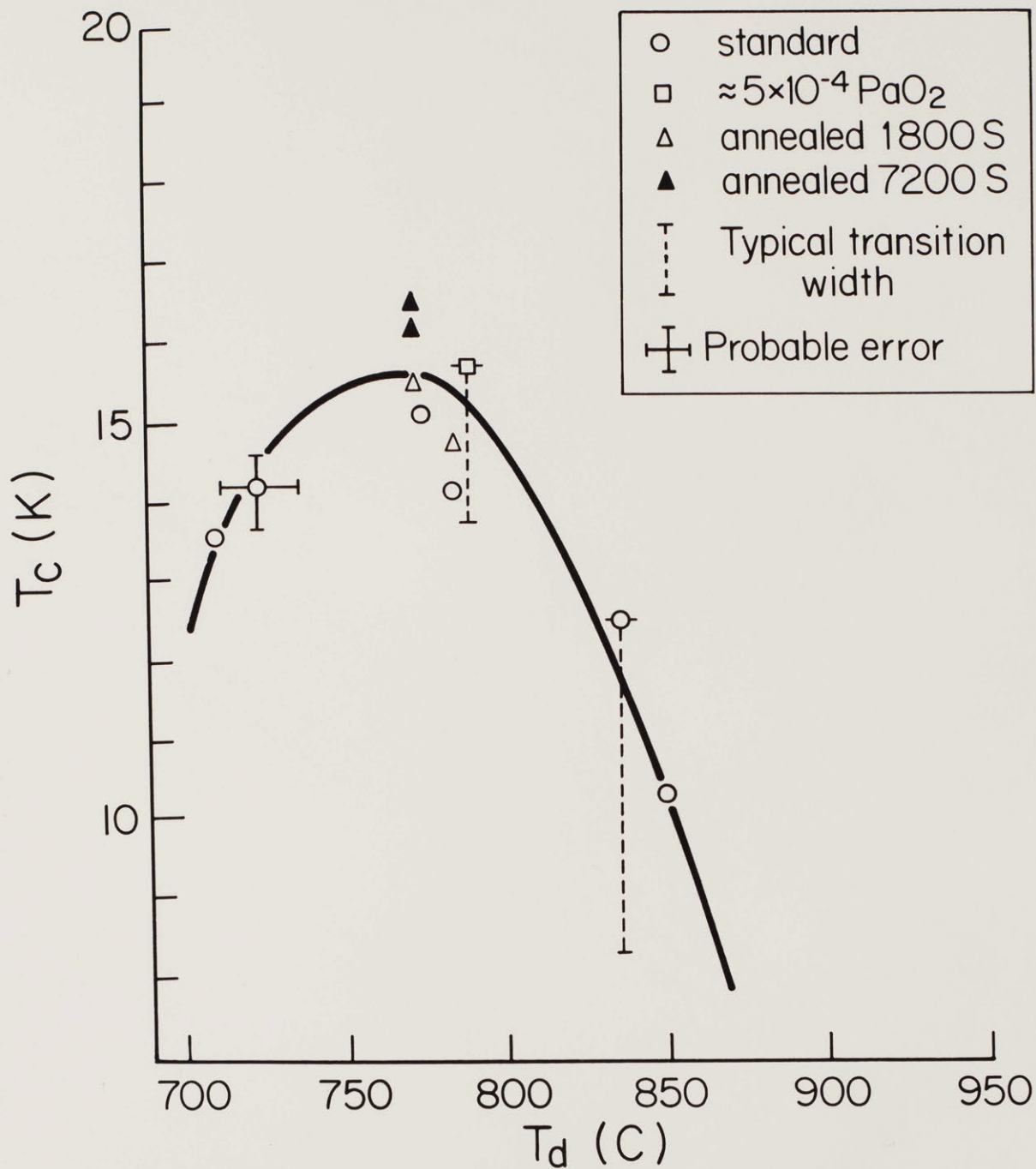
Fig. 34. Transition temperature vs. deposition
temperature: 21% Ge target.
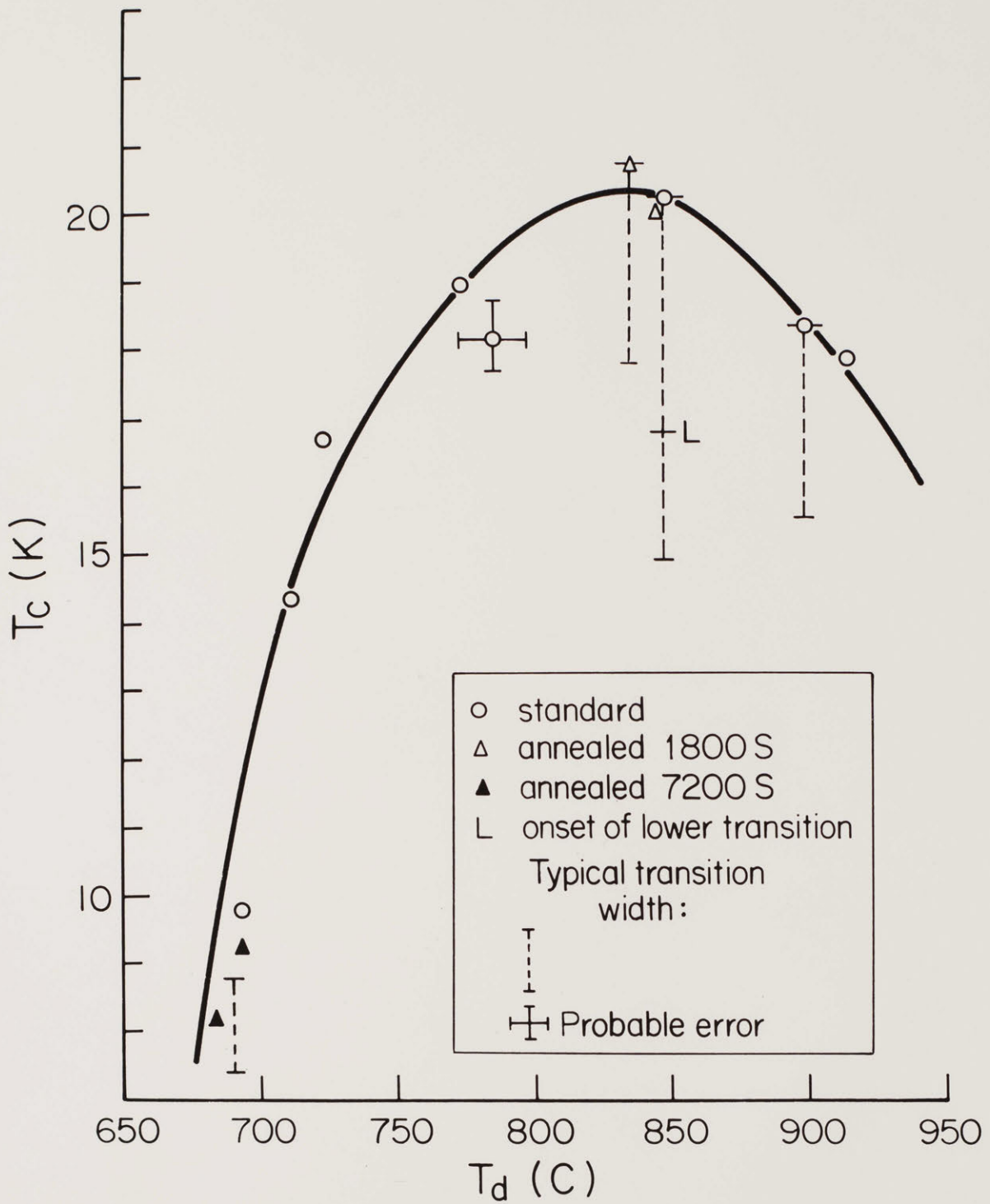
Fig. 35. Transition temperature vs. deposition
temperature: 23% Ge target.
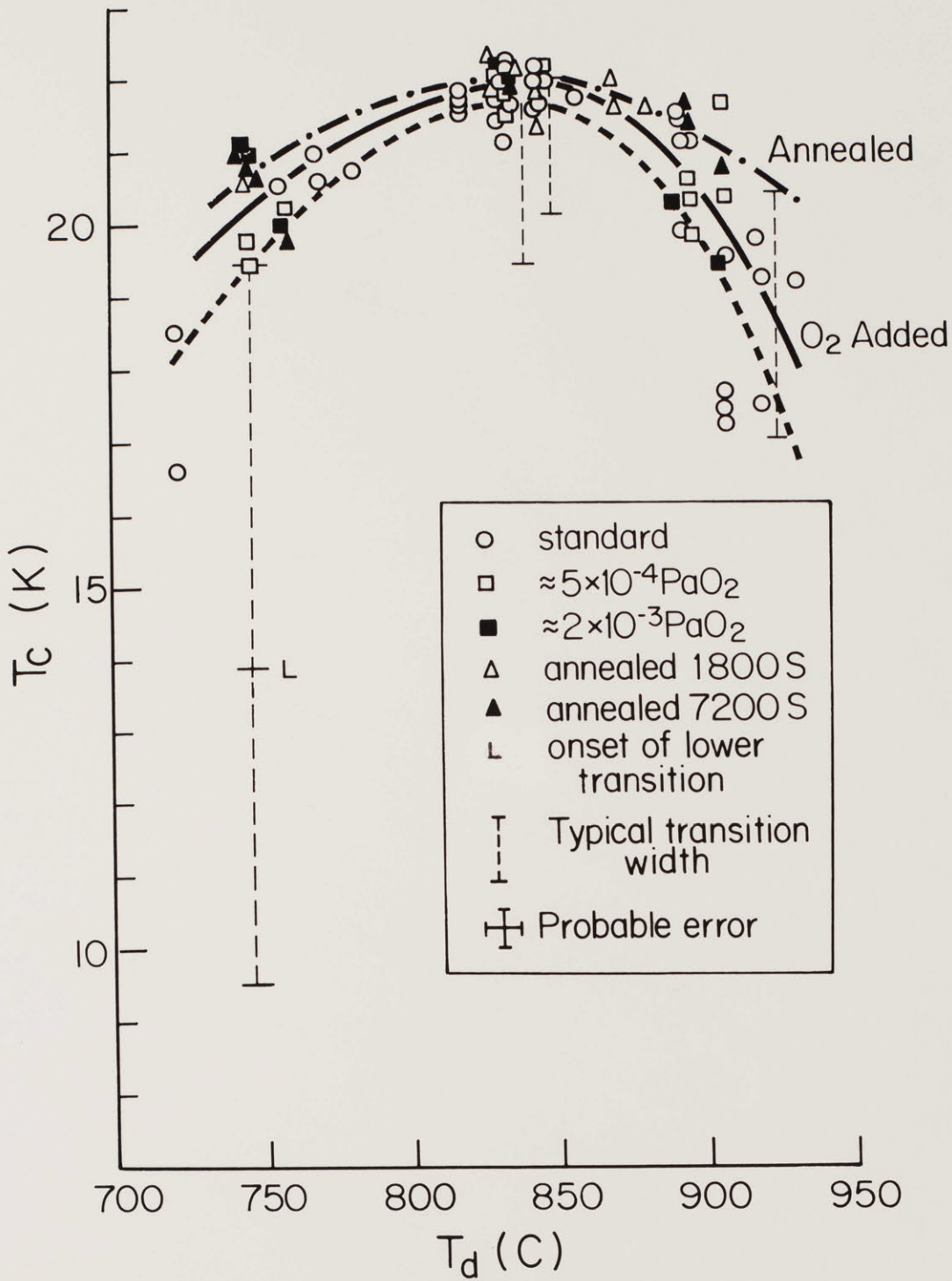
Fig. 36. Transition temperature vs. deposition
temperature: 28% Ge target.

with a higher partial pressure of O_2 during deposition.

Although extensive tests have not been made of the effect of Ar pressure on the properties of the film, and despite the uncertainty in absolute measurements of T_d (± 20 C), the data in Table V, representing samples sputtered from the 28% Ge target, suggest that at 33 or 53 Pa argon the width of the transition increases at the T_d which is the optimum for 40 Pa. This increase in width can be reduced by raising T_d as the Ar pressure rises. Since the highest T_c samples also appear to have the narrowest transitions, the data suggest the optimum T_d increases as the deposition pressure does.

The effect of annealing on the T_c of very thin films ($\approx$ 100-200 nm) is shown in Fig. 37 where it has been assumed that the as-deposited film has been annealed for 300-500 seconds (half the deposition time). The plot of T_c vs. $(\text{seconds})^{\frac{1}{2}}$ indicates the T_c first rises with annealing but then eventually declines; this degradation in T_c occurs earlier for films deposited from the 28% target than for the 23% target films.

Referring again to Figs. 34-36, it is apparent that the T_c of 1 μm samples are generally increased by annealing, and for the 28% Ge target this increase tends to flatten the T_c vs. T_d curve, that is, to extend the range of deposition temperatures over which T_c's above 21 K occur. For the 28% target the incidence of T_c's above 22 K increased for samples deposited at the optimum T_d and then subjected to annealing; for the

Table V - Sample Transition Temperature
and Argon Sputtering Pressure

Sample	P_{Ar} (Pa)	T_d (C)	T_c (K) onset	T_c (K) midpoint	T_c (K) finish	ΔT_c
21291	33	840	22.0	19.8	18.4	3.6
21292	"	850	22.0	19.6	18.2	3.8
21293	"	840	22.1	20.2	18.6	3.5
2011	40	840	22.3	21.0	20.2	2.1
2012	"	850	22.6	21.5	20.8	1.8
2013	"	840	22.1	20.8	20.0	2.1
19251	"	850	22.4	21.1	20.3	2.1
19252	"	860	22.2	19.9	19.0	3.2
19253	"	850	22.4	20.7	19.8	2.6
21261	53	840	22.7	21.1	19.3	3.4
21262	"	850	22.3	20.7	19.7	2.6
21263	"	840	22.5	20.7	18.7	3.8
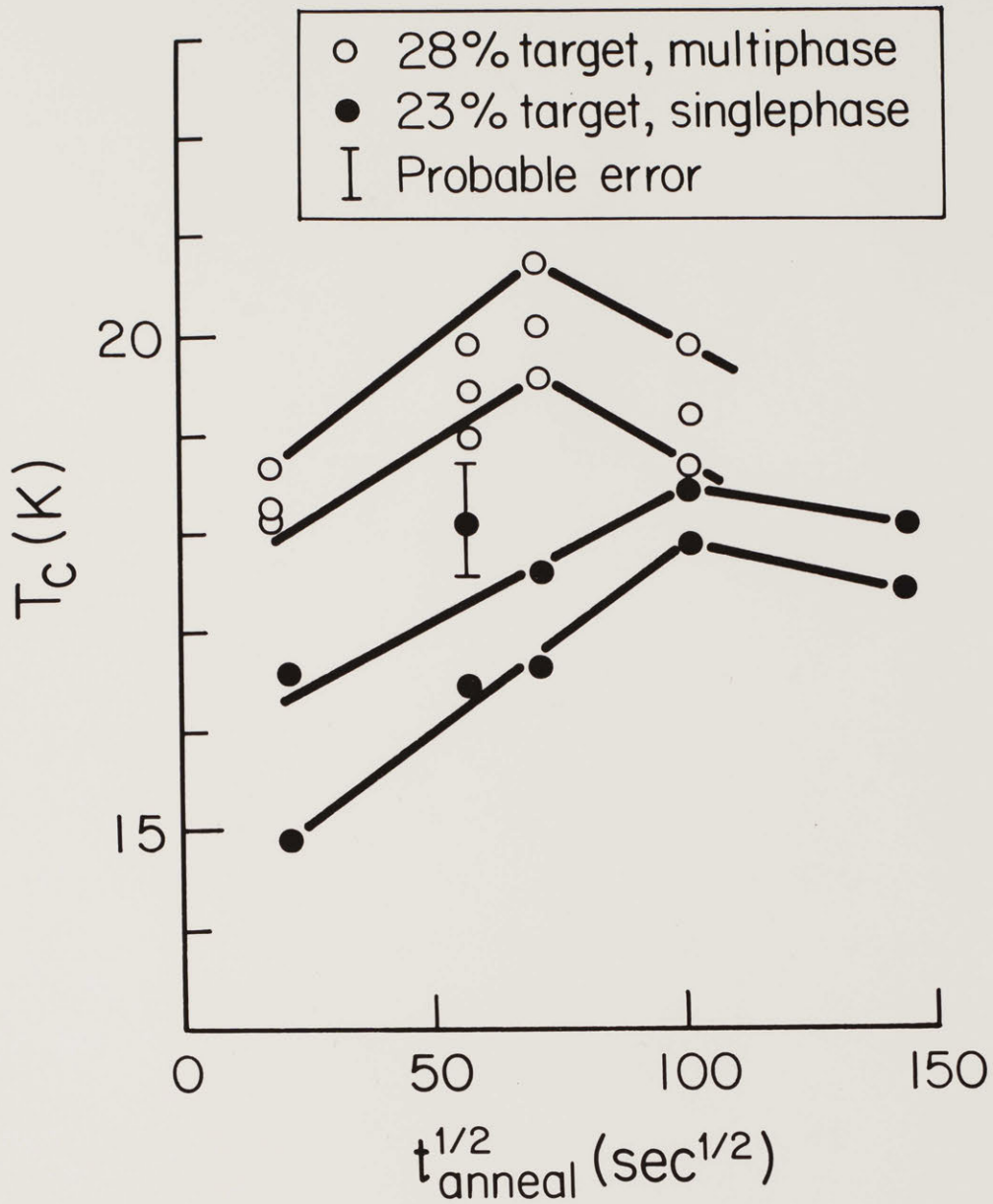
Fig. 37. Transition temperature vs. $(t_{anneal})^{\frac{1}{2}}$, $T_d = 840$ C, film thickness approximately 150 nm.

samples annealed for times up to two hours, the onset of the transition did not decline substantially but the midpoint and completion of the transition did. (In general, annealing took place _in_ _situ_ immediately upon the completion of deposition. Similar increases in T_c were, however, observed for samples that had been sputtered, characterized, annealed, and then recharacterized.)

The effect of sample thickness on T_c is included in Table II. For a given composition and annealing treatment after deposition, the T_c rises as the thickness increases from the vicinity of .15 μm to 1 μm. For the 28% target the T_c continues to increase with thickness up to 1 μm, above which T_c changes little. Table II also contains information on the T_c of films held at T_d for equal times but of different thicknesses. The results of heat treatment on the final performance of Nb_3Ge films indicate that T_c and the total time the sample is held at T_d are not independent. The data suggest the T_c's are slightly higher for the thicker films, which have larger grains than thinner films.

The effect of substrate species on T_c is not entirely clear. Comparing the data in Table III to that in Figs. 34-36, it can be seen that the T_c of a film deposited on alumina is about the same as a film deposited on a sapphire substrate with the same composition, O_2 partial pressure, and heat treatment. However, for the films deposited on metallic substrates,

accurate measurements of T_c from a direct reading of the voltage across the sample as the temperature is varied cannot be obtained because of substrate shunting effects. That is, the resistance of the substrate is much less than the normal state resistance of the film so the substrate acts as a shunt until the resistance has dropped to a value of 1% or less of its normal state. Assuming the 99% to 1% width of the transition in Nb_3Ge films on Hastelloy is the same as the width of films on sapphire, then the onset of superconductivity of films deposited on Hastelloy could be $\approx$ 22 K. In addition, sputtering pressures have to be increased for deposition of high T_c films on metallic substrates so that direct comparisons with ceramic substrate films are not possible. For these reasons comparisons are made only between trends on each substrate type. Within these limitations, the effect of a metallic substrate on T_c can be seen in Table VI in which the "99% onset" temperatures are recorded for Hastelloy substrate samples. Although the lower T_c's may be due in part to the shunting effect on the Hastelloy, they might also be real and attributable to the interdiffusion of the Nb, Ge, Ni, and Mo. A plot of the "99% onset" temperatures also reveals that there is an optimum T_d (near 870 C) for the metallic substrates as well as for the ceramic ones. Whether or not there is a real difference between the sapphire and the Hastelloy optimum T_d's, however, is not clear since the error in measuring the substrate temperature ($\pm$20 C) is approximately the same as the observed difference in T_d's. The superconducting

Table VI - Transition Temperature and Processing Parameters of Films Deposited on Metallic Substrates

Sample	T_d (C)	Target (% Ge)	Thickness (µm)	PAr (Pa)	X-Ray Patterns	T_c^* (K)	Comments
					Hastelloy B Substrates		
2231	840	28	.7	40	Hastelloy, Nb-Ni	15.0	5×10^{-4} Pa O_2
2232	850	"	.7	"	"	15.2	
2251	840	"	2.3	"	"	15.0	3×10^{-4} Pa O_2
22101	920	"	2.1	"	Hastelloy, other phases	19.3	"
22102	930	"		"	"	19.6	
22103	920	"		"	"	19.3	
22191	850	"	1.3	59	A15, Hastelloy, Nb-Ni	20.0	
22192	860	"		"	"	19.4	
22193	850	"		"	"	19.4	
22211	850	"		"	"	19.8	annealed 1800s
22212	860	"		"	"	19.3	
22213	850	"		"	"	19.5	
22281	860	"	1.4	"	A15 strong, Hastelloy	19.8	5×10^{-4} Pa O_2

Table VI

Sample	T_d (C)	Target (% Ge)	Thickness (μm)	PAr (Pa)	X-Ray Patterns	T_c* (K)	Comments
					Hastelloy B Substrates		
22282	880	28		59	A15 strong, Hastelloy	20.8	
22283	860	"		"		19.1	
28101	840	23	1.7	"	A15, tetragonal, Nb-Ni, Hastelloy	13.6	
28102	850	"		"		13.4	
28121	840	"	1.8	67	"	17.7	4×10^{-4} Pa O_2
28122	850	"		"	"	18.1	
28141	900	"		"	A15 stronger	18.1	3×10^{-4} Pa O_2
28142	910	"		"		19.8	
28181	770	"	1.9	"	poor pattern	<4.2	"
28182	780	"		"		<4.2	
28211	970	"	1.8	"	A15, Nb-Ni strong	<4.2	"
29151	900	"	2.1	"	A15, Nb-Ni, Hastelloy	14.7	2×10^{-5} Pa O_2
29152	910	"		"	"	14.4	

Table VI

Sample	T_d (C)	Target (% Ge)	Thickness (μm)	PAr (Pa)	X-Ray Patterns	T_c^* (K)	Comments
					Hastelloy B Substrates		
29171	900	23	2.7	67	A15, Nb-Ni, Hastelloy	10.1	2×10^{-5} Pa O_2 annealed 1800s
29172	910	"			"	9.8	
					Splat-Cooled Substrates		
18211	910	28	.8	40	many peaks	17.7	24% Ge flake
18212	930	"	"	"	"	20.2	"
22261	850	"	1.2	59	"	21.2	"
22262	850	"	"	"	"	12.0	29% Ge flake
					Nb Substrates		
22311	850	28	1.5	59	many peaks, strong tetragonal	20.4	
22312	860	"	"	"	"	21.0	

*Actual onset of superconductivity of these samples
is obscured by shunting effect of substrate and
can be expected to be somewhat higher.

onsets of films on the other metallic substrates used (Nb and splat-cooled Nb-Ge flakes) are approximately the same as for the Hastelloy, but the transitions are several degrees wider.

The effect of an applied tensile or compressive strain on T_c was only measured for films deposited on Al_2O_3 and Hastelloy substrates. The results of this effect on films deposited on Al_2O_3, given in Table IV and shown in Fig. 38a, indicate that although there is a fair scatter in the data, T_c does not seem to change within the precision of measurement (.05 K) until strains of about $\pm$.09% are reached. T_c then decreases upon fur- ther straining of the samples in either tension or compression and the decrease in temperature is uniform across the width of the transition; both of these effects are counter to what should be expected from incipient crack formation in the film itself. The rate of decrease is hard to estimate due to the scatter, but it appears to be about .05 K for each .01% increment of strain up to the breaking strain. The changes in T_c were rever- sible up to fracture; that is, T_c returned to its initial value when the four-point bending device was disengaged. (unfortu- nately, since the Au overlayer that increased the breaking strain of the A15-alumina domposite did not make a low noise contact to the A15 film reliable measurements of T_c with strains above approximately $\pm$.12% could not be made on polycrystalline ceramic substrates.)

Films deposited on Hastelloy substrates seem to exhibit a
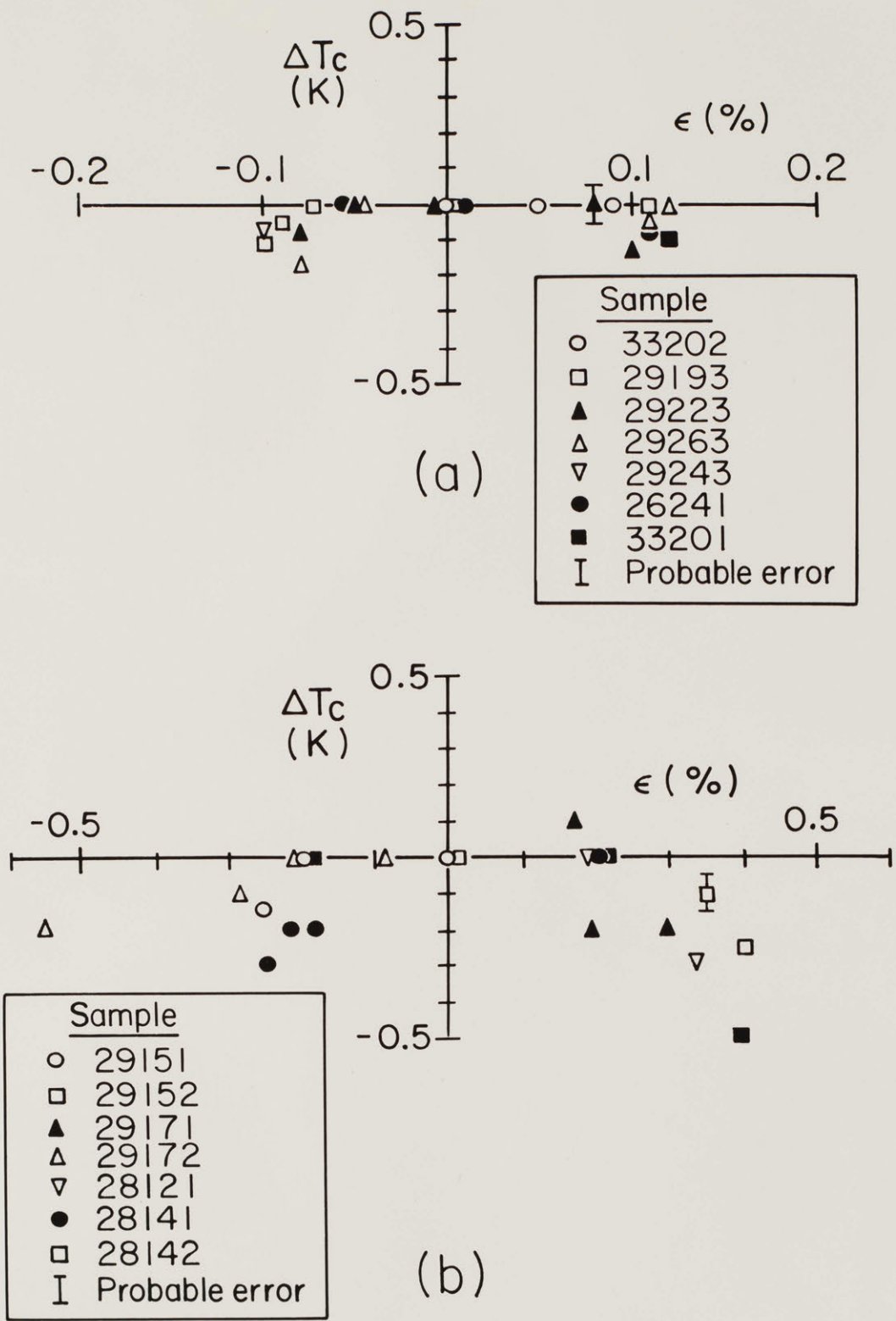
Fig. 38. Strain dependence of transition temperature of (a) ceramic and (b) metallic substrates. (See Table IV and Table VII, respectively.)

higher threshold for strain before T_c decreases. The data in
Table VII (and shown in Fig. 38b) indicate this threshold
strain is about $\pm.18\%$, beyond which T_c decreases for both ten-
sion and compression at a rate of about .25 K for an increment
in strain magnitude of .1%. Above about $\pm.3\%$ total strain, the
decrease in T_c of the samples is not reversible and some re-
sidual strain remains after the four-point bending device dis-
engages.

H. Effects of Processing Variables on Observed Properties

Film composition depends primarily on target composition
and T_d. The 21% and 23% Ge target films exhibit a peak in
c_{Ge} as T_d is increased, while the 28% Ge films appear to in-
crease in Ge content as T_d is increased. The composition of
the film does not appear to depend on thickness except near the
film-vacuum and film-substrate interfaces, as seen with the
Auger spectrometer. After an interface region is passed, in
which the species (and perhaps morphology) of the substrate is
influential, the composition of the film appears to be indepen-
dent of both the nature of the substrate and the thickness of
the film.

The phases present in the film depend mainly on target
composition, T_d, and length of annealing time: the amount of
tetragonal and hexagonal phases increase significantly be-
tween the 23% and 28% Ge targets, the higher Ge concentration

Table VII - Degradation of T_c with Applied Strain and Processing Parameters of Samples Deposited on Hastelloy B Substrates

Sample	Target (% Ge)	T_d (C)	Comments	Strain (%)	T_c# (K) midpoint
29151	21	900		0.00	12.37
				− .20	NC
				− .25	12.23
29152	"	910		0.00	11.70
				+ .35	11.60
				+ .40	11.45*
29171	23	900		0.00	15.70
				+ .17	15.80
				+ .19	15.50
				+ .30	15.50
29172	"	910		0.00	15.10
				− .09	NC
				− .21	NC
				− .28	15.00
				− .55	14.90*
				0.00	15.00
28121	28	840	5×10^{-4} Pa O_2	0.00	15.10
				+ .18	NC
				+ .34	14.80
28141	"	900	"	0.00	15.70
				− .18	15.50
				− .22	15.50
				− .25	15.40
				+ .20	15.70

Table VII

Sample	Target (% Ge)	T_d (°C)	Comments	Strain (%)	T_c# (K) midpoint
28142	28	910	5×10^{-4} Pa O_2	0.00	16.90
				+.20	NC
				+.40	16.40
				−.20	NC

#Actual <u>midpoint</u> of superconducting transition of these samples is obscured by shunting effect of substrate and can be expected to be somewhat higher.

NC - No change

* - irreversible

See Fig. 38 for graphical presentation of T_c vs. strain data.

films undergo a decrease in the amount of tetragonal phase present as T_d is increased, and annealing the films increases the amount of tetragonal phase while decreasing the amount of hexagonal phase present.

The lattice parameter follows both film composition and phase assemblage: decreasing with increasing film composition only up to $\approx$ 23% Ge where it becomes constant, and increasing with annealing time for a given composition. It may also be that films $\approx$ 150 nm thick may have a lattice parameter $\approx$ .003 nm larger than thicker films.

The A15 grain size of the films depends most strongly on T_d and film thickness. As T_d is increased the grain size increases to a point where it is $\approx$ 400 nm and then increases only very slowly or saturates, the "saturation" temperature increasing with c_{Ge}. The grain size also increases with thickness such that as the film thickens, the grain shape becomes less equiaxed and more columnar.

The morphology of the film depends on that of the substrate: so, for example, pits in the alumina surfaces manifest themselves as flaws in the A15 film and the grain boundaries and twins in the Hastelloy B grains are reflected in the morphology of the Nb_3Ge. The grain size of the A15 phase, on the other hand, is not affected. The nature of the substrate itself is the most significant factor observed to govern the breaking strain of the Nb_3Ge films. The pits

in the surface of the sintered alumina and the grain boundaries of the Superstrate apparently lowered the breaking strains of the composites. These strain values are then raised to the breaking strain of sapphire by including a 1 μm thick layer in the Al_2O_3 composite.

The T_c of the film depends on nearly all of the processing parameters to a greater or lesser degree; i. e., it may depend on some parameters secondarily through their influence on the structural elements described above. Increasing the Ge composition of the film raised T_c until a limiting Ge composition of approximately 23% was reached. Increasing T_d also raised T_c until an optimum T_d was reached, after which T_c decreased. This optimum T_d value itself changed directly with Ge content of the film.

The T_c also depends on heat treatment of the films and thickness, although these effects may well be linked together. Although unannealed films have a lower T_c than thick films, a significant fraction of this difference may be eliminated by annealing the thinner film. Annealing increased the incidence of T_c's above 22 K for films 1 μm or greater in thickness.

The application of strain decreases T_c. For ceramic substrates, strain magnitudes above .1% cause a decrease in T_c of about .1 K before fracture. For Hastelloy substrates a strain magnitude $\approx$ .18% had to be exceeded before T_c was lowered; it then decreases by about .3 K for an additional

strain of $\approx .2\%$ before plastic deformation of the substrate occurred.

The resistivity and residual resistance ratio may depend both directly and indirectly on the processing parameters. Increasing the target composition from 21% to 23% has little effect on the resistivity; however, a sharp decrease in ρ accompanies the change from the 23% to the 28% target. The resistivity of the film drops as T_d is increased, with a break in these curves occurring at a T_d near the optimum for T_c. Annealing lowers ρ for low T_d samples. The resistivity decreases upon increasing film thickness from 150 nm to 1 μm.

The residual resistance ratio, Γ, rises at low T_d and then saturates near the optimum T_d for 21% and 23% target films. The 28% target samples exhibit a nearly linear Γ as a function of T_d for high O_2 partial pressures and/or for long anneals.

It is noteworthy that the peak in Ge concentration for the 21% and 23% targets, the minimum in diffuse background, the attainment of maximum grain size, the maximum in T_c, and the change in slope of ρ and Γ all occur at about the same T_d for a given target. This T_d for maximum T_c and well developed grain size, increases from ≈ 790 C for 21% Ge films to ≈ 820 C for 23% Ge. The 28% Ge films in the multiphase region, have an optimum T_d at about 840 C where the films have approximately 24% Ge incorporated in the A15 phase (as determined by lattice parameter measurements).

VI. Discussion and Interpretation of Results

In this chapter the effect of the structure of the films on their properties is discussed, and a comparison made with work done in other laboratories. Whether an attribute of the film is seen as structure or property will depend on the context of the discussion (see Chapter I). For example, the lattice parameter will be interpreted as an element of structure in the discussion of T_c since it is the unit of translation in the lattice, while later, a_o will be treated as a property itself, influenced by composition and other factors. The means of controlling the structure of the films so that desired properties are obtained are also discussed. The key elements in the discussion are film composition, long-range order and/or the presence of film defects, and, finally, phase distribution and grain size and shape.

A. Relationship Between Structure and Properties

Lattice parameter behavior is influenced by composition and, for a given composition, by the long-range order of the film. If one considers composition alone, it is interesting to note the extrapolation of the A15 lattice parameter to "A15 Nb_3Nb" in Fig. 14 and in the literature[95] yields a value of .523 nm, or a volume per atom of 1.79×10^{-29} m^3, which differs from the volume per atom of bcc Nb by only .3%. Thus, the interatomic distance along the A chains of the

hypothetical A15 Nb_3Nb compound is .262 nm, fairly close to twice the covalent radius of Nb which is .268 nm. The short A chain Nb-Nb distance has been interpreted as evidence of a strong covalent bond between atoms along these chains such that the bond is believed to become more metallic in character as this distance increases.[78,96,97] While the Nb-Nb bond can be regarded as partially covalent, the Nb-Ge bond length is larger and thus this latter bond has more metallic character.[78]

It was observed in A15 compounds that changing the B element changes the lattice parameter independently of the A element and, similarly, when the A element is changed the change in lattice parameter does not depend on the B element.[40] This has led to the derivation of radii of the elements in A15 compounds that predict the lattice parameter by assuming the A and B elements make contact along [210] in the crystal. That is, $r_A + r_B = \sqrt{5}/4 \, a_o$ where r_i is referred to as the Geller radius of the constituent.[8] However, to determine the effective Geller radius of Ge in Nb_3Ge for a disordered material one must determine an effective Geller radius of Nb on the A15 B sites. This can be done by using the data in Fig. 14 and the Geller radii of Nb and Ge on their proper sites, .151 and .136 nm, respectively, and assuming the radius of the B site is weighted by the concentration of Nb and Ge present. This leads to an estimate of .141 nm

for Nb on a B site, which is in accord with Zachariasen's
Rule: a site with lower coordination number has a lower
effective radius.[49]

If one now considers, for a given composition, that Ge
and Nb atoms interchange themselves to some degree by neutron
irradiation then this will change the lattice parameter.
Irradiation data[19] indicate the lattice parameter of a
$Nb_{76}Ge_{24}$ sample has a value of .519 nm when the T_c has been
degraded to about 3 K from 10.7 K. Assuming that the sample
was virtually free of antisite defects before irradiation
and completely disordered afterwards and that the radii
of both the disordered A and B sites are averages of Nb
and Ge radii weighted 76:24, this implies a Ge A site radius
of .146 nm, which is .010 nm larger than the B site radius.

The above estimate of the Ge A site radius may be more
tenuous than the Nb B site radius because the change in a_o
may be partly due to introduction of vacancies or inter-
stitials during irradiation or partly to a departure from
equilibrium positions with very low long-range order. The
vacancies would be expected to decrease a_o while the latter
effects would be expected to increase the lattice parameter
and the Geller radii; that is, a weaker bond implies less
overlap of orbitals. This estimate of the Ge radius on the
A site indicates a break should occur in the a_o vs c_{Ge}
plot at 25%. Although such behavior is consistent with

the behavior of codeposited films,[61] it was probably not
observed in the present research because the highest Ge
content incorporated in the A15 phase appeared to be 23% -
24%.

Resistivity and residual resistivity ratio have been
used as indicators of the T_c of the films[30,98] in the belief
that they depend on the same structural parameters as the
T_c of the film. There is also interest in the resistivity
of Nb_3Ge for its own sake, since it determines the electrical
behavior of the material should its superconductivity be
quenched for any reason in an applications environment.

There is no clear dependence of resistivity, ρ , on
the composition of the film, as seen in Figs. 27-29. It
is not surprising that the resistivity increases as T_d is
lowered because this change could be expected to decrease
grain size, to increase the vacancy concentration, or to
lower the long-range order in the films as the atoms have
less mobility and remain in the positions where they land.
Increased grain boundary area, vacancy concentration and
antisite defects would be expected to increase the resis-
tivity of the material by decreasing the mean free path of
the electrons. The decrease of the maximum ρ obtained
with Ge concentration may only be a manifestation of these
effects. Films with the lowest Γ 's are those that were

deposited at temperatures below the optimum T_d. Apparently
the contribution of phonon scattering to the room tempera-
ture resistivity is not sufficient to increase ρ signi-
ficantly, due to the great amount of disorder in these
samples. In fact, there is little difference between
the resistivity of films deposited from 19%, 21%, and 23%
Ge targets at the same temperature; this may simply mean
that compositional sensitivity of ρ is secondary to that
of the effects of disordered regions, grain boundaries, and
defects. The large change in resistivity for 28% Ge target
films compared to the 21% and 23% target films appears to
be due to the presence of multiple phases, as is apparent
in Table I.

Annealing samples lowered the resistivity of the films
deposited at the lowest temperatures. This may be due to
the elimination of vacancies in the material, increasing
the grain size at a level below the resolution of the SEM,
or to elimination of antisite defects in the material. On
the other hand, for these films, Γ was not affected by anneal-
ing. This again indicates that the phonon contribution to
ρ for low T_d samples is small; the structural defects re-
maining in the films after annealing are still significant
and probably continue to be a collection of grain boundaries,
vacancies, and antisite defects.

As mentioned above, the resistivity of the films is

markedly influenced by the presence of other phases in the samples, with ρ being reduced by 50% or more with the introduction of approximately 20 volume percent tetragonal phase while the A15 phase has approximately the same grain size, Ge concentration, order, and T_c. Percolation theory suggests that approximately 15% concentration is the regime where the resistivity of a composite drops sharply as low ρ material is added to it.[99] No data exists to preclude the possibility of Nb_5Ge_3 being a low resistivity phase; the data are not sufficiently accurate to estimate its resistivity. If the tetragonal phase has the same phonon scattering contribution as the A15 phase and Mathiessen's rule is approximately valid, films which have a low resistivity at low temperature and a significantly higher ρ at room temperature would be predicted, yielding a higher Γ. This is the observed behavior of the films described in this work.

Breaking strain appears to depend only on the film substrate and the presence of a ductile auxiliary film either above or below the A15 layer. An overlay of approximately 1 μm of Au, a thin overlayer of epoxy, and a 1 μm deposited Au layer between the Al_2O_3 and Nb_3Ge were each able to raise the breaking strain of such composites to the vicinity of $\pm$ .15% while the A15 films deposited on alumina without an overlayer failed at $\approx \pm$ .06% and those on Superstrates

near $\pm$.11%. The as-received alumina substrates broke at

strains $\approx$ $\pm$.09% while the as-received Superstrates broke at

about $\pm$.15%. Sapphire substrates failed at $\approx$ $\pm$.15%, irrespec-

tive of the presence of A15 or other films. The failure of

the composites at the breaking strain of sapphire suggests the

maximum strength of the A15 films is at least .15%; this could

be determined by breaking the films that had been removed from

their substrates although this was not done in the present work

because of the difficulty in removing these films intact. The

observed flaws in the other ceramic substrate materials probably

acted to degrade the breaking strain of the substrates; this

degradation could, however, be partially compensated for by an

under or overlayer film in the composite. It can be shown

(Appendix B) that the compressive strains induced at the surface

of either an Al_2O_3 substrate or an A15 film lying on an Al_2O_3

substrate due to thermal expansion mismatch of Au, Nb_3Ge, and

Al_2O_3 are negligibly small compared to the strains applied to

break the samples while incipient cracks would presumably lead

to asymmetric behavior in T_c vs. ϵ . It therefore appears that

the function of the Au or epoxy layer is to remove the stress

concentrating flaws that occur either in the surface of the sub-

strate-film composite or in the substrate itself. It may be

that the ductile layer is acting to reduce the stress concen-

tration factor of a sharp crack, which is given by $2\sqrt{\frac{c}{\rho}}$ where

C is the depth of the crack, and ρ the crack-tip radius.[100]

This factor is multiplied by the applied stress present to deter-

mine the stress at the tip of the crack. Depositing material in the crack can act to blunt the crack tip (increase ρ) or decrease the depth of the crack (decrease C). Both effects will, of course, lower $\sqrt{\dfrac{C}{\rho}}$ and therefore the stress at the crack tip, allowing a higher stress to be applied before the fracture stress is attained. A ductile material deposited in a sharp crack can plastically deform under applied stress rather than dissipate the work done by the creation of new surface area which propagates a crack. A propagating crack would increase C and thereby aid further crack propagation. Therefore higher levels of stress can be reached before crack propagation by depositing a ductile material in the crack. (Note, however, the exact function and role of the overlayer films, which have a weak adherence to the A15 films, remain undetermined.)

The transition temperature of the Nb_3Ge is most strongly influenced by the Ge content of the A15 phase which in turn is determined by the Ge content of the film. Referring to Fig. 33 note that the highest T_c for a given concentration increases at a fairly linear rate with increasing Ge concentration until a composition around 23% Ge is reached. At higher Ge concentrations the T_c's fall in a band between 19 K and 23 K. The general trend of these data and the absolute values measured are in good agreement with data[30,31,34,49,63] from other laboratories,

given the 1% uncertainty in composition most groups cite.

The saturation of T_c around 23% Ge might be due to entry

into a two phase region in the binary phase diagram; support

for this argument comes from a plot of A15 lattice para-

meter with film composition. In Fig. 14, the lattice

parameter varies smoothly with composition, decreasing as

the Ge concentration increases until a value of approximately

23% Ge is reached; a_o is then very close to this same value

when the films contain 26-29% Ge. Such behavior is often used

in physical metallurgy to define the extent of single phase

regions in binary systems: the lattice parameter follows

the change in composition in a monotonic fashion in the

single phase region and in the two phase region the com-

position of the phase of interest does not change and

neither does its lattice parameter. The intersection of

the extrapolated one phase lattice parameter and the two

phase lattice parameter occurs at the composition where the

second phase first appears.[64]

This procedure relies on the assumption that the com-

position of the phase of interest is known in the region

where the lattice parameter is varying. In our case this

means the films are either single phase or the amount and

composition of the extra phases are known. However, as

discussed in detail in Chapter V, an absolute determination

of the amounts of second and third phases present in the

films is not possible. On the other hand, it seems reasonable to assume that films with weak tetragonal or hexagonal peaks in the 2θ range from $20°$ to $150°$ (despite preferred orientation) are nearly single phase, i. e., that essentially single phase material is contained on the Nb rich side of the 1% uncertainty of the film composition.

Accepting this assumption, and further assuming that the lattice parameter of Nb_3Ge varies linearly with composition, the data in Fig. 33 imply that the films with T_c's above 20 K contain more than 23% Ge and that the films of overall composition of about 26-28% Ge contain 23-24% Ge in the A15 lattice (recall that the maximum solubility of Ge in the A15 phase is 22%,[63] corresponding to a $T_c \approx 17$ K).

Along with the apparent supersaturation of Ge content in the nearly single phase samples mentioned above, a_o decreases as T_c and Ge concentration in the A15 phase increase (Fig. 39); that is, the amount of Ge dissolved in the lattice is not an absolute number and can be altered by experimental conditions. In addition to varying the target composition, the supersaturation can be changed by varying the deposition temperature, varying the time at that temperature, and varying the partial pressures of impurity gases[33,51] present in the sputtering can. In one set of experiments, undertaken in a different laboratory, 26% Ge was dissolved in the A15 lattice by depositing the film on a polycrystalline
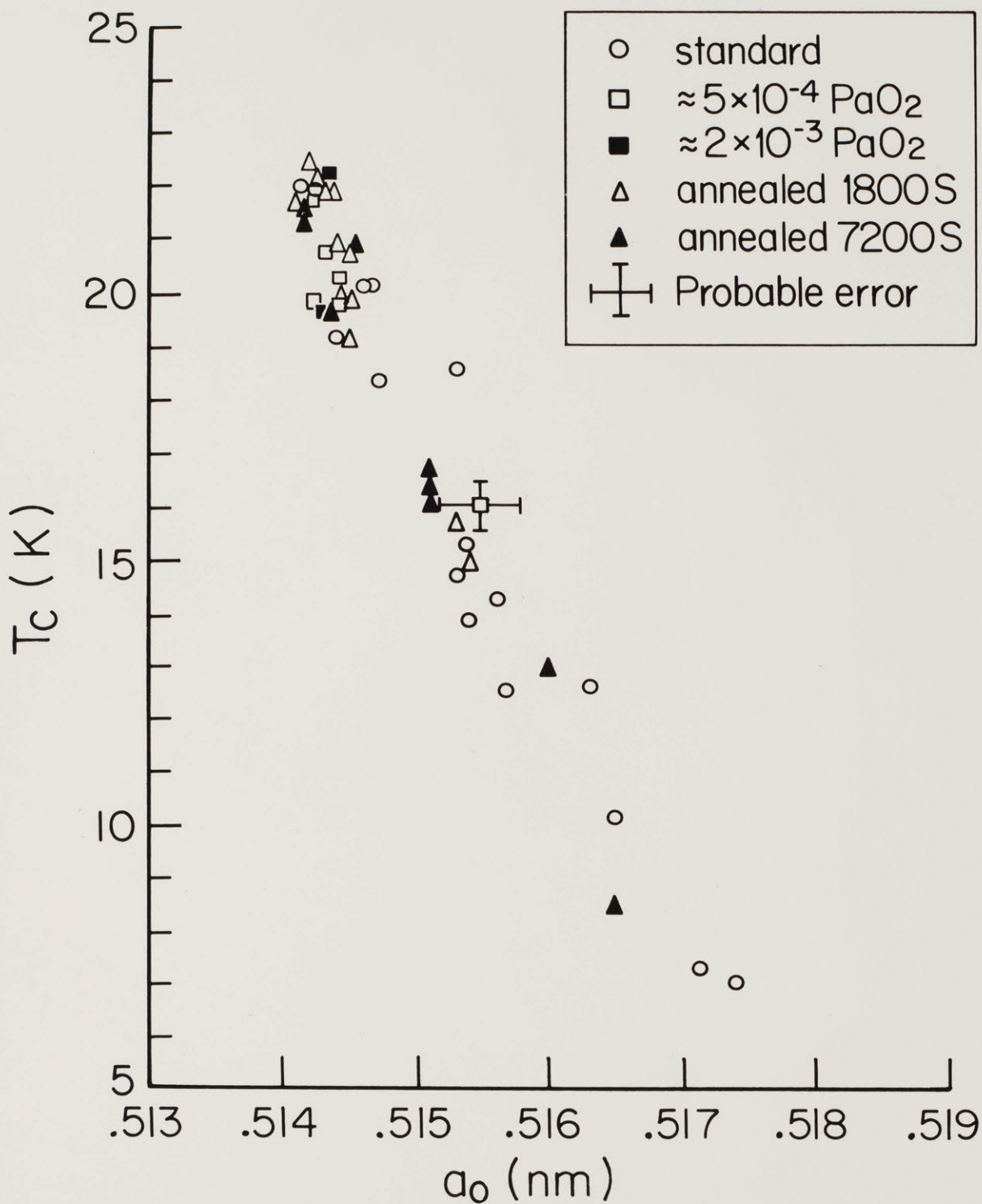
Fig. 39.   Transition temperature vs. A15 lattice parameter.

Nb_3Ir substrate; T_c increased smoothly with Ge content to over 22 K at a composition close to 25% and then declined.[56] Therefore, although it appears that composition is the most important parameter in obtaining high T_c Nb_3Ge, the equilibrium concentration of Ge in the lattice must be exceeded and raised to the vicinity of 25% to obtain T_c's above 22 K.

Other influences on T_c are grain size, crystallinity, and long range order of the film. In the present context "crystallinity" refers to the extent of translational symmetry around a given point in a film, and implies a grain size of a few nm or larger. "Long range order" refers to occupancy of lattice sites of a particular point symmetry by particular constituents. In the case of Nb_3Ge this means occupancy of the primitive cell face sites by Nb and the bcc-like sites by Ge; interchanging the Nb and Ge atoms creates what are known as antisite defects.

The effect of long-range order on the T_c of A15 materials has been investigated extensively in the past.[11,16-19] These studies have led to the general conclusion that T_c of the material is increased by as much as several degrees when the antisite defects present in the compound are decreased. For example, interchanging 1% of the Nb atoms on the A element sublattice with Ge atoms has been shown to lead to a decrease of 3.0 K in T_c.[19] An estimate of the

long-range order parameter, S, can be obtained by measuring
the relative intensity of the A15 (110) and (440) peaks; this
ratio should be proportional to the square of the difference
of the scattering factors of the A and B sites, which is
in turn proportional to the square of the long-range order
parameter. This ratio will be zero when the lattice is com-
pletely disordered and reaches a maximum when completely ordered.
Furthermore, the choice of these two peaks, which correspond
to parallel planes, should eliminate complications from pre-
ferred orientation of the films (see Chapter IV). Besides
consideration of preferred orientation and multiple phases
present in the films, large uncertainties exist in the exact
thickness of the films, the film density, the level of diffuse
background, the exact vacancy concentration, and the precise
Debye-Waller factor for A15 Nb-Ge. These uncertainties in
combination with the large noise levels present in the inten-
sities of the (110) and (440) peaks led us to believe that
including more peaks in the computer refinement to deter-
mine long-range order could not be expected to increase sig-
nificantly the accuracy of the value of S extracted for the
sample sizes of films fabricated in this work. Indeed, only
a general trend in the ordering of the films as a function
of T_c can be determined from the (110) and (440) intensity
ratio data (Table I).

The behavior of T_c vs. S is shown in Fig. 40 for annealed samples produced from the 21% Ge target. The calculations of the theoretical intensity ratio of these peaks are given in Appendix D; they take into account the sample composition, thickness, reported Debye-Waller factor,[49] and the Bragg angle of the beam. These calculations indicate that the measured values of the ratio of the (110) and (440) peaks are larger than is theoretically possible. Considering the uncertainties in these measurements, it is not surprising the least-squares-fit slope of T_c vs. S disagrees significantly with and contains within the scatter that value derived from the work at Brookhaven where several x-ray peaks were used to determine the long-range order parameter of samples in 20 to 100 mg quantities (as opposed to <1 mg in this work). This gross disagreement probably arises because the effect of the individual experimental uncertainties in measuring S and T_c is to cause even greater uncertainty in the slope of S vs. T_c. For instance, decreasing S by 1% in the Brookhaven data accompanies a decrease in T_c of .7 K; this is approximately equal to the error in measuring T_c in the present work and corresponds to a change of S of 11%, approximately the noise level of the (110) and (440) peak ratio.

Despite the discrepancy in the behavior of long-range order and T_c between this work and the Brookhaven work, the behavior of T_c as a function of annealing agrees quite well.
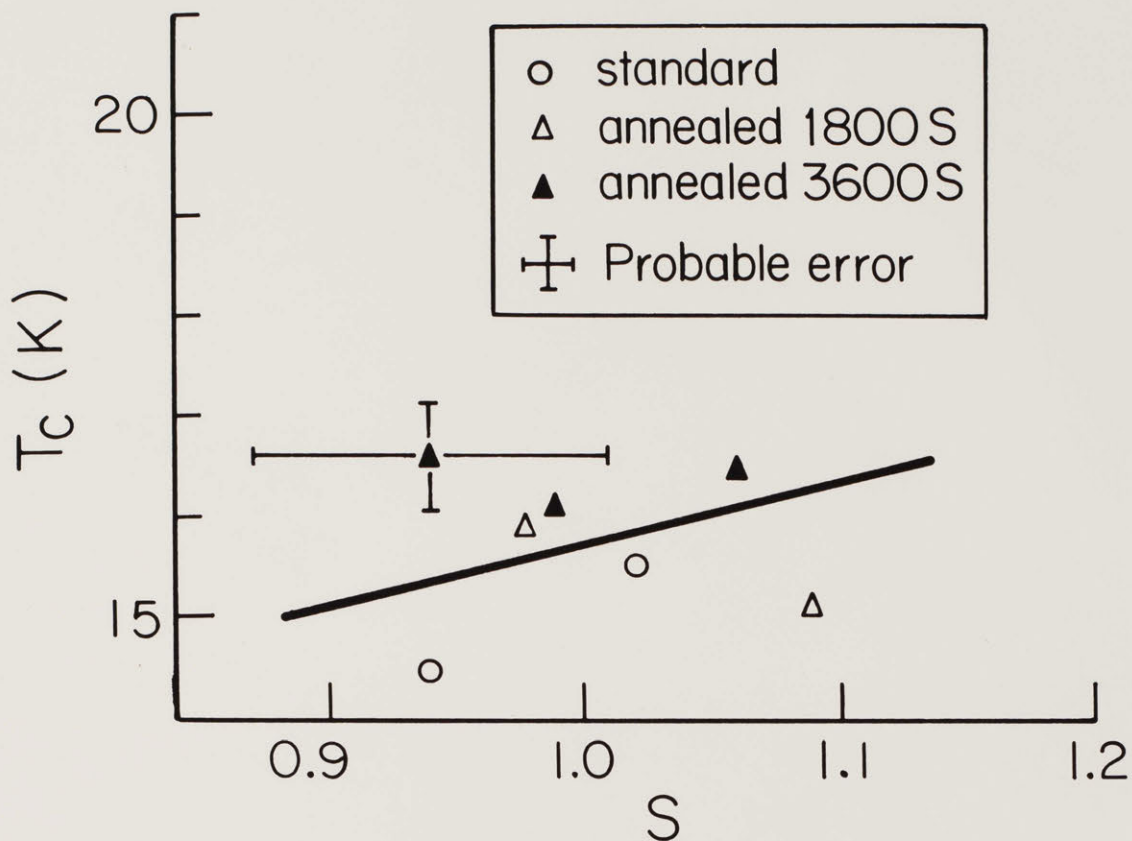
Fig. 40. Transition temperature vs. long-range order parameter: 21% Ge target, T_d = 770 C.

In the Brookhaven work, the Nb_3Ge samples showing a decrease in long-range order parameter and T_c upon irradiation returned to approximately their original values after an anneal of two hours at temperatures between 700 and 900 C;[19] this behavior is similar to that presented in Fig. 37 where samples reach their peak values of T_c after 1½ to 2 hours annealing time at 840 C. Note also that T_c increases at a less than linear rate, which agrees with the expected rate of change in order parameter with annealing:[19] the lattice approaches perfect order by diffusion of antisite defect-atoms to the appropriate sites. These defects become fewer in number and more widely separated in distance as ordering progresses; as a consequence the rate of ordering decreases. After approximately two hours, the rate of increase of T_c with ordering falls below the rate of decrease of T_c due to the formation of tetragonal phase and the increase of Nb content of the A15 phase because of the precipitation of this second phase. Similar behavior is observed for bulk A15 compounds upon annealing; i. e., order increases, T_c initially increases and then decreases as segregation occurs.[101] The trend towards equilibrium during long anneals is also suggested by the decrease in the amount of hexagonal phase present (Table I). (The hexagonal phase itself is believed to be a metastable phase in the Nb-Ge system.[63])

The Brookhaven samples exhibited an increasing lattice parameter with progressive irradiation and decreasing long-range order. That data indicates T_c decreases with increasing a_o. The slope of T_c vs. a_o is about 20% greater[19] than that shown in Fig. 39. The change in a_o observed in this study depends on compositional variation but also includes effects of ordering. Removing the samples deposited at T_c's below optimum from the data set reduces the slope in Fig. 39 by $\approx$ 5%. The change in T_c of these low T_d samples with a_o is intermediate between that caused by compositional variation and that caused by irradiation induced change in long-range order parameter.[19] The diffraction patterns of these low T_d samples also showed more diffuse background than those at higher temperatures, indicating less well ordered material. (A vacancy model to explain this T_c vs. a_o behavior is not really reasonable because of the large vacancy concentrations required.[17,49])

There is, however, another possible interpretation of the irradiation studies of A15 compounds;[78] i. e., the defect responsible for the decrease in T_c is a "puckering" of the A chains caused by a bombardment-induced displacement of atoms from their equilibrium A15 positions. This explanation, on the other hand, disregards the Huang-Borie or size effect where disordered alloys experience a displacement due to a change in size or valence of the constituent atoms on a particular

lattice site.[79] The observed displacement increases with
the decrease in the long-range order parameter of these
samples. Indeed, if the displacements are not caused by a
change in long-range order parameter and the accompanying
change in the outer electrons of neighboring atoms, what
keeps these atoms in their non-equilibrium, and presumably
high energy, positions? Evidence for the presence of inter-
stitials is negative,[76,78] vacancies are possible but are re-
quired in large concentrations,[49] and TEM work has shown
no peculiar defect-related contrast in the A15 phase[82,83]
except for a possible high temperature superlattice.[28]
Therefore, if puckering of the chains is the mechanism be-
hind the change in T_c with disordering, it seems to the
author as if the cause of the puckering is simply the natural
antisite defects inherent in these irradiated films.

According to Mathiessen's Rule, the residual resis-
tance ratio is related to the quantity of defects in the
sample; the higher Γ is, the more perfect the sample.
The plot of T_c vs. Γ , including samples deposited from
different composition targets, is shown in Fig. 41. Al-
though there is considerable scatter in the data, especially
at lower Γ , T_c does increase with Γ . However, it
appears the relationship of T_c and Γ depend on composi-
tion and at higher Γ values, T_c begins to decrease as
the multiphase region is entered. If the plots of T_c vs.
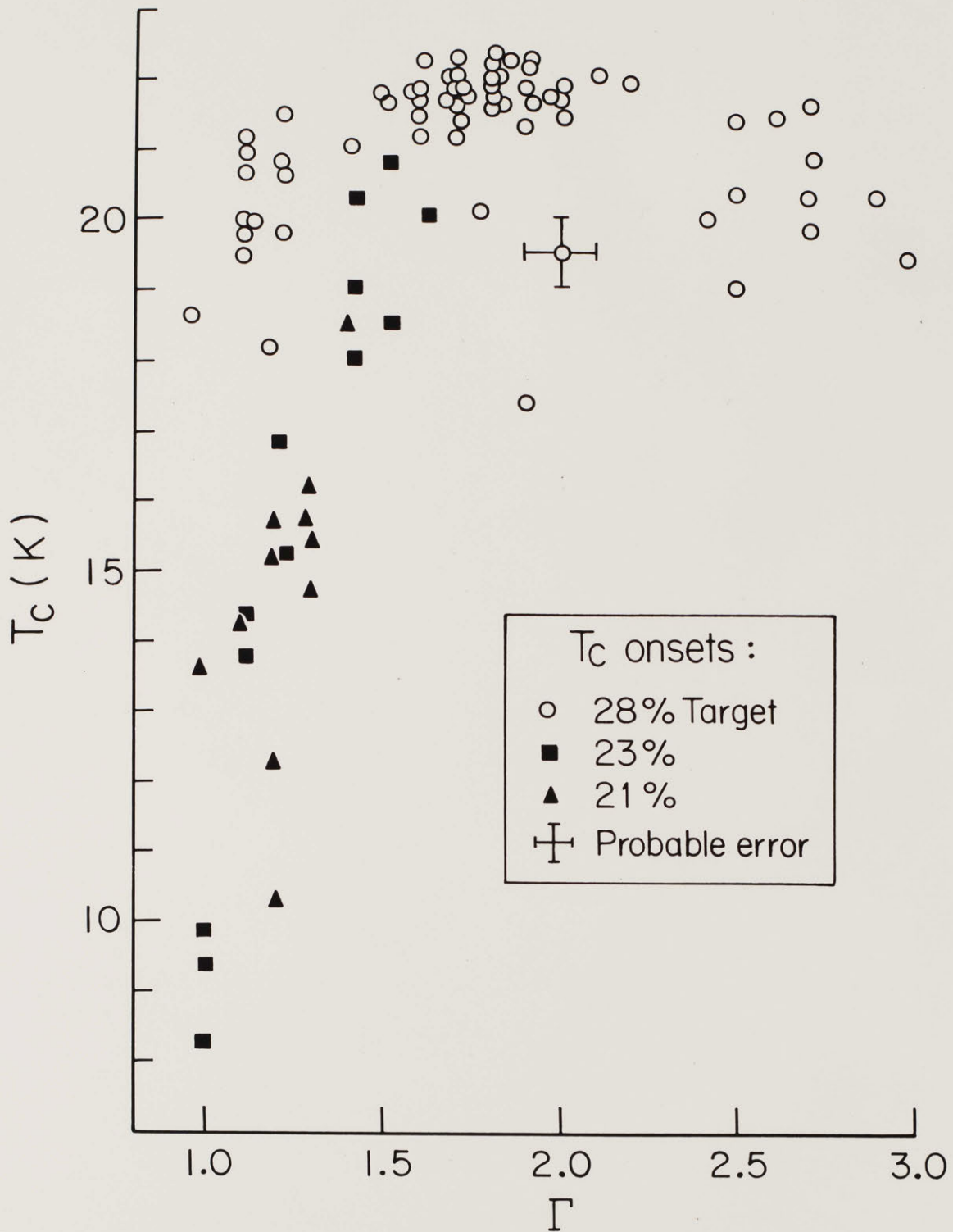
Fig. 41. Transition temperature vs. residual resistance ratio.

⌐   of different research groups[30,34,55,98] are super-
imposed, there is a general trend suggesting T_c increases
up to a ⌐ of 2 or 2.5, but the scatter of the data is so
large that prediction of T_c from ⌐ becomes imprecise.

Although it seems that the mechanism of long-range
order can incorporate all the data on the reduction of T_c
by irradiation or its increase by annealing, grain size of
the A15 phase also has an influence on T_c of the samples.
This influence is seen in the variation of T_c with sample
thickness (Table II). For films deposited from a 28% Ge
target, T_c increased from 19.9 K for an annealed film of
0.12 μm thickness and a grain size below the resolution of
the SEM, to ≈ 21.6 K for a film .9 μm thick and a
grain size of approximately .4 μm; above this grain size
T_c saturates (the grain size of the thin films is probably
20 to 50 nm, as determined by the FWHM of the diffraction
peaks). Although a thin film may have a higher average O
concentration than does a thick film and T_c is degraded
by this contamination,[33] it appears that T_c increasing with
grain size is a monotonic effect. On the other hand, small
grain size does not always imply a low T_c since films de-
posited on Nb_3Ir films have a grain size below the resolu-
tion of the SEM, but T_c onsets ≈ 22 K.[102]

The effect of grain size on T_c may also play a part in

the variation of T_c with T_d since grain size is observed to decrease rapidly below the optimum T_d; however, these results are probably influenced by reduced long-range order within the smaller grains and changes in film composition as T_d is lowered, as well. For the 28% Ge target samples with a T_d of $\approx$ 750 C, T_c onset is in the vicinity of 18-19 K and the grain size is below the resolution of the SEM but there are sharp peaks in the diffraction pattern. When T_d is around 700 C, these diffraction peaks broaden to one large peak cen-tered at $2\theta \approx 39°$ and T_c onsets fall to between 10 and 15 K; in addition, the transitions grow to several degrees in width, suggesting the existence of a significant amount of amorphous material.

Another study based on the extended x-ray absorption fine structure (EXAFS) also investigated the effect of the presence of fine-grained material on T_c.[103] It was shown later that the change in T_c in a series of samples with varying amorphous phase fraction could be explained by a proximity effect in which the low T_c amorphous phase degraded the T_c of the A15 material when as little as 5% of the sample was amorphous material.[104] In addition, structural considerations indicated that the Ge atoms had a coordination number of 8 in the amorphous phase (vs. 12 for A15 material) and the distance between Nb and Ge nearest neighbors in this phase was about .266 nm, .021 nm less than in the A15 structure. Since no tetragonal phase was

observed, per se, the authors concluded that only the A15

and amorphous phases were present in the diffraction

patterns.[103] However, certain of the Ge atom sites in the

Nb_5Ge_3 tetragonal phase are separated from Nb atom sites

by .265 nm and these sites also have a coordination number

of 8. Furthermore, in samples produced from the 23% and 28%

Ge targets of the current work the amount of tetragonal

phase in the diffraction pattern increases as T_d decreases

from optimum and the diffraction pattern approaches the single

large peak characteristic of an amorphous phase. It appears,

therefore, that the amorphous phase present in certain

samples is structurally similar to the tetragonal phase in

the Nb-Ge system. Similarly, the difference between the A15

and tetragonal phases disappears as the grain size of the

samples decreases. Therefore, as the grain size decreases

disordered or low T_c material is in contact with a larger

proportion of the A15 material and lowers T_c by the proximity

effect. Above a certain grain size, however, the low T_c

material does not affect enough A15 material to lower the

resistive T_c. In this work little degradation of T_c onset

of films containing 10 to 15% tetragonal phase (as estimated

by application of the lever rule) was observed, while ΔT_c

increases for these same samples. This suggests that in-

homogeneities in the films increase as T_c decreases; this is

the expected behavior if a low T_c phase is widely dispersed

in varying amounts.

Uniaxial strains applied to A15 films and wires have been observed to degrade T_c when corrections for thermal mismatch have been taken into account.[105,106] It is thought that this change in T_c may stem from the effect of strain on the crystal structure. In the four-point bending measurements reported here, not only were strains applied uniaxially but the effects of thermal mismatch of the films and substrates were documented. There appears to be a correlation between the rate of decrease of T_c with strain and the substrate material; for the ceramic substrates T_c decreases by about 5 K/% strain for strains $\approx$ ±.11% while for the Hastelloy substrates T_c decreases at approximately 2.5 K/% strain at strains $\approx$ ±.2%.

The thermal contraction of Nb_3Ge between 1200 K and 0 K can be estimated[107,108] at .73% to .78% while that of alumina is .72% and Hastelloy[110] is $\approx$ 1.4%. This indicates the A15 films are subjected to a tensile strain of 0.01 to .06% when deposited on an alumina substrate and a compressive strain of about .7% when deposited on Hastelloy. These estimates of strain agree well with those calculated in this work from the curvature of a 1 μm film deposited on a 100 μm thick sapphire substrate. Deflection of the center of the film-substrate composite from the ends was less than

20 μm, which indicates the radius of curvature was greater

than 900 mm. This radius, along with the thickness of the

A15 and sapphire and the Young's modulus of each indicates

the mismatch of thermal contraction between $\approx$ 800 C and

room temperature is .06% or less. (See Appendix C.)

The effect of strain on T_c for the sapphire substrate

films used in this research compares well to the observed

behavior in Nb_3Sn wires[105] and various other types of A15

films.[111] For Nb_3Sn there is a parabolic maximum in T_c

when the applied tensile strain just cancels the difference

in thermal expansion mismatch.[105] The decrease on either

side of this maximum is symmetric: for an excursion of .10%

strain on either side of this peak the T_c decreases by about

0.06 K. The application of quasi-hydrostatic pressure to

the A15 films on sapphire substrates[111] indicates the T_c

of the film decreases linearly at the rate of .14 K for

approximately .10% compression along the length and width

of the film. (These values are, of course, only approximate

because the stress state cannot accurately be described

as hydrostatic since the compression of the film will be

restricted by the substrate, which has a Young's modulus

about twice that of the Nb_3Ge.)

These values of $\Delta T_c / \Delta \epsilon$ are close to those

reported here in that the present data is bracketed

by these values. In addition, the decrease in T_c for a

given strain was found in both this work and other studies to be independent of the initial T_c of the material. This data agrees fairly well with the behavior expected from the thermodynamic properties of A15's near T_c.[112] Theory predicts that $T_c(0) - T_c(\epsilon) = 10^5 \epsilon^2$ for high T_c superconductors. For a strain of .1% this indicates T_c is degraded by .1 K and that this degradation remains the same no matter what the initial T_c had been. The present values of T_c under strain are very close to these and although the functional dependence of T_c on strain is uncertain it does appear that T_c drops more rapidly in the interval .06% to .12% than in the interval 0 to .06%, as it would following a parabolic dependence.

If the observed strain behavior were due to microcracks instead of an inherent strain dependence of T_c a different behavior would be observed. That is, the behavior would be similar to that of samples which have T_c measured at different current densities where it is observed that the temperature difference between the midpoint and 10% normal state resistance increases with current density. In fact, the degradation of T_c with applied strain is about the same for samples at the midpoint and at 10% normal state resistance.

The behavior of T_c with applied strain for films deposited on Hastelloy is unexpectedly symmetric about zero

applied strain in contrast to the data on Nb_3Sn wires[105]
and thin films[106] and CVD Nb_3Ge films.[62] In these latter
studies the T_c or critical current density increased as
the applied strain increased probably because of the large
difference in thermal contraction of the A15 and its sub-
strate.

One reason for the disparity may be the presence of
an interfacial layer between the Hastelloy and the A15
which can only tolerate a strain in the neighborhood of
0.2% and then plastically deforms or fractures so the imposed
strain on the A15 is far less than expected from thermal
contraction mismatch of the A15 and Hastelloy. Indeed,
Auger depth profiles of samples deposited on Hastelloy B
show a region approximately 500 nm thick where the Nb, Ni,
and Ge peak-to-peak heights are of comparable magnitude.
Further, the diffraction patterns of these samples show
peaks at d-spacings corresponding to Nb-Ni and Nb-Ni-Ge
intermetallic compounds. Both the Auger and x-ray data
support the contention for an interfacial layer, but do
not address the question of the relative strength of the
A15 and interfacial layers. If the A15 layer has a greater
flow or breaking strain, however, then the A15 layer would
be subjected to applied strains only in the neighborhood
of the interfacial layer strength or yield stress before
this interfacial layer cracked or flowed. This interfacial

layer slippage may be the source of the irreversible de-
gradation of T_c for strains above .3% on Hastelloy sub-
strates. The thinner this interfacial layer is compared

to the thickness of the A15 film, of course, the less effect

it will have on the observed mechanical properties of the

films. This is, perhaps, why CVD processed films[62] do

not show the symmetric mechanical behavior observed for

the dc-sputtered Nb_3Ge films.

B. Control of the Film Structure

As was indicated in Chapter V, the composition of the

film is very close to that of the target such that any

deviation of the film composition from the target stoichio-

metry outside the 1% accuracy of the microprobe appears

to be on the Nb rich side. Although the composition of

the A15 phase probably depends on a number of parameters

such as composition of the vapor deposited, sticking

coefficient, deposition temperature, and sputtering gas

composition, only changes due to the variation of deposi-

tion temperature or the presence of impurities in the

sputtering gas could be documented in the present research.

It has previously been observed that small amounts of O_2,

N_2, or other gases aids the deposition of high T_c Nb_3Ge

films.[34,51,54] Oxygen additions at both the 5×10^{-4} and

2×10^{-3} Pa levels in the present work also resulted in

increases of T_c although the effects were the same at both levels. This may be because of the very high O_2 level inherent to the system ($\approx 4 \times 10^{-5}$ Pa) which is considerably above the reported lower limit that is effective in obtaining high T_c material.[34,51] On the other hand, no clear changes in the optimum T_d were observed even for O_2 pressures varying by a factor of 50 from the background level.

In the absence of solid evidence to the contrary the following hypothesis is accepted: a partial pressure of O_2 in the region of 10^{-5} to 10^{-2} Pa is necessary to increase the A15 Ge content beyond that allowed in the binary phase diagram and to obtain high T_c material on substrates that do not have the A15 structure.[33,51,54] Laboratory air has been found to be beneficial in producing high T_c material, in this study and by Sigsbee.[51] With the exception of H_2 noted below, it is assumed all other impurities in the gas phase act in a manner analogous to O_2 to stabilize the phases (e. g., Cl_2 stabilizes the tetragonal T_2 phase[53]). At least under certain conditions, however, the supersaturation of Ge in the A15 lattice is metastable despite the presence of O_2 in the deposition system. This was seen in the present work when films were held near their deposition temperatures too long: T_c declined and the amount of second phase increased, consistent with observations reported by other groups.[46]

The means by which the impurity in the films increases the Ge content of the A15 phase is still in question since it is

difficult to determine the exact amount of oxygen in the A15 phase and whether this O is substitutional or interstitial in nature. What is known is that the presence of oxygen stabilizes other structures in binary systems that possess an A15 compound;[63] e. g., in the V-Ga[70] and Nb-Ga[71,72] systems the phase with the Nb_5Ge_3 crystal structure is very sensitive to oxygen contamination. It is possible that O raises the free energy of the tetragonal phase relative to the A15 and hexagonal phases, raising the solubility of Ge in the A15 phase and stabilizing the hexagonal phase (see Fig. 42). Another situation in which a normally unstable phase is stabilized due to gaseous contamination is in CVD samples deposited with a low H_2 to Cl_2 ratio in the gas phase in the reaction chamber.[53] Thus, the appearance of phases missing in the binary phase diagram upon the introduction of impurities implies the chemical potential of Nb and Ge are changed by the inclusion of O or some other impurity, such as carbon,[113] in the intermetallic phases of the Nb-Ge system allowing the A15 phase to form near stoichiometry, thereby raising the T_c. However, adding O to bulk A15 Nb-Ge did not extend the solubility range of Ge,[63] suggesting that the effects of O_2 additions are probably kinetic in films as well as in bulk Nb_3Ge.

The depth profile of oxygen has been reported to show a large decrease through CVD Nb_3Ge films, i. e., the oxygen concentration dropped to $<$ .1% from a much higher value near the
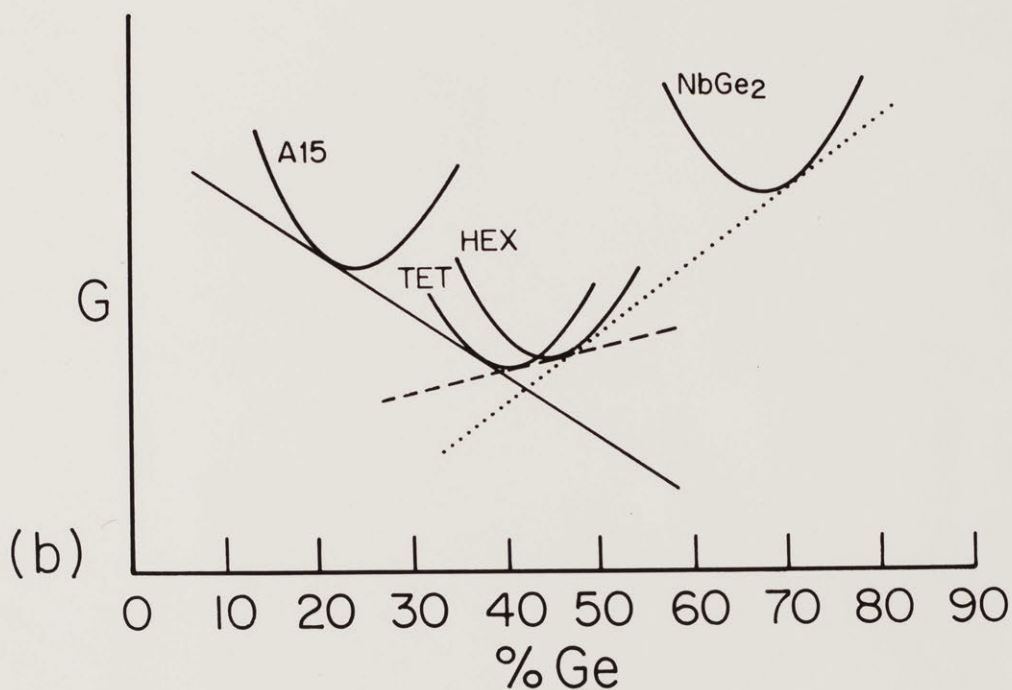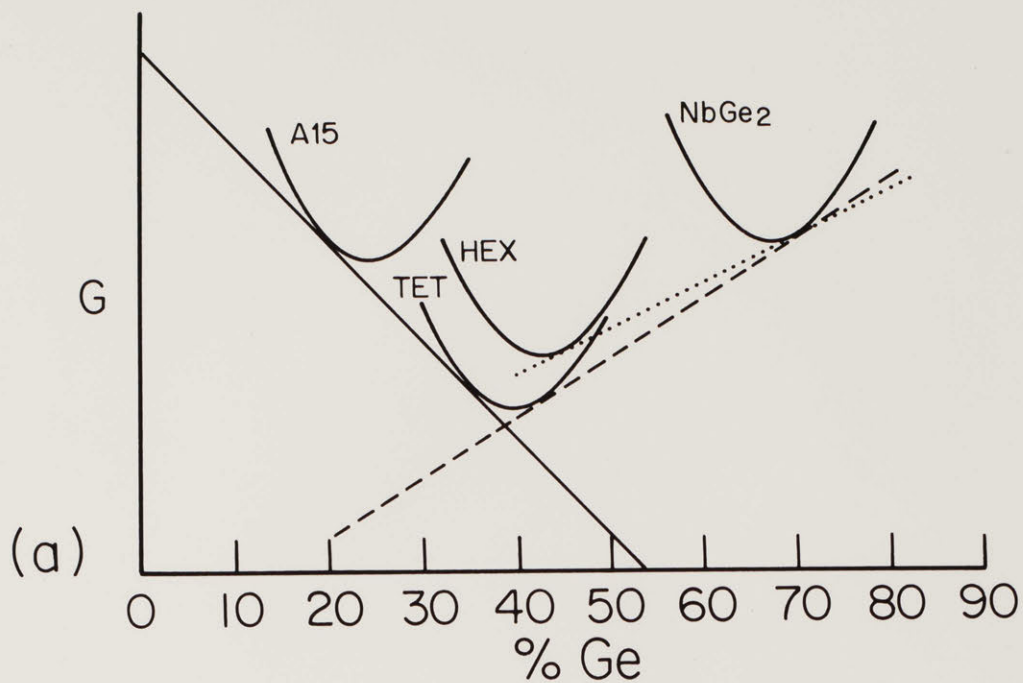
Fig. 42. Hypothetical free energy vs. composition plots of
the Nb-Ge system near 800 C. (a) stable equili-
brium (b) metastable equilibrium in which the free
energy of the tetragonal phase is raised relative
to that of the A15 and hexagonal phases by inclusion
of oxygen. Note the Ge concentration in the A15
phase increases and the hexagonal phase is now
stable.

substrate interface, suggesting that perhaps only in the early
stages of film growth is an impurity required for phase stabi-
lization.[33] The sputtered Nb_3Ge films deposited on ceramic
substrates in the current work qualitatively followed the
same oxygen depth profile behavior. However, films deposited
on metallic substrates (on Au underlayers and Hastelly B) did
not show this behavior. These data suggest that oxygen coming
from the substrate-film interface may play a major role in the
final profile of the CVD films and the Nb_3Ge films on ceramic
substrates. (It is worth noting that sputtered Nb_3Ge films on
oxidized metallic substrates were reported to have similar in-
creasing oxygen profiles to the samples deposited on ceramic
substrates near the substrate interface and simultaneously to
exhibit higher T_c's than non-oxidized metallic substrates.[33])
If the impurity is required only at the outset of deposition
then it is possible the impurity has an effect other than al-
tering the free energies through chemical means, e. g., by
straining the lattices so they match the lattice of the sub-
strate. This lattice stretching is similar to what is believed
to occur in the diffusion growth of Nb_3Sn from Sn vapor de-
posited on Nb single crystals although in that particular case
the reason for this phenomenon is unknown. If this is the
case then oxygen, which is present in high concentration, may
alter the surface structure of the substrate, perhaps forming
an oxide, and thereby create a lattice or nucleus that is

favorable to the deposition of high T_c Nb_3Ge. The present

work gives some evidence, however, that a partial pressure

of O_2 is required throughout the deposition of the film

if optimum T_c's for a given deposition temperature are

to be obtained. For example, films that had O_2 added to

the system at the beginning of the deposition and then ter-

minated had T_c's that were intermediate between those of

films where O_2 was not added and those of films where O_2 was

added throughout the deposition of the film.

Although the requirement of O_2 additions for high T_c

films not grown on A15 substrates has been established,

the mechanism and role of inclusion of O or other impurities

in the A15 phase is still not known and will probably re-

main a point of controversy until the atomic positions

can be determined by precision x-ray analysis. It should

be noted, however, that oxygen and other impurities may

not be necessary to form high-T_c A15 Nb_3Ge if a substrate

with a lattice parameter close to that of the desired A15

is used.[61] The Stanford group has deposited Nb_3Ge with

T_c's above 22 K and Ge concentrations up to about 26%

on A15 Nb_3Ir substrates, apparently without any O_2 or other

impurities introduced into the vacuum chamber.[56,61]

As with oxygen, the grain size varied with distance

from the substrate-film interface.[33,60] Thin sputtered

A15 films deposited on ceramic and metallic substrates
appeared to have a smaller grain size and a greatly in-
creased lattice parameter as compared to thicker films.
Since O concentration decreases at positions farther from
the substrate and grain size increases, the idea that the
small grain size allows the lattice to relax and assume
a larger lattice constant follows. If the thin films
with fine grains contain a high O concentration this could
help to explain the difference in T_c between the 1 μm thick
films and the 150 nm films that were annealed for forty-
five minutes, since high O contamination appears to lower
T_c.[54]

The oxygen near the substrate-film interface may reside
mainly in the grain boundaries as opposed to within the
grains. Thus, as the films thicken and the grains grow,
the proportion of grain boundary material decreases and so
does the oxygen concentration. One might then expect that
a large grain film would have a lower oxygen concentration
overall than does a small grain film. Auger analysis does
not seem to substantiate this prediction: the oxygen con-
centration of low T_d samples, with grain sizes in the re-
gime of 50 to 100 nm, is not significantly different from
samples prepared in comparable vacuum and with grain sizes
around 400 nm. On the other hand, in the absence of a

standard specimen, the calculated O concentration may vary
by a factor of four for a given peak-to-peak height ratio in an
Auger profile, making the expected change in O concentration
well within the limits of uncertainty of the Auger analysis.

One might also expect that if sputtering were inter-
rupted and then resumed, a region of small grain size and
large oxygen concentration would exist within the interior
region of the film. Such small grain, high oxygen layers
have been observed for multiple interruptions in fabrication.[60]
The role of the ambient oxygen may be either to surround
the new grains and prevent their coalescence or to enhance
the nucleation of new grains.[33,60]

The effect of oxygen in enlarging the lattice parameter
may be to enhance lattice registry, thereby promoting nuclea-
tion and growth of A15 material.[73] If this mechanism were the
dominant one, the lattice matching should cause the lattice
parameter in the plane of the film and normal to the plane to
be strained in opposite senses. To date, TEM and x-ray
measurements[33] do not provide evidence for this mechanism
although the observed variation in the two directions is at
the limit of resolution of the TEM ($\approx 1\%$ of a_o). It is more
likely, however, that this observed change in lattice parameter
would be accomplished by oxygen atoms (and/or ions) incorpo-
rated substitutionally on the Nb chains or interstitially
in the lattice.

It has been proposed that another effect of O on the properties of the films is that it prevents hydrogen from entering the A15 phase and degrading the superconducting properties.[85] To determine if the essential effect of post deposition annealing is to drive off H that was introduced during sputtering, a set of 28% Ge target films were annealed in 40 Pa Ar; no difference in their T_c with films annealed in vacuum was observed. Although 40 Pa may not be a high enough pressure to prevent partial evolution of the hydrogen from the film, it should decrease the rate of boil-off if H is present in significant amounts. Thus, the absence of any measurable effect on T_c implies that H evolution during annealing is not a problem in this work.

Samples produced from the 21% and 23% Ge targets have a peak in Ge composition close to the T_d which produced the highest T_c films. Although this maximum in composition is not sharp and in some cases not any larger than the uncertainty in the microprobe results, its presence is supported by a larger lattice parameter for samples deposited at non-optimum T_d. This variation in a_o is consistent with the variation indicated by the microprobe and the data in Fig. 14 (a_o vs. Ge concentration). The change in Ge content with T_d could explain the low Ge concentration value of the sample sputtered from the 19% Ge

target. Assuming behavior similar to that of the 21% and 23% targets, the peak for this composition should be in the vicinity of 700 C and a few percent higher than 16% Ge, as shown in Fig. 10.

An explanation for the decrease of Ge concentration at high T_d might be that the vapor pressure of the Ge has risen so that its effective sticking coefficient, relative to that of Nb, has decreased. In addition, for low T_d samples it might be that the sticking coefficient of the Ge relative to Nb is decreased by the higher impurity concentration, poisoning Ge adsorption sites, or to the larger effective grain boundary area of the smaller grains. However, this last possibility runs counter to the theory of Williams and Nason,[114] which predicts segregation of the component with the higher vapor pressure, i. e., Ge, to the grain boundaries.

The effect of T_d on the composition of the 28% target samples in Fig. 10 seems to be either a slight increase in Ge content with T_d or no change. If the second phases also have behaviors of composition with T_d that show maxima, it may be that the relative displacements of the curve maxima along the T_d axis serve to maintain the overall composition of the film as nearly constant because the decreasing Ge composition side of the A15 phase curve is complemented by the increasing Ge composition of the second phase curves.

The deposition temperature has a very strong influence
on the grain size and phase distribution. In agreement
with Thornton's model of film properties, SEM studies and
FWHM measurements indicate that the films are undergoing
a change from a fine-grained to a coarser structure at a
deposition temperature that is close to half the absolute
melting temperature.[66] Above this T_d grain size is not
expected to change significantly until recrystallization
begins,[66] a T_d much higher than those used in the present
study. Since the T_d at which the crossover from fine to
coarse grains occurs increases as the system pressure does,[66]
the increase in optimum T_d with Ar pressure may be related
to this change. The optimum T_d and the T_d at which the
grains reach a size of about .2 μm decreases for lower Ge
concentration.

Order and perfection are also important in determining
the properties of the Nb_3Ge. Perfection appears to depend
on some of the same parameters that are influential in ob-
taining a high Ge concentration in the A15 phase such as
T_d and gas composition as well as deposition rate and grain
size. Ordering appears to be the most likely explanation
for the effect of annealing on T_c: the films are deposited
on the substrate in a highly disordered state with a low
T_c but with high atomic mobility; the initial layer of A15

material is established by impurity or substrate stabilization
and as time progresses each A15 layer is covered by a new layer
of disordered material which then crystallizes to lower its
free energy. The long-range order of the underlying layers is
simultaneously increased by holding the samples at T_d during
or after deposition. As ordering proceeds the displacements[78]
of atoms from their equilibrium position decrease.

The FWHM of high angle x-ray peaks increase for long term
anneals; this larger range of d-values for the peaks indicates
the films are becoming more inhomogeneous due to precipitation
of the tetragonal phase and growth of Nb-rich Nb_3Ge. This
latter possibility is supported by the increase of lattice para-
meter of annealed films initially in the single phase region.

However, not all material can be expected to form single
phase A15 because of the character of the fabrication process.
If tetragonal and hexagonal phases are initially present, de-
pending on free energy considerations, a decomposition of mater-
ial in the A15 phase to these second phases might be more likely.
On the other hand, if little or no second phase material is pre-
sent in the initial layers, the energy required to nucleate
those layers is probably higher than the energy required to or-
der the A15 film. Both alternatives can be inferred from the
annealing data shown in Fig. 37.

In addition, for the 21% and 23% Ge target compositions
there are ranges of T_d in which single phase A15 material is

deposited and these ranges appear to be bracketed by deposi-
tion temperature intervals in which multiphase material is de-
posited. For the 28% Ge films there is never single phase
material, probably because the limit of solid solubility of
Ge in the A15 lattice for the present apparatus has been ex-
ceeded, although there appears to be an intermediate T_d at
which the fraction of second phases is at a minimum. Despite
the single or multiphase nature of the films, the amount of
amorphous material present decreases as T_d is raised from
very low deposition temperatures, indicating ordering is occur-
ring at an increasing rate. High T_d films, on the other hand,
appear to have an increased amount of second phase present
which indicates that precipitation occurs more rapidly in
this temperature region.

It is interesting to consider the possibility that low T_d
films have some of the disorder of freshly deposited atoms
frozen in and to speculate that the disordered films contain
fine-grained material that could be interpreted as either the
A15 or tetragonal phases. The similarity of these two phases
has been noted before,[49,82] and in one case,[49] it was suggest-
ed that the diffuse background in the diffraction patterns
was due to small compositional fluctuations that favored the
formation of small domains of the tetragonal phase. An even
stronger similarity exists between the tetragonal phase and an
A15 structure that has a high dislocation density, however.

Partial dislocations with Burgers vectors of the type $\frac{1}{2}$ $[011]$ could shift the A15 cells (shown in Fig. 43a) relative to each other and produce a region that has a tetragonal structure (shown in Fig. 43b). The extra Ge atoms necessary to achieve proper stoichiometry are contained in the dislocation cores.

If a square grid of the dislocations were introduced every 0.5 nm, the A15 structure transforms into the tetragonal in a manner similar to the conversion of the fcc structure to hcp by the introduction of stacking faults. Of course, the dislocation density required to achieve this purpose is prohibitively high if the whole film were to be transformed, but the model does indicate that an A15 film with a high density of growth-induced stacking faults could be viewed as fine-grained material with a Nb-Ge nearest neighbor distance of 0.266 nm and a coordination number of 8 about the Ge atom; depending on the grain size or partial dislocation spacing (which could be interpreted as a grain boundary) this A15 material could give a diffraction pattern similar to either the tetragonal or amorphous phase, both of which have the above Nb-Ge nearest neighbor distance and coordination number.[89] The large amount of tetragonal phase present in the low T_d samples for the 23% and 28% Ge target samples might be an indication of the tendency of the amorphous phase to crystallize in the tetragonal structure or of the presence

Nb₃Ge legend: ○ Nb ⊘ Ge

Nb₅Ge₃(T) legend: ⬤ Nb(1) ○ Nb(2) ⊘ Ge(1) ⊗ Ge(2)

(a)

(b)
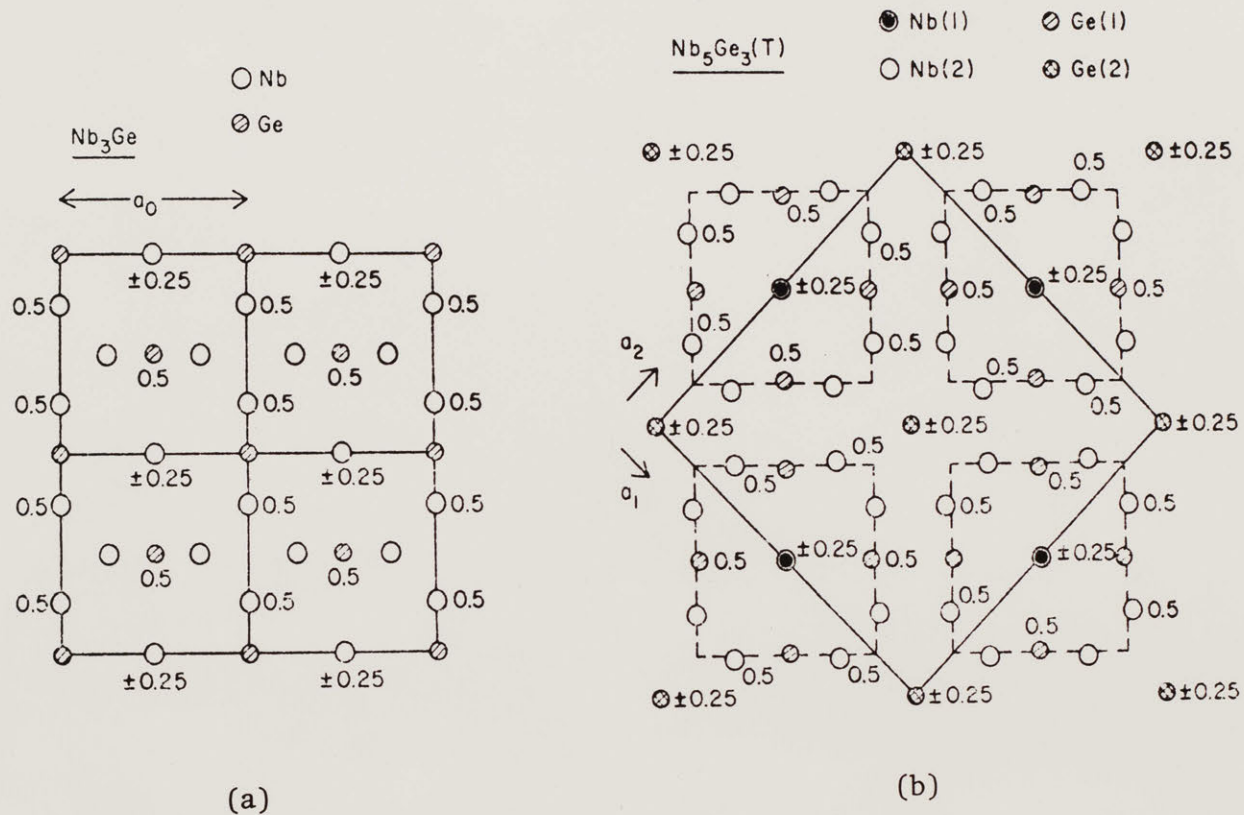
Fig. 43. Projection on (001) of the structures of (a) Nb₃Ge
(b) Tetragonal Nb₅Ge₃. The small numerals denote
the heights of the atoms in fractions of the verti-
cal cell edge. The respective unit cells are shown
by the solid lines and the broken lines show the
A15 unit cell "block" surrounding the Nb(1) atoms
in Nb₅Ge₃. Used with permission of D. E. Cox (ref. 49).

of stacking faults of the kind mentioned above that were not
annealed out during deposition. This possible interpretation
would, of course, be reinforced by the observation that after
annealing low T_d films have a significant decrease in resis-
tivity which might also be indicative of the second phases
present in the samples.

VII. Summary and Recommendations for Future Research

A wide variety of Nb_3Ge films were fabricated by dc getter-sputtering. Although commercially, perhaps, the most interesting films are those with optimal superconducting parameters, films with non-optimum superconducting parameters must be investigated to obtain insight into the role which the elements of film structure play in determining the final superconducting attributes of the films. Since the elements of structure are determined by the particulars of film processing conditions, this study undertook a systematic examination of film composition, lattice parameter, phase assemblage, crystalline order, grain size and morphology, breaking strain, and superconducting transition temperature as a function of fabrication parameters: sputtering target composition, temperature of the substrates, sputtering gas composition and pressure, annealing time, film thickness, substrate species, and applied strain. Both single and multiphase films with T_c ranging from the equilibrium A15 Nb_3Ge value of ≈ 7 K to over 22 K were obtained. Whereas annealing, and thus ordering, is known to increase the T_c of almost all A15 materials, and such increases were observed in this research, for metastable Nb_3Ge annealing, even at optimum temperatures, eventually causes the precipitation of undesirable second phase material and consequently decreases the superconducting transition temperature.

The Ge and Nb concentrations of the deposited films
are close to the stoichiometry of the sputtering targets;
deviations are $\approx$ 2% - 3%. The elemental concentrations
vary with the temperature of the sputtering table. These
concentrations are relatively insensitive to sample thick-
ness or substrate type (except at the substrate-film and
vacuum-film interfaces), while the O and C concentrations
exhibit gradients in the film that are substrate dependent.
For example, the oxygen content of films rises significantly
$\approx$ 100 nm before the ceramic substrate-film interface
while an increase in O concentration does not occur in
films deposited on Hastelloy B.

The lattice parameter of the A15 phase depends primarily
on the Ge content of that phase, with a_o decreasing as the
Ge content increases. The lattice parameter appears to
decrease as the order of the film increases and, perhaps,
as the film thickens. The phases present in the film
have a strong dependence on target composition; when the
equilibrium solubility limit of Ge ($\approx$ 18%) in the A15 phase
is exceeded the tetragonal and hexagonal Nb-Ge phases
are produced. The solubility limit was raised to $\approx$ 23%
Ge by using a Ge rich target but these supersaturations
were unstable with respect to annealing the films either
during or after deposition. In addition, for deposition

temperatures (T_d) below a T_d characteristic of a given target composition a significant amount of fine-grained or amorphous material is deposited. This characteristic T_d decreases with Ge content of the target and decreases with increasing film thickness for a given target composition.

Germanium rich, multiphase films have a lower resistivity than single phase films perhaps because the second phases have lower resistivities than the A15 phase. The resistivity of a film of given composition decreases as T_d is increased; annealing decreases the resistivity of the lowest T_d samples. The thinnest films tend to have higher resistivities along with smaller grain sizes.

The breaking strain of the samples depends primarily on the substrate material. Breaking strains of films deposited directly on sapphire appear to be limited by the breaking strain of sapphire itself. Flaws in other ceramic substrates lead to lower breaking strains, but composites of films interfaced with a ductile layer on these substrates have a breaking strain equal to that of sapphire. Films deposited on Hastelloy B have interfacial reaction layers which appear to have a lower yield stress than the breaking stress of Nb_3Ge.

The superconducting transition temperature, T_c, depends strongly on the A15 phase composition (T_c increases as the

Ge concentration approaches stoichiometry) and on the de-
position temperature. The T_d that produces the highest

T_c is defined as the optimum T_d; its value is not too

different from that T_d where the amount of fine-grained

material has been significantly reduced; i. e., the grain

size has reached $\approx$ 200 nm. This optimum T_d increases

from $\approx$ 770 C for a 21% Ge target to $\approx$ 840 C for a 28% Ge

target. At deposition temperatures higher than the optimum,

T_c is degraded by the Ge concentration of the A15 phase

decreasing towards equilibrium due to the precipitation

of second phases. At low T_d, on the other hand, the de-

crease in T_c is due to the smaller grain size and higher

disorder. The influences of composition and ordering

can be seen in the behavior of T_c vs. a_o.

Additions of O_2 (on the order of 10^{-2} Pa) during film

deposition increase T_c only slightly, this is, perhaps

because of the high O_2 background level initially in the

system. Certainly, thin films of the same material do

have a degraded T_c which might be caused by overall high O

contamination levels throughout the film. Finally, strain-

ing the films either in tension or compression decreased

T_c reversibly, except in the case of Hastelloy B substrates

where T_c was decreased irreversibly beyond certain limiting

strains.

In summary, the T_c of the Nb_3Ge films depends on a

number of factors; for the maximum T_c the films should
have a composition near 25% Ge, be nearly single phase,
possess high long-range order, and have grain sizes at
least .3 μm. To achieve the above structure, the film
should be deposited in a system that contains $\approx 5\times10^{-3}$
Pa O_2 on a substrate $\approx$ 840 C and the sample should be
held at this temperature after the completion of deposi-
tion for $\approx \frac{1}{2}$ hr. for a film thickness $\approx$ 1 μm. The substrate
material should be chosen so there is little differential
thermal mismatch between 1100 K and 0 K.

It is significant that the optimum T_d for a high T_c
film for a given composition is also close to the deposi-
tion temperature at which there appears to be a minimum
second phase content, at which grain size first reaches
its saturated value, at which the Ge composition of the
21% and 23% targets reaches a maximum, and at which ρ
and resistivity ratio exhibit a change in slope for the
21% and 23% target films. The key behavior appears to
be that of grain size and composition, since a limiting
grain size and high Ge composition will contribute to a
high T_c and a lower ρ . The kinetics favoring a limit-
ing grain size also promote ordering in favor of precipi-
tation of other phases. Indeed, the small grain size
at low T_d may also alter the relative sticking coefficient

of Ge to Nb, decreasing the Ge content of the film while
at higher T_d the more volatile species (i. e., Ge) should
also decrease its concentration.

To explain the growth and structure of the A15 films
the following hypothesis is advanced. The Nb and Ge atoms
are deposited on the substrate in a highly disordered state.
An elevated T_d provides the atoms with sufficient mobility
for the disordered layer to lower its free energy by order-
ing and/or growth of the equilibrium phases. One of the
first crystalline structures assumed by the film is the
A15. The nucleation of this phase containing a super-
saturation of Ge appears to be aided by the presence of O_2
in the deposition system[33] or the presence of an A15 sub-
strate that has a lattice parameter near that of super-
saturated Nb_3Ge.[61] It might be that the O_2 molecules inter-
act with the Nb and Ge atoms on the film to form nuclei
for the A15 grains. Perhaps the incident atoms have a
higher sticking coefficient at the nucleation sites pre-
sented by the already adsorbed or reacted O and as these
nuclei grow in cross-sectional area, the sticking coeffi-
cients of the Nb and Ge rise, increasing the Nb and Ge
concentrations and decreasing the O concentration in the
film.[115] Given the special affinity of Nb for O the
relative Nb and Ge sticking coefficients are probably
altered, leading to a lower Ge concentration. Once the

initial layers order into a crystalline structure the sub-
sequent deposited material easily crystallizes into the
same lattice structure and enhances grain growth. The
coherency of these layers helps to stabilize the super-
saturated Nb_3Ge and impede precipitation of the tetragonal
phase. If, on the other hand, the film is held at T_d for
too long a period of time, precipitation will occur be-
cause of the metastability of the supersaturated A15 phase.
The thicker the film becomes, the more likely it is that
the initial film layers experience precipitation of second
phases and degradation of T_c while the later layers are
still optimizing their T_c. This effect may explain, for
example, why annealing thick films for a long period of
time decreases the superconducting transition midpoint
and finish but not the onset temperature. In addition, this
hypothesis might explain the occurrence of an optimal T_d:
below the optimum, ordering of the film does not occur very
rapidly but as T_d is increased and ordering accelerates so
does precipitation of the tetragonal phase, therefore a
temperature at which these effects are balanced exists and
at this T_d the superconducting transition temperature is the
maximum for a given target composition.

Although the above hypothesis is consistent with the
data observed in this work and previous research, its

quantitative details should be confirmed and its applicability
to other A15 materials determined. To reduce the annealing
time inherent during the deposition of thick films the deposi-
tion rate should be increased; this could be accomplished by
converting the system to a dc triode arrangement or simply by
increasing the allowable limits for Ar pressures and sputter-
ing voltages in the present system. Increasing the deposition
rate should also improve the quality of films deposited on
metallic substrates because the reduced time for film fabri-
cation may decrease the thickness of any interfacial layer.
A thinner interfacial layer would make it more likely that TEM
examination could be done on layers corresponding to almost
all stages of growth because the metallic substrate and inter-
facial layer could be dissolved away.

Since the supersaturation of Ge in the A15 lattice may de-
pend on a combination of impurities in the films,[33,51,54] tests
should be undertaken to determine if the impurity gases alter
the kinetics of film growth, the kinetics of ordering, or
even the thermodynamic stability of the material. Thicker
films deposited at a higher rate would make measurement of
long-range order of the films more accurate. Precision re-
flection-electron diffraction lattice parameter measurements
might show the decrease in lattice parameter predicted as the
surface layers of the film order upon annealing.

Implantation of oxygen ions in bulk Nb_3Ge might incorporate

the O into the material in a manner which is not possible with conventional melting and solidification techniques. It would also be interesting to implant O into thin films and observe changes in superconducting properties and defect structure, especially for films subjected to further annealing where growth of the equilibrium phases might occur. To determine the effect of implantation on Nb_3Ge material the density of "virgin" and irradiated material should be determined precisely. These measurements would also test the validity of the Brookhaven group's suggestion that the vacancy concentration in Nb_3Ge films is below 1%.

Further studies should also be made to determine the effect of thickness, background gases, and annealing on impurity profiles of the films. These studies may also reveal whether the 23% Ge solubility limit observed in this work is an artifact of the fabrication variables in this deposition system, particularly the annealing and loss of Ge to the tetragonal phase during deposition. In any case, the modification of the present system to produce 25% Ge A15 films should be pursued since the well-ordered, stoichiometric Nb_3Ge may have a T_c significantly higher than that observed in this work.

Since the data in Chapter V suggests that multiphase samples have a lower resistivity than do nearly single phase A15 films in the normal state, even at low grain size, the tetragonal and/or hexagonal material might serve as effective

flux pinners in their dispersed form. Therefore, the resistivity of single phase tetragonal and hexagonal films should be measured and the effect of fine-grained multiphase material on the superconducting critical current density and critical magnetic field should be studied. Dr. Robert Meservey at the Francis Bitter National Magnet Laboratory has shown that a measurement of the magnetic properties of sputtered films is feasible, using a Nb_3Ge sample provided by the author. (T_c = 21.4 K, J_c = 2×10^{10} A/m^2 at zero magnetic field, J_c = 2×10^9 A/m^2 at 10 T). Extrapolating from the present work, it appears that nearly single phase tetragonal Nb-Ge films, required for these measurements, could be made by merely changing the Ge content of the targets at the same deposition temperatures used herein.

To understand fully the dependence of T_c on uniaxial strain and breaking strain on film-substrate composites more work is required. It is curious the breaking strain of the film-substrate composite was increased equally by Au film overlayers and underlayers, especially since the overlayers did not adhere well to the A15 film. To learn more about the mechanical bonding of these layers fatigue experiments should be undertaken and cross sections of the samples should be prepared for examination in the SEM. Auger depth profiling would also be useful in determining the chemistry of the interface of the Au with the A15 or the substrate.

The presence of incipient cracks in the A15 film and their influence on T_c might be determined by subjecting the samples to four-point bending in the SEM (at room temperature). Or, by measuring the reversible behavior of T_c vs. strain (at low temperatures) with a device more sensitive to changes in temperature than the one employed in this work ($\approx$ .05 K) more information could be obtained since a crack initiated at some strain would lead to a slight irreversible degradation of T_c at a lesser strain than the maximum applied, upon partial unloading of the sample. These studies should also be undertaken on films deposited on metallic substrates to verify the hypothesis that the Nb-Ni layer prevents the full thermal mismatch strain from being applied to the Nb-Ge film.

To learn more about the basic properties of the A15's it would be useful to search for the low temperature structural transformation of Nb_3Ge and other A15 superconductors in their thin film form. Although x-ray evidence for this transformation in Nb_3Ge is negative,[30] a thin film strain gauge deposited on the film (of a thickness such that the moment of inertia of the A15 film is comparable to or greater than that of the film strain gauge) might be able to detect the strains associated with a cubic to tetragonal transformation if $\approx$ 1-10% of the sample was transforming.

Finally, it would also be interesting to investigate the effect of film texturing on the superconducting properties

of the Nb_3Ge films.[86]   Texturing effects have been observed

recently in A15 Nb_3Sn layers fabricated by a vapor diffusion

process on Nb single crystal substrates.[29]   In that study

the (111) orientation of the A15 phase exhibited compositional

and T_c behaviors that were dramatically different from those

exhibited by other orientations.[29] This anisotropy is believed

to be due to lattice registry effects on layer growth kinetics

and to sensitivity to impurity contamination. The existence

of texturing effects in Nb_3Ge films might offer the possibility

of further optimizing its superconducting properties by mani-

pulating, for example, substrate orientation.

VIII. Appendices

Appendix A

Purity of Sputtering Gas and Background Pressure
of Sputtering System

__Typical Lot Analysis of Ultra High Purity Argon Sputtering Gas__

(Supplied by Matheson Gas Products, Gloucester, MA)

$$1-2 \quad ppm \quad O_2$$
$$3-4 \quad ppm \quad N_2$$
$$3-4 \quad ppm \quad H_2O$$

__Residual Gas Analysis of Vacuum System__

(Determined with a Model 21-614 RGA supplied by

Consolidated Electrodynamics Corp., Torrance, CA)

At the ultimate	O_2	.15
pumping pressure:	N_2	2.1
	H_2O	8.0
	CO_2	.6
	Ar	.25
	CH_3OH	.02
	CH_3COCH_3	.25
	Total Pressure	11.4 μPa

At throttled pressure
obtained before back-
filling for sputtering:

O_2	4.1	
N_2	12.0	
H_2O	8.0	
CO_2	1.1	
Ar	.25	
CH_3OH	.00	
CH_3COCH_3	.2	
Total Pressure	25.6	μPa

Appendix B

Bending of Film and Substrate Due to

Differential Thermal Contraction

The strain associated with differential contraction of a
thin film and its substrate is calculated by assuming no
slippage of the film relative to the substrate. The forces
P_1 and P_2 exerted on the film and substrate by constraining
them not to slip generates bending moments $M_1 - M_4$ (see Fig. 44).
Neglecting terms of order $\frac{t}{h}$ where t is the thickness of the
film and h is the thickness of the substrate, the relations
between forces and moments are given by:

$$\frac{P_1 h}{2} = M_1 + M_2 \qquad\qquad \frac{P_2 h}{2} = M_3 + M_4$$

and

$$M_1 = \frac{E_s I_{s2}}{1 - \nu_s^2}\left(\frac{1}{r_2} + \frac{\nu_s}{r_1}\right), \quad M_2 = \frac{E_f I_{f2}}{1 - \nu_f^2}\left(\frac{1}{r_2} + \frac{\nu_f}{r_1}\right)$$

$$M_3 = \frac{E_s I_{s1}}{1 - \nu_s^2}\left(\frac{1}{r_1} + \frac{\nu_s}{r_2}\right), \quad M_4 = \frac{E_f I_{f1}}{1 - \nu_f^2}\left(\frac{1}{r_1} + \frac{\nu_f}{r_2}\right)$$

so

$$\frac{P_1 h}{2} = \frac{E_s I_{s2}}{1 - \nu_s^2}\left(\frac{1}{r_2} + \frac{\nu_s}{r_1}\right) + \frac{E_f I_{f2}}{1 - \nu_f^2}\left(\frac{1}{r_2} + \frac{\nu_f}{r_1}\right)$$

$$\frac{P_2 h}{2} = \frac{E_s I_{s1}}{1 - \nu_s^2}\left(\frac{1}{r_1} + \frac{\nu_s}{r_2}\right) + \frac{E_f I_{f1}}{1 - \nu_f^2}\left(\frac{1}{r_1} + \frac{\nu_f}{r_2}\right)$$

where: E_i is Young's modulus for (i=f) film or

(i=s) substrate

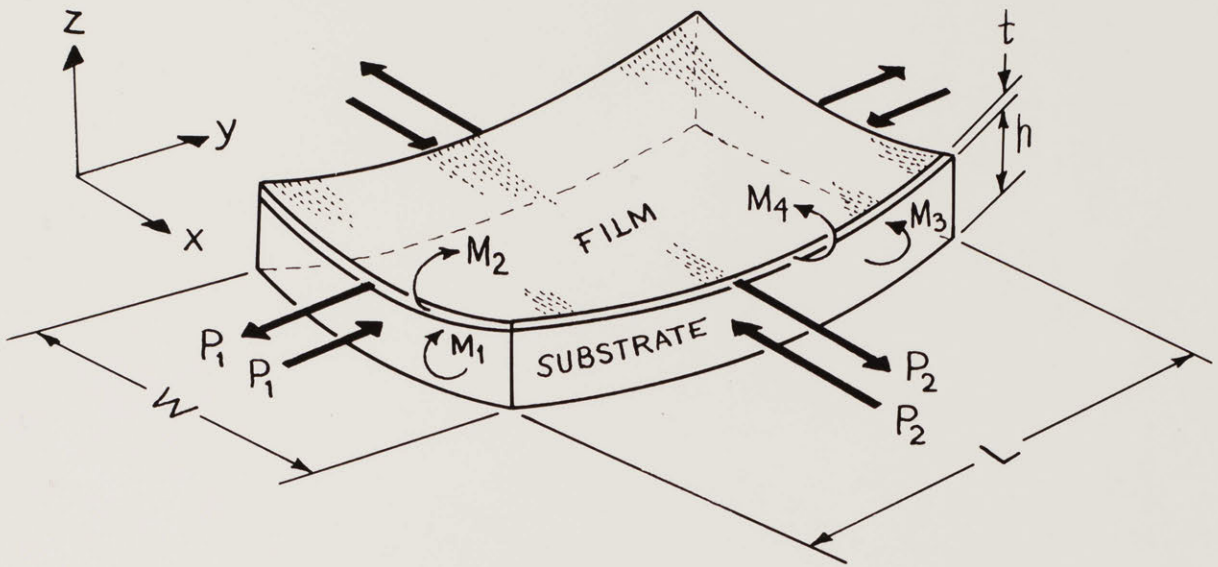ν_i is Poisson's ratio for film or substrate

Fig. 44. Schematic of forces acting on film-substrate
         composite due to thermal contraction mismatch.

I_{ij} is the moment of inertia of the film or substrate about the (j=1) y or (j=2) x axis

r_j is the radius of curvature of the film-substrate composite about the y or x axis.

To insure continuity across the film-substrate interface the following two relations must hold (neglecting $\frac{h^2}{r^2}$):

$$\frac{\delta L_s}{L} - \frac{P_1}{E_s hW} + \frac{\gamma_s P_2}{E_s hL} - \frac{h}{2r_2} = \frac{\delta L_f}{L} + \frac{P_1}{E_f tW} - \frac{\gamma_f P_2}{E_f tL} + \frac{t}{2r_2}$$

$$\frac{\delta W_s}{W} - \frac{P_2}{E_s hL} + \frac{\gamma_s P_1}{E_s hW} - \frac{h}{2r_1} = \frac{\delta W_f}{W} + \frac{P_2}{E_f tL} - \frac{\gamma_f P_1}{E_f tW} + \frac{t}{2r_1}$$

where: L is the length of the sample

W is the width of the sample

δL_i is the unconstrained thermal contraction of the length of the film or substrate

δW_i is the unconstrained thermal contraction of the width of the film or substrate.

Assuming isotropic thermal contraction,

$$\frac{\delta L_s}{L} = \frac{\delta W_s}{W}, \quad \frac{\delta L_f}{L} = \frac{\delta W_f}{W} \quad \therefore \quad \frac{P_1}{W} = \frac{P_2}{L} = P', \quad \frac{1}{r_1} = \frac{1}{r_2} = \frac{1}{r}.$$

Substituting in the continuity equation, a relation between the thermal contraction mismatch and forces generated is determined:

$$\frac{\delta L_s}{L} - \frac{p'(1-\gamma_s)}{E_s h} - \frac{h}{2r} = \frac{\delta L_f}{L} + \frac{p'(1-\gamma_f)}{E_f t} + \frac{t}{2r}$$

Biographical Note

The author was born on October 14, 1951 in New Rochelle, N.Y. and was raised in Eastchester, N.Y. The author graduated from the Massachusetts Institute of Technology in June, 1973 with the degree of Bachelor of Science in Metallurgy and Materials Science. He entered graduate school in Materials Science at the Massachusetts Institute of Technology in September, 1973 with a National Science Foundation Fellowship. He is the author of two papers and a member of Tau Beta Pi and Sigma Xi.

On July 27, 1974 the author married Nancy Anne Hellens of West Simsbury, Conn.

or
$$\frac{\delta L_s - \delta L_f}{L} = \frac{h+t}{2r} + p'\left(\frac{1-\nu_f}{E_f t} + \frac{1-\nu_s}{E_s h}\right)$$

$$\approx \frac{h}{2r} + p'\frac{1-\nu_f}{E_f t} \quad .$$

Substituting r for r_1 and r_2 and the expression for I_{ij} into the moment-force equation gives after some algebra:

$$\frac{p'h}{2} = \frac{E_s h^3}{12(1-\nu_s)r} + \frac{E_f t^3}{12(1-\nu_s)r} \approx \frac{E_s h^3}{12(1-\nu_s)r} \quad .$$

$$\therefore \quad \frac{\delta L_s - \delta L_f}{L} \approx \frac{h}{2r}\left(1 + \frac{E_s h}{3E_f t}\right) \approx \frac{E_s h^2}{6 E_f t r}$$

$$\frac{1}{r} \approx \frac{\delta L_s - \delta L_f}{L} \cdot \frac{6 E_f t}{E_s h^2}$$

$$p' \approx \frac{\delta L_s - \delta L_f}{L} \cdot \frac{E_f t}{1-\nu_s} \quad .$$

Thus, the physical parameters of interest in this approximation are:

$$\overline{\sigma}_{yf} = \overline{\sigma}_{xf} \approx \frac{p'}{t}$$

(average stress in the plane of the film),

$$\overline{\epsilon}_{zf} = \frac{-\nu_f}{E_f}(\overline{\sigma}_{xf} + \overline{\sigma}_{yf}) \approx \frac{-2\nu_f}{1-\nu_f} \cdot \frac{\delta L_s - \delta L_f}{L}$$

(average strain normal to the film),

$$\overline{\epsilon}_{xf} = \overline{\epsilon}_{yf} = \frac{1-\nu_f}{E_f}\sigma_{xf} \approx \frac{1-\nu_f}{1-\nu_s} \cdot \frac{\delta L_s - \delta L_f}{L}$$

(average strain in the plane of the film).

At the film-substrate interface,

$$\epsilon_{xs}(h) = \epsilon_{xs} + \frac{h}{2r} \approx \frac{1-\nu_f}{1-\nu_s} \cdot \frac{\delta L_s - \delta L_f}{L} \cdot \frac{t}{h} + \frac{\delta L_s - \delta L_f}{L} \cdot \frac{6 E_f t}{E_s h^2} \cdot \frac{h}{2}$$

and since $\frac{1}{3} \approx \frac{1}{4}$ and $E_s \approx 2E_f$,

$$\mathcal{E}_{xs}(h) = \frac{5}{2} \cdot \frac{\delta L_s - \delta L_f}{L} \cdot \frac{t}{h} .$$

Also since $t \ll h$ and $\mathcal{E}_{xf} \approx \frac{\delta L_s - \delta L_f}{L}$,

$$\mathcal{E}_{xs} \ll \mathcal{E}_{xf} .$$

Therefore, within the limitations of these approximations the compressive strain induced at the interface is very small compared to the tensile strain induced in the Nb_3Ge ($\approx .1\%$) and, thus, this compressive strain will not act to strengthen the film-substrate composite.

Differential Thermal Contraction of Film-Substrate Composite

The differential thermal contraction of the A15 film and
the sapphire substrate can be estimated by measuring the
bowing of the film-substrate composite as shown in Fig. 45
where: t is the thickness of the A15 layer

h is the thickness of the sapphire substrate

L is the length of the sample

d is the deflection of the sample due to thermal

mismatch strains deforming the sample to a

radius of curvature r.

Using plane geometry it can be shown that:

$$\left(\frac{L}{2}\right)^2 = d(2r-d);$$

taking L= 12 mm and d .02 mm, then r $\geqslant$ 900 mm.

From Appendix B:

$$\frac{1}{r} \underset{\sim}{\approx} \frac{\delta L_s - \delta_f}{L} \cdot \frac{6 E_f t}{E_s h^2}$$

where: δL_i is the unconstrained thermal contraction of

the length of the (i=f) film or the (i=s)

substrate

E_i is Young's modulus for the film or the

substrate.

Since $\frac{E_f}{E_s} \approx \frac{1}{2}$, $t \approx 1 \ \mu m$, $h \approx 100 \ \mu m$, then $\frac{\delta L_s - \delta L_f}{L} \underset{\sim}{\leqslant} 6 \times 10^{-4}$.
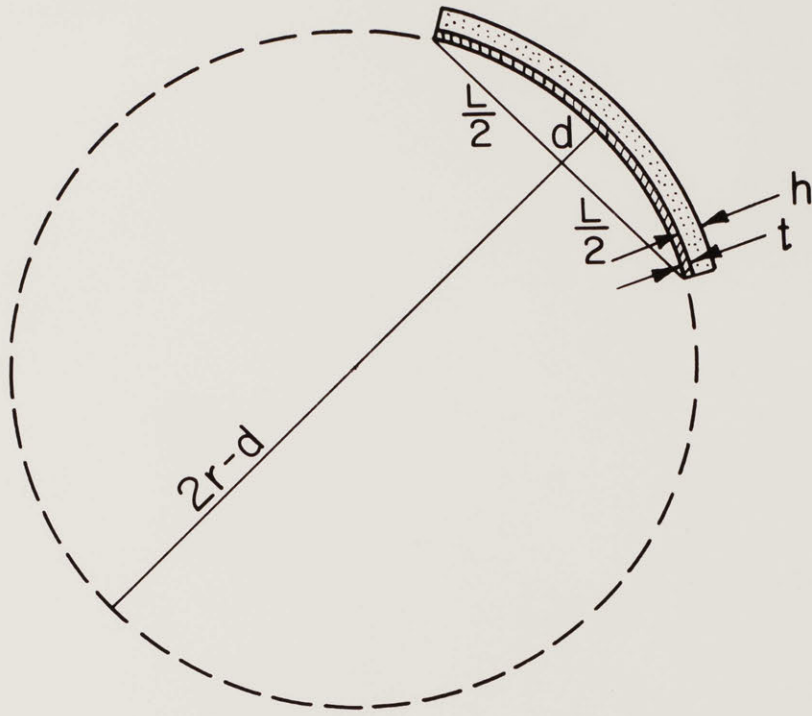
Fig. 45. Bending of film-substrate composite due to thermal contraction mismatch.

Appendix D

Calculation of X-Ray Intensities of

Perfectly Ordered Thin Nb$_3$Ge Films

The intensity of the x-ray reflection from the (hkl)
plane of a crystal can be written as:

$$I_{hkl} = A m |F_{hkl}|^2 \left(\frac{1+\cos^2 2\theta}{\sin\theta \sin 2\theta}\right)\left(1-e^{-2\mu t/\sin\theta}\right)e^{-2B\frac{\sin^2\theta}{\lambda^2}}$$

where: A is a geometric constant that does not vary

for the conditions considered

m is the multiplicity of planes

F_{hkl} is the structure factor for the (hkl)

plane

θ is the Bragg angle

μ is the absorption **coefficient** = 1183 cm^{-1}

(ref. 49)

t is the film thickness

B is the Debye-Waller factor = .7 Å^2 (ref. 49)

λ is the wavelegth of the x-rays = 1.54 Å.

For a 1.2 μm thick layer of Nb$_{79}$Ge$_{21}$:

hkl	$\left(\frac{1+\cos^2 2\theta}{\sin\theta \sin 2\theta}\right)$	m	$\left(1-e^{-2\mu t/\sin\theta}\right)$	$e^{-2B\frac{\sin^2\theta}{\lambda^2}}$	F_{hkl}	$|F_{hkl}|^2$
110	41.9	12	.74	.97	$2(f_B - f_A)$	232.3
440	3.08	12	.28	.65	$2(f_B + 3f_A)$	20,580

where f_A and f_B are the scattering powers of A and B sites,
respectively.   Therefore $\frac{I_{110}}{I_{440}} = .61$ for maximum order.

IX. Bibliography

1. B. B. Schwartz, S. Foner, Phys. Today 30, JUL 34 (1977).

2. R. W. Keyes, IEEE Trans. Magn. Mag-15, in press.

3. R. A. Hein, The Science and Technology of Superconduc-
    tivity, edited by W. D. Gregory, W, N. Mathews, and
    E. A. Edelsack (Plenum Press, New York, 1973) p. 333.

4. B. T. Matthias, Ibid., p. 263.

5. R. M. Rose, Ibid., p. 289.

6. D. M. Gualtieri, J. Appl. Phys. 45, 1880 (1974).

7. M. Cohen, Mater. Sci. Eng. 25, 3 (1976).

8. D. Dew-Hughes, Cryogenics 15, 435 (1975).

9. F. E. Wang, J. Phys. Chem. Solids 35, 273 (1974).

10. R. Flukiger, J. L. Staudenmann, P. Fischer, J. Less-Common
    Met. 50, 253 (1976).

11. E. C. Van Reuth, R. M. Waterstrat, Acta Cryst. B24,
    186 (1964).

12. M. Weger, Rev. Mod. Phys. 36, 175 (1964).

13. M. Weger, I. B. Goldberg, Solid State Phys., edited by
    F. Seitz and D. Turnbull (Academic Press, New York, 1973)
    vol. 28, p. 1.

14. L. F. Mattheis, Phys. Rev. B 12, 2161 (1975).

15. J. E. Cox, R. A. Hein, R. M. Waterstrat, Proc. XII Int.
    Conf. Low Temp. Phys., edited by E. Kanda (Plenum Press,
    New York, 1970) p. 333.

16. J. Labbé, E. C. Van Reuth, Phys. Rev. Lett. 24, 1232
    (1970).

17. J. G. Kohr, Ph. D. Thesis, M. I. T., Dept. of Met. and Mat. Sci., 1971, unpublished.

18. R. D. Blaugher, R. A. Hein, J. E. Cox, R. M. Waterstrat, J. Low Temp. Phys. $\underline{1}$, 531 (1969).

19. A. R. Sweedler, D. E. Cox, S. Moehlecke, J. Nucl. Mater. $\underline{72}$, 50 (1978).

20. L. R. testardi, R. R. Soden, E. S. Greiner, J. H. Wernick, V. G. Chirba, Phys. Rev. $\underline{154}$, 399 (1967).

21. B. W. Batterman, C. S. Barrett, Phys. Rev. $\underline{149}$, 296 (1966).

22. R. Mailfert, B. W. Batterman, J. J. Hanak, Phys. Lett. $\underline{24A}$, 315 (1967).

23. L. R. Testardi, Rev. Mod. Phys. $\underline{47}$, 637 (1975).

24. J. Labbé, Phys. Rev. $\underline{172}$, 451 (1968).

25. R. Viswanathan, D. C. Johnston, Mater. Res. Bull. $\underline{8}$, 589 (1973).

26. G. Shirane, J. D. Axe, Phys. Rev. B $\underline{4}$, 2957 (1971).

27. J. J. Hauser, D. D. Bacon, W. H. Hammerle, Phys. Rev. $\underline{151}$, 296 (1966).

28. P. H. Schmidt, E. G. Spencer, D. C. Joy, J. M. Rowell, Superconductivity in d- and f-Band Metals, Second, edited by D. H. Douglass (Plenum Press, New York, 1976) p. 431 and references therein.

29. V. Diadiuk, Sc. D. Thesis, M. I. T., Dept. of Phys., 1978, unpublished.

30. L. R. Testardi, R. L. Meek, W. A. Royer, A. R. Storm, J. H. Wernick, Phys. Rev. B $\underline{11}$, 4304 (1975).

31. D. A. Rogowski, Ph. D. Thesis, Penn. State Univ., Dept. of Solid State Sci., 1976, unpublished.

32. B. T. Matthias, T. H. Geballe, R. H. Willens, E. Corenzwit, G. W. Hull, Phys. Rev. $\underline{139}$, A1501 (1965).

33. J. R. Gavaler, M. Ashkin, A. I. Braginski, A. T. Santhanam, Appl. Phys. Lett. $\underline{33}$, 359 (1978).

34. A. B. Hallak, R. H. Hammond, T. H. Geballe, Appl. Phys. Lett. $\underline{29}$, 314 (1976).

35. J. M. Poate, R. C. Dynes, L. R. Testardi, R. H. Hammond, Phys. Rev. Lett. $\underline{37}$, 1308 (1976).

36. L. R. Testardi, J. M. Poate, H. J. Levinstein, Phys. Rev. B $\underline{15}$, 2570 (1977).

37. G. F. Hardy, J. K. Hulm, Phys. Rev. $\underline{93}$, 1004 (1954).

38. J. H. Carpenter, Ph. D. Thesis, Purdue Univ., Dept. of Chem., 1955, unpublished.

39. J. H. Carpenter, J. Phys. Chem. $\underline{67}$, 2141 (1963).

40. S. Geller, Acta Cryst. $\underline{9}$, 885 (1956).

41. B. T. Matthias, T. H. Geballe, V. Compton, Rev. Mod. Phys. $\underline{35}$, 1 (1963).

42. T. B. Reed, H. C. Gatos, W. J. LaFleur, J. H. Roddy, Metallurgy of Advanced Electronic Materials, edited by G. E. Brock (Interscience Press, Philadelphia, 1963) p. 71.

43. S. Foner, E. J. McNiff, B. T. Matthias, E. Corenzwit,
Proc. XI Int. Conf. of Low Temp. Phys., edited by
J. F. Allen, D. M. Finlayson, D. M. McCall (St. Andrews
Univ. Press, St. Andrews, Scotland, 1968) p. 1025.

44. A. Muller, Z. Naturforsch. 25A, 1659 (1970).

45. J. R. Gavaler, Appl. Phys. Lett. 23, 480 (1973).

46. J. R. Gavaler, M. A. Janocko, C. K. Jones, J. Appl.
Phys. 45, 3009 (1974).

47. F. J. Cadieu, N. Chencinski, IEEE Trans Magn. Mag-11,
227 (1975).

48. G. W. Roland, A. I. Braginski, Adv. Cryog. Eng. 22, 347
(1977).

49. D. E. Cox, S. Moehlecke, A. R. Sweedler, L. R. Newkirk,
F. A. Valencia, Superconductivity in d- and f-Band
Metals, Second, edited by D. H. Douglass (Plenum
Press, New York, 1976) p. 461.

50. L. R. Newkirk, F. A. Valencia, A. L. Giorgi, E. G. Sklarz,
T. C. Wallace, IEEE Trans. Magn. Mag-11, 221 (1975).

51. R. A. Sigsbee, Appl. Phys. Lett. 29, 211 (1976)

52. A. I. Braginski, G. W. Roland, A. T. Santhanam, K. W.
Guardipee, J. Appl. Phys. 49, 736 (1978).

53. A. I. Braginski, J. R. Gavaler, G. W. Roland, M. R.
Daniel, M. A. Janocko, A. T. Santhanam, IEEE Trans. Magn.
Mag-13, 300 (1977).

54. J. R. Gavaler, <u>Superconductivity in d- and f-Band Metals</u>, <u>Second</u>, edited by D. H. Douglass (Plenum Press, New York, 1976) p. 421.

55. R. E. Somekh, Phil. Mag. B <u>37</u>, 713 (1978).

56. A. H. Dayem, T. H. Geballe, R. B. Zubeck, A. B. Hallak, G. W. Hull, Appl. Phys. Lett. <u>30</u>, 541 (1977).

57. R. H. Buitrago, L. E. Toth, A. M. Goldman, J. Schwanebeck, M. Dayan, Appl. Phys. Lett. <u>32</u>, 341 (1978).

58. M. Kudo, Y. Tarutani, IEEE Trans. Magn. <u>Mag-13</u>, 331 (1977).

59. E. I. Alessandrini, R. B. Laibowitz, C. C. Tsuei, J. Vac. Sci. Tech. <u>15</u>, 377 (1978).

60. A. T. Santhanam, J. R. Gavaler, J. Appl. Phys. <u>46</u>, 3633 (1975).

61. A. H. Dayem, T. H. Geballe, R. B. Zubeck, A. B. Hallak, G. W. Hull, J. Phys. Chem. Solids <u>39</u>, 529 (1978).

62. J. W. Ekin, A. I. Braginski, IEEE Trans. Magn. <u>Mag-15</u>, in press.

63. J. L. Jorda, R. Flukiger, J. Muller, to be published in J. Less-Common Met. and references therein.

64. B. D. Cullity, <u>Elements of X-Ray Diffraction</u> (Addison-Wesley, Reading, MA, 1956) p. 346.

65. N. N. Mikhailov, I. V. Voronova, O. A. Lavrova, E. V. Melnikov, M. N. Smirnova, JETP Lett. <u>19</u>, 271 (1974).

66. J. A. Thornton, Ann. Rev. Mat. Sci., edited by R. A. Huggins, R. H. Bube, R. W. Roberts (Annual Reviews,

Palo Alto, CA, 1977) vol. 7, p. 239.

67. R. E. Somekh, J. E. Evetts, IEEE Trans. Magn. Mag-15, in press.

68. D. F. Moore, private communication.

69. W. A. Lanford, P. H. Schmidt, J. M. Rowell, R. C. Dynes, P. D. Dernier, Appl. Phys. Lett. 32, 339 (1978).

70. R. Flukiger, J. L. Staudenmann, J. Less-Common Met. 50, 253 (1976).

71. J. L. Jorda, R. Flukiger, J. Muller, J. Less-Common Met. 55, 249 (1977).

72. D. A. Ashby, R. D. Rawlins, J. Less-Common Met. 50, 111 (1976).

73. K. L. Chopra, Thin Film Phenomena (McGraw-Hill, New York, 1969) p. 191 and references therein.

74. B. Letellier, J. C. Renard, IEEE Trans. Magn. Mag-15, in press.

75. D. E. Cox, J. A. Tarvin, Phys. Rev. B 18, 22 (1978).

76. O. Meyer, B. Seeber, Solid State Commun. 22, 109 (1977).

77. L. R. Testardi, J. M. Poate, W. Weber, W. M. Augustyniak, J. H. Barrett, Phys. Rev. Lett. 39, 716 (1977).

78. R. D. Burbank, R. C. Dynes, J. M. Poate, to be published.

79. B. E. Warren, X-Ray Diffraction (Addison-Wesley, Reading, MA, 1969) p. 241.

80. B. S. Brown, R. C. Birtcher, R. T. Kampwirth, T. H. Blewitt, J. Nucl. Mater. 72, 76 (1978).

81. J. C. Phillips, Solid State Commun. <u>18</u>, 831 (1976).

82. A. G. Cullis, J. M. Poate, L. R. Testardi, Phil. Mag. B <u>36</u>, 1035 (1977).

83. A. T. Santhanam, J. Appl. Phys. <u>48</u>, 3347 (1977).

84. A. T. Santhanam, P. M. Yuzawich, J. Mater. Sci. <u>12</u>, 1161 (1977).

85. R. H. Hammond, private communication.

86. R. E. Somekh, J. Physique <u>39</u>, 398 (1978).

87. H. C. Theurer, J. J. Hauser, J. Appl. Phys. <u>35</u>, 554 (1964).

88. H. C. Theurer, J. J. Hauser, Trans. AIME <u>233</u>, 588 (1965).

89. J. H. Wernick, W. A. Royer, D. D. Bacon, A. R. Storm, J. Appl. Phys. <u>45</u>, 446 (1974).

90. P. H. Schmidt, D. D. Bacon, H. Barz, A. S. Cooper, J. Appl. Phys. <u>46</u>, 2237 (1975).

91. J. M. Rowell, P. H. Schmidt, Appl. Phys. Lett. <u>29</u>, 622 (1976).

92. R. W. Strachin, Ph. D. Thesis, M. I. T., Dept. of Met. and Mat. Sci., 1967, unpublished.

93. L. E. Davis, N. C. MacDonald, P. W. Palmberg, G. E. Riach, R. E. Weber, <u>Handbook of Auger Electron Spectroscopy</u> (Physical Electronics Industries, Inc., Edina, MN, 1976) p. 5.

94. <u>XRD-5 Instruction Manual</u> (General Electric Co., Milwaukee, WI, 1958) Dir. 11690E.

95. L. J. Vieland, A. W. Wicklund, Phys. Lett. 49A, 407 (1974).

96. J. L. Staudenmann, P. Coppens, J. Muller, Solid State Commun. 19, 29 (1976).

97. K. M. Ho, W. E. Pickett, M. L. Cohen, Phys. Rev. Lett. 41, 580 (1978).

98. H. Lutz, H. Weisman, O. F. Kammerer, M. Strongin, Phys. Rev. Lett. 36, 1576 (1976).

99. A. Davidson, M. Tinkham, Phys. Rev. B 13, 3261 (1976).

100. A. S. Tetelman, A. J. McEvily, Fracture of Structural Materials (John Wiley, New York, 1967) p. 48.

101. R. Flukiger, J. L. Jorda, Solid State Commun. 22, 109 (1977).

102. A. H. Dayem, private communication.

103. G. S. Brown, L. R. Testardi, J. H. Wernick, A. B. Hallak, T. H. Geballe, Solid State Commun. 23, 875 (1977).

104. C. S. Pande, R. Viswanathan, Solid State Commun. 26, 893 (1978).

105. T. Luhman, M. Suenaga, C. J. Klamut, to be published in Adv. Cryog. Eng.

106. W. A. Pupp, W. W. Sattler, E. J. Saur, J. Low Temp. Phys. 14, 1 (1974).

107. G. W. Hull, L. R. Newkirk, J. Low Temp. Phys. 29, 297 (1977).

108. A. I. Braginski, G. W. Roland, M. R. Daniel, Appl. Polymer Symp., edited by J. Economy (John Wiley, New York, 1976) vol. 29, p. 93.

109. S. Touloukian, Thermophys. Prop. Matter (Plenum Press, New York, 1977) vol. 13, p. 175.

110. Ibid., vol. 12, p. 1245.

111. C. W. Chu, L. R. Testardi, P. H. Schmidt, Solid State Commun. $\underline{23}$, 841 (1977).

112. L. R. Testardi, Phys. Rev. B $\underline{5}$, 4342 (1972) and references therein.

113. H. Nowotny, A. W. Searcy, J. E. Orr, J. Phys. Chem. $\underline{60}$, 677 (1956).

114. F. L. Williams, D. Nason, Surf. Sci. $\underline{45}$, 377 (1974).

115. C. A. Neugebauer, Handbook of Thin Film Tech., edited by L. I. Maissel and R. Glang (McGraw-Hill, New York, 1070) p. 8:15.

Biographical Note

The author was born on October 14, 1951 in New Rochelle, N.Y. and was raised in Eastchester, N.Y. The author graduated from the Massachusetts Institute of Technology in June, 1973 with the degree of Bachaelor of Science in Metallurgy and Materials Science. He entered graduate school in Materials Science at the Massachusetts Institute of Technology in September, 1973 with a National Science Foundation Fellowship. He is the author of two papers and a member of Tau Beta Pi and Sigma Xi.

On July 27, 1974 the author married Nancy Anne Hellens of West Simsbury, Conn.